UNIVERSITY OF OKLAHOMA

GRADUATE COLLEGE

REMOTE SENSING OF HYDROLOGIC VARIABLES IN RIVERS

A THESIS

SUBMITTED TO THE GRADUATE FACULTY

in partial fulfillment of the requirements for the

Degree of

MASTER OF SCIENCE

By

MUHAMMAD MUSHFIQUR KHAN
Norman, Oklahoma
2020

REMOTE SENSING OF HYDROLOGIC VARIABLES IN RIVERS

A THESIS APPROVED FOR THE
SCHOOL OF CIVIL ENGINEERING AND ENVIRONMENTAL SCIENCE

BY THE COMMITTEE CONSISTING OF

Dr. Yang E. Hong, Chair

Dr. Jonathan J. Gourley, Co-Chair

Dr. Pierre-Emmanuel Kirstetter

ACKNOWLEDGEMENT

I start with expressing my gratitude to the almighty; the more I relied on Him, the easier He made everything. I would like to thank my supervisor Dr. Jonathan J. Gourley for his wisdom and constant guidance throughout this whole endeavor. I would also like to thank Dr. Yang Hong and Dr. Pierre-Emmanuel Kirstetter for sharing their thoughts with me. Special thanks go to Danny Wasielewski and Jorge Duarte from ANCHOR project for consistently helping me with information and materials.

I am always grateful to my family for their never-ending love and inspiration throughout my whole life. For any achievement in my life, they are the ones who should be thanked first. I especially thank my elder brother Sourav for helping me with the coding.

Last but not the least, I want to express love and gratitude to my dear wife. The almighty always presented her as the rescuer to me whenever I was stuck with something and she helped me to get rid of that. I am truly grateful to her.

ABSTRACT

The use of a “rating curve”, an empirical relationship between water depth in a river and the volumetric flux of water, or discharge, is subjected to uncertainty in data extrapolation, complexity due to changes in channel bathymetry, and high labor costs to maintain it. To potentially overcome these limitations, this study evaluates the efficacy of remote-sensing technologies in measuring river stage and surface velocity, which are the primary input variables for discharge computation, using automated, non-contact methods. Eight pulsed Doppler microwave radars (stream radars) have been installed on cables, culverts, and bridges across rivers at pre-determined, high-priority locations and provided year-round measurements with a temporal resolution of 5-10 minutes. Three of them are collocated with conventional streamgages operated by the U.S. Geological Survey (USGS) and U.S. Department of Agriculture (USDA), which are used as validation. The channel cross-sections are measured by total-station surveying method, while a constant (k-value) is adopted to convert the surface velocity to mean channel velocity for computing discharge. This study discovers and quantifies error in stage measurements induced by the thermal expansion and contraction of supporting structures due to diurnal temperature variation; however, these errors are deemed small and negligible. The impact of ambient wind on the retrievals of surface velocity are found to be negligible too. The results for the three collocated stations show that the radars can accurately measure stage as long as the river depths are not less than 0.08 ft. With the selection of the appropriate k-value, stream radar discharge estimates are as accurate as the conventional USGS and USDA measurements. In examining the time series of river stage and velocity, there are some events identified where the surface velocity reaches its peak 60 – 120 minutes earlier than the peak of the river stage. This time-lag has some levels of positive correlation with the magnitude of the rainfall-runoff events and is negatively correlated with channel slope, indicating a wave celerity effect. Overall, non-contact streamgaging by radars appear both effective and reliable for providing continuous, real-time discharge estimates in an operational setting.

TABLE OF CONTENTS

LIST OF TABLES

LIST OF FIGURES

Chapter 1

INTRODUCTION

1.1 BACKGROUND

Streamflow (discharge) is the key hydrologic variable of a river. It is of paramount importance for stormwater management, flood forecasting, estimating load for water quality control, water resource management, etc. Conventional stream gauges, such as those operated and maintained by the United States Geological Survey (USGS), use an empirical relationship of water depth and discharge, called a "rating curve" to estimate the streamflow. These rating curves need manual, in-situ measurements over a wide range of river flow conditions and must be updated in response to changes in the channel bathymetry, which is time-consuming and costly. In this regard, remote sensing technologies that utilize commercially available radars capable of continuously measuring water level and surface velocity, can potentially address the shortcomings of relying on a rating curve.

Streamflow of a river is the product of cross-sectional area (i.e., wetted area; hence it is a function of water depth) and mean channel velocity at that location. USGS uses different methods for measuring water depth (alternatively known as stage, or, gage height) that include float/stilling-well method, pressure transducers, gas-purge (bubbler) systems, and stage radar. (USGS, 2020a). The instruments that measure, record, and transfer stage data to database are kept in a structure (streamgage), which is generally located beside the river of interest. On the other hand, for over a century USGS has kept unchanged their velocity measurement technique with the "current meter"; however, recently, it has introduced a technologically more advanced technique that involves using an Acoustic Doppler Current Profiler (ADCP) (USGS, 2020b). Both are direct measurement methods as in the case with a current meter, the instrument needs to be directly immersed into

water to obtain the rotation rate of its wheel around a vertical axis (Rantz, 1982), while in order to transmit a sound pulse into the water and measure the difference in frequency with its echo, the ADCP requires to be mounted on a boat or similar vessel.

The annual operating and maintenance costs of a traditional streamgage are similar to the initial purchasing cost of the instruments. During floods, direct measurements may produce high percentage of error as well as put operators' lives at risk due to increased turbulence. Moreover, floods can damage the streamgage structure and wash away valuable equipment. On the contrary, remote sensing equipment are situated well-above a stream surface, hence, less likely to be lost during a flood and have less stringent requirements for annual maintenance, power, and access.

This study uses a "Stream Radar" that integrates two contact-free radar methods in one frame to retrieve both the stage and surface-water velocity of a stream simultaneously. Eight stream radars have been installed on cables or bridges across rivers at pre-determined, high-priority locations and are providing measurements continuously. Therefore, the complete system offers a non-contact solution to retrieve all variables needed to estimate discharge in a stream. This research is being conducted as a part of the "Automated Non-Contact Hydrologic Observations in Rivers" (ANCHOR) project, funded by the National Oceanic and Atmospheric Administration (NOAA), which aims to investigate and demonstrate the use of remote sensing technologies for streamflow estimation.

1.2 HYPOTHESES AND OBJECTIVES OF THE STUDY

1.2.1 Hypotheses

The hypotheses of this study are as follows:

1. The stream radars will be able to accurately measure the stage and surface water velocity of the selected streams. The cause of systematic and random biases will be identifiable and quantified.
2. When the river cross-sections are known, discharge can be accurately estimated from the remote-sensing observations with uncertainty estimates supplied.
3. There will be specific sites and events which reveal offsets in the evolution of velocity & stage.

1.2.2 Objectives

The three objectives of this research are given below:

1. To compare the stage measurements with gauge observations for the radars that are collocated with a USGS streamgage, quantify the errors, and identify their sources.
2. To compare the discharge estimates with gauge observations for the radars that are collocated with a USGS streamgage, quantify the errors, and identify their sources.
3. To understand the information content of the velocity measurements. Do they merely mirror the stage measurements (as is assumed in the construction of a rating curve) or do they provide additional details and under what settings?

1.3 THESIS OUTLINE

This thesis intends to introduce the reader to remote sensing of streams using a stream radar. A comprehensive literature review is provided in Chapter 2 to explore the existing methods and challenges they faced during discharge estimation. Chapter 3 describes the hydrologic variable measurement technique by the stream radars and the methods carried out for different analyses in this study. The findings of this research and discussion of the results are presented in Chapter 4, while Chapter 5 lists the conclusions and recommendations for future work.

Chapter 2

LITERATURE REVIEW

To address the direct measurement issues, numerous attempts have been made in the last couple of decades. Some notable non-contact techniques that have been previously used to estimate discharge are described in this chapter.

2.1 INDIRECT MEASUREMENT

Typically, peak discharges after any flood event are measured by different indirect measurement methods such as flow over dam, contracted opening, flow through culvert, etc. (Benson & Dalrymple 1967). The most commonly adopted one by USGS is the slope-area measurement which is based on Manning's formula as given in equation 1.

$$Q = \frac{k}{n} A R^{2/3} S^{1/2} \qquad \text{Equation (1)}$$

where, Q is the discharge (ft^3/s), A is the cross-sectional area (ft^2), R is the hydraulic radius (ft), S is the friction slope and n is the Manning's roughness coefficient, and k is equal to 1.49.

The accuracy of discharge measurement by the slope-area method is sensitive to the accuracy of friction slope in equation 1. It is assumed that Manning's can be applicable for non-uniform channels when the energy gradient is changed to represent the friction losses at the boundaries and the slope is calculated from the difference in water surface elevation and velocity heads along the reach of the channel. For calculating the water surface difference, the highest water level is determined from the traces of flow on the side wall of a reach. These marks may mislead in representing the actual slope in the main section of the flow due to diffusion and downslope creep of debris, bank roughness, difficulty induced by the smaller events after the big one, etc. (Smith et al., 2010).

Another challenge of slope-area method is the selection of the channel reach. To best retain the mark, the channel should have accessibility to survey right after a large event, sidewalls made of rocks, least amount of morphological changes, uniform cross-sections above the reach, etc. (Dalrymple & Benson, 1984). Moreover, the hydrograph of an event cannot be generated from slope-area method since it only allows computing the peak flow. Overall, the slope-area method is less reliable, and the accuracy level of the discharge estimate is very poor (Costa et al., 2006).

2.2 RATING CURVE METHOD

A very popular way of determining discharge is to use the "rating curve" that allows to extract the flow rate corresponding to a stage value from a numerous, direct stage-discharge measurements, which are called "gaugings" (Rantz, 1982). In this method, stage is measured and reported automatically, and then the rating curve is used to get the corresponding discharge value for this stage. To establish a rating curve, discharge measurement must be done manually (i.e., direct measurement of velocity and cross section) during a variety of conditions.

A rating curve is a simple function for relating the flow rate with the stage that is assumed to prevail at a cross-section of the flow in the reference hydraulic conditions. The definition of this reference hydraulic regime is hardly straightforward. In most cases, these conditions refer to the ideal situations like steady flow, constant channel roughness, unchanging geometry, no backwater effects, etc. (Schmidt, 2002). Whenever there is a deviation from these conditions, the derived discharge may have significant errors. These errors should be identified from the ones that are directly related to the reference stage-discharge relation. If the reference regime is permanently altered, for example, due to the change in channel geometry after a flood event, a new regime should be established. The regime can be changed temporarily due to changes in the downstream boundary condition (Petersen-Overleir & Reitan, 2009), seasonal vegetation growth (WMO,

2010), dune-flat bed transitions due to floods, or, hysteresis due to transient flow effects (Le Coz et al., 2012).

A detailed description on uncertainty analysis related to gaugings and rating curve was given by McMillan et al. (2012). The gaugings are difficult to get especially at extremely low or high flow events and the derived discharge can vary by 5-20% of the actual (measured) one. The relationship between river stage and discharge is not always a straightforward one when the stream has unsteady flow (Dottori et al., 2009). The discharges for a single stage are different based on their rising, or, descending behavior, where higher values are typically obtained for the rising one (Di Baldassarre et al., 2009). In extreme cases, the extrapolation may result in a bias of 100% or even higher than that (Lang et al. 2010). To establish a rating curve and benefit from it, it requires proper understanding of the hydraulics of any river. Therefore, managing these curves and properly dealing with the associated uncertainties are still not easy tasks and research work is being developed to improve the condition (Le Coz et al., 2012).

2.3 MEASUREMENT USING TRACERS

For small channels, the USGS uses tracer dilution method when discharge measurements become difficult due to increased turbulence, movement of debris, frequently changing cross-section, inaccessible flow conditions, etc. (Kilpatrick & Cobb, 1985). There are two techniques to apply this method: slug injection and constant rate injection. Due to relatively simple principle, the latter one is frequently used, which is based on the conservation of mass principle. When a tracer is injected into a stream at a constant rate, its concentration will be reduced (i.e., dilution) proportionally with the streamflow rate (Kilpatrick & Cobb, 1985). In this method, concentration of the tracer is measured at three stages: before, during and after the it crosses the gauging station (Capesius et al., 2004). Discharge is then measured by the following equation,

$$Q_s = 5.89 \times 10^{-7} \frac{c_i Q_i}{(c_g - c_b)}$$ Equation (2)

where, Q_s is the discharge of the stream (ft^3/s), c_i is the concentration of the tracer injected (mg/L), Q_i is the rate of tracer injection (mL/min), c_g is the concentration of tracer at the gaging station (mg/L), c_b is the background concentration of the tracer at the gaging station (mg/L). This method assumes that 1) the tracer is conservative 2) it is completely mixed with the stream and 3) the amount of tracer does not change due to chemical reactions (Rantz, 1982).

Recently some research works have been conducted on tracer gauging method, such as, Capesius et al. (2004) used the tracer dilution technique for measuring discharge in some ice-affected streams in Colorado. They found different results based on the elevation and weather condition of the gauging station. For example, at a low altitude and warmer site, the tracer method overestimated by 14% from the discharge by current meter method, whereas at a high altitude and colder site, it underestimated by 52%. The poor performance in colder station was attributed to the low reliability of the tracer pump and limitation of the tracer-probe accuracy. However, they found the discharge measurement by the current meter method in winter season was unreliable too. Clow and Fleming (2008) used tracer dilution method to measure discharge in ice-affected streams in Colorado too. The average error obtained was 6.3% in comparison with the USGS gauge measurement. To get the best outcome, they emphasized examining the primary assumption of the test prior to the test such as, uniform mixing and total conservation of the tracer, no chemical reaction or sorption, etc.

2.4 MEASUREMENT BY IMAGE ANALYSIS

The idea of measuring surface velocity using remote sensing technologies started with image analysis. In the 1960's, the first image-based velocimetry method was introduced that was labelled as Particle Image Velocimetry (PIV). In this method, as Adrian (1991) quoted, "particles in the

fluid are illuminated by a sheet of light that is pulsed. The particles scatter light into a photographic lens located at 90° to the sheet, so that its in-focus object plane coincides with the illuminated slice of fluid. Images are formed on a photographic film or on a video array detector, and the images are subsequently transferred to a computer for automatic analysis". The selection of any component in traditional PIV method such as visualizing the flow, illumination, or, recording, is determined by some rules-of-thumb that are based on the particle size and concentration with respect to the image processing parameters and expected particle movement in several pictures. These conditions are mostly available in a laboratory environment, and possibly for very small streams (Bradley et al., 2002). In the mid-1990s, PIV was first implemented for rivers in Japan (Fujita & Komura, 1994; Aya et al., 1995). After some changes in traditional PIV method such as illumination, seeding procedures, pre-processing of the recorded images etc. and adding new component (e.g., image orthorectification), Fujita et al. (1998) applied this method for greater surface area than those were used in the conventional PIV method and was renamed as Large Scale PIV (LSPIV). During course of time, LSPIV could measure surface velocity and provide discharge estimates for areas up to 5000 m^2 (Fujita et al., 1998; Muste et al., 2000; Bradley et al., 2002; Creutin et al., 2003; Hauet et al., 2006).

Several studies were conducted in the last few decades that used LSPIV for discharge measurement in natural streams. Harpold et al. (2006) developed a LSPIV prototype for measuring surface velocity and discharge in a hydraulic flume and then adjusted parameters to apply it to an actual river system. They found that for low Froude number (< 0.10), the accuracy of LSPIV measurement can be reduced by 15% due to aggregation of the tracer elements. On the other hand, for higher Froude number (> 0.25), discharge estimates will be underestimated due to lack of proper tracer density. The discharge estimates were overestimated by 28% than that of a control

structure (e.g., weir) for relatively high flow conditions, since appropriate tracer distribution is difficult to maintain at high flows. Dramais et al. (2011) conducted discharge measurements with a mobile LSPIV (i.e., a remotely controlled mobile telescopic mast containing a video camera) system for a flood event of 10-year return period and for a reservoir release event. In an attempt of identifying the parameter that provides major error for mobile LSPIV measurements, they found that the velocity coefficient could solely induce up to 15% error in discharge estimates due to its multiplicative nature. However, for a flood event especially in case of peak flow, this percentage of error is significant, which can potentially imply the inability to accurately measure channel velocity for big events by LSPIV method. MacVicar et al. (2012) used videography for their river monitoring study. It was found that using conventional cameras at nighttime was a major source of error. Even the use of infrared sensitivity could not improve the situation, while during daytime intense sunlight, reflections from random sources, etc. also caused deterioration in the data quality.

A remotely piloted aircraft system (RPAS) method was used by Bolognesi et al. (2017) to extend the PIV method for measuring low surface velocity and small discharges. The method of velocity measurement was simply based on analyzing the movement of a float in a specific time period from series of digital photos. However, for such method, constant presence of several ground control points (GCPs) is required, which is difficult to achieve for wider rivers considering all the points need to be present in the captured image; at the same time quality is also ensured for image processing. On the other hand, without GCPs, the stability of the RPAS is essential since the displacement of the aircraft will result in scale-change of an image and mislead the tracer. Increased wind speed for higher altitude above the ground can potentially affect the stability. In a study (Tauro et al., 2017) that evaluated the applicability of the LSPIV method for natural streams, it was found that LSPIV method largely underestimated the surface velocities with respect to some

gauged velocities due to tracer aggregation and inconsistent light intensity. They argued that the velocity vectors, obtained from the LSPIV method, were mean values for a specific period of time that can be accurate for a laboratory condition only since users can homogenously and uninterruptedly add tracers there. They further concluded that LSPIV can provide good discharge estimates for small rivers provided that the seeding is quite high there as it was done by Creëlle et al. (2018) in a vegetated stream.

While working with PIV methods such as LSPIV for an actual river system, some specific conditions must be fulfilled. For example, one should have a suitable recording position that has a constant light intensity and enough floats (e.g., debris, foam, etc.) at the surface of the channel (Muste et al., 2008). But unlike a laboratory lighting system, natural light intensity is not the same during day and nighttime. Also, presence of glare and shadows on water surface deteriorate image quality (Hauet et al., 2008). On the other hand, tracers do not always present themselves in sufficient amount in a natural stream which require addition of artificial tracers. It indicates potential discontinuity in getting accurate data as well as constant human involvement. However, only addition of tracers does not completely solve the issue since their moving direction must coincide with that of the stream. Strong winds or clustering of the floats, due to electrostatic force, can potentially hamper the proceedings (Muste et al., 2008). Any tilting angle (of camera) less than 10 degrees can hurt the image quality that will eventually impose trouble in image transformation (Kim et al., 2007). Also, for image orthorectification, accuracy of the GCPs is essential, which makes this technique unsuitable for the environment that are not easily accessible (Tauro et al., 2017).

On the contrary, in LSPIV method, initial measurement of water depth is directly taken from photos that is further converted into actual stage using the topographic information. The

orthorectification process of LSPIV is affected by the error in stage that eventually generates error in discharge computation (Dramais et al., 2011). Le Boursicaus et al. (2016) found water depth was the major source of error for discharge computation in their study. For a difference of 15 cm in water depth from the photo resulted in up to 28% error in the final discharge output.

2.5 MEASUREMENT BY RADARS

Streamflow computation by radar was first carried out in 2000 (Costa et al., 2000), where surface velocity was measured by a pulsed Doppler radar (10 GHz) and channel cross section was measured by a ground penetrating radar (GPR) (60-300 MHz). The experiment site had an active gauging station from USGS, and the output discharges were within 1% of rating curve provided discharge value. It was a proof-of-concept experiment and only three discharge measurements were made. Success of this experiment inspired further application of non-contact radar technique in streamflow measurements, such as by helicopter-mounted radar (Melcher et al. 2002), using an X-band pulse radar (Lee et al., 2002), coherent microwave systems (Plant et al., 2005), etc. Costa et al. (2006) further applied three different non-contact radar systems (e.g., continuous wave microwave, monostatic UHF Doppler and pulsed Doppler microwave radar) for continuous surface velocity measurement and cross section measurement method by a GPR was kept unchanged. The maximum data acquisition was made for 16 weeks for a single station and the discharge estimates for all the three radars were highly correlated (e.g., correlation coefficient: 0.883 ~ 0.992) with the rating curve discharge values. Welber et al. (2016) deployed handheld surface velocity radar (SVR) for surface velocity measurement and the output discharge estimates were 10% of the directly measured discharge value. However, the SVRs provided neither the water depth nor the bathymetry of the channel, rather both were measured manually. So, technically, it was not a complete non-contact measurement.

An extensive work on radar velocimetry was provided by Fulton et al. (2020), which evaluated the efficiency of Doppler and pulsed radars to provide automated, real-time discharge data. Ten radars were installed to monitor streams representing a variety of hydrologic and hydraulic characteristics, all of them were collocated with a USGS streamgage and most of them provided data for one year or so. A strong correlation was found for mean velocities (R^2= 0.993) and discharge estimates (R^2 = 0.999) between the radar and streamgage data. The composite average and absolute percentage of error between the radar and streamgage data were -0.3 and 5.1%, respectively. However, they found that the deployed radars were not effective in measuring velocity less than 0.15 m/s. They also reported that gravity waves and wind drift can induce additional drift in the surface velocities leading to highly biased discharge estimates. Finally, they concluded that remote sensing observations can provide real-time river variable data that can be used operationally and in absence of previous records.

Previous studies on remote sensing by radars are primarily experimental and highlight the basic measurements of stage and surface velocity in rivers. However, more comprehensive analysis is needed using commercial sensors placed on a variety of streams in different hydrologic regimes that can provide data over long periods of time. In this study, we have used eight stream radars that monitor streamflow in small channels, rivers with frequent morphological changes, a flume, and a spring-fed creek. These radars provide year-round measurements of stage and surface velocity with a temporal resolution of 5-10 minutes. Besides discharge estimation, these long timeseries data are analyzed to identify the correlation between the variables like how they behave during rainfall events, behavioral comparison for different sites, and topographical effect on surface velocity. These analyses will provide information for better error characterization and

quantification in non-contact measurements by radars, which will eventually be useful in applying these sensors in an operational setting.

Chapter 3

METHODOLOGY

3.1 STUDY AREA

Eight stream radars have been installed on cables or bridges across rivers at the pre-determined and high-priority locations in four states. As shown in Figure 1, three of them are installed in Texas, two in both Arizona and Oklahoma and one is installed in Colorado.

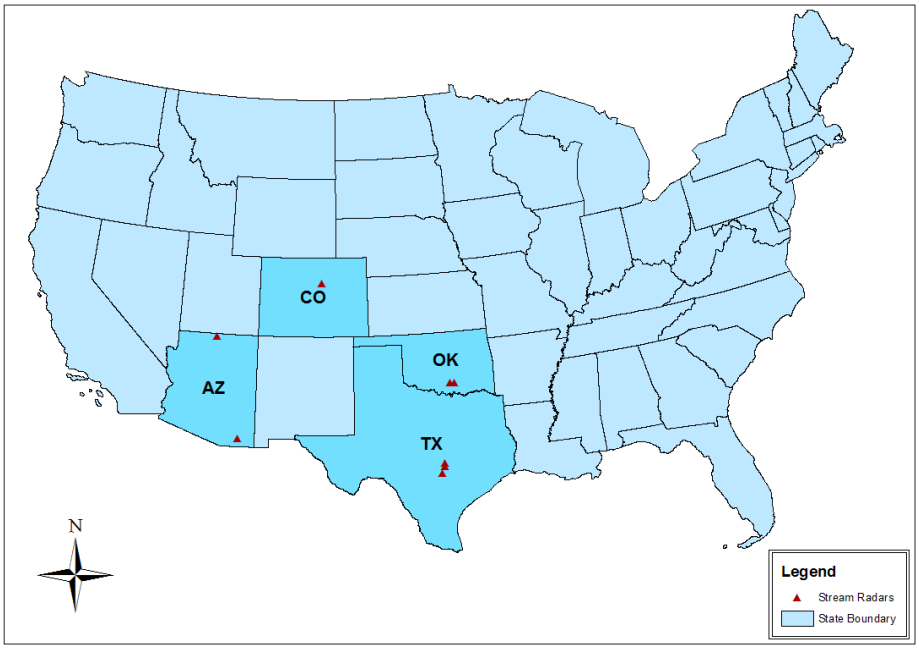

Figure 1: Locations of all the stream radars in the United States

3.1.1 Cherry Creek

Cherry Creek is a tributary of the South Platter River that runs near Denver, Colorado. The area of the watershed is about 1058.9 square kilometers (Figure 2). According to the National Land Cover Database 2011 (NLCD 2011) (Homer et al., 2015), land use in the upper part of the watershed is mostly vegetation (e.g., herbaceous and shrub/scrub), whereas the lower part is a

complete developed area. The relative proportions of sand, silt, and clay are 53.9, 29.7 and 16.4% respectively as per CONUS soil datasets (Miller and White, 1998). The area has a mean watershed slope of 7.92%. The mean annual precipitation at the radar location is 404 millimeters (PRISM, 2004). The stream radar is mounted on a bridge here (Figure 3) and situated approximately 200 ft upstream from a USGS streamgage (station ID – 06713500).

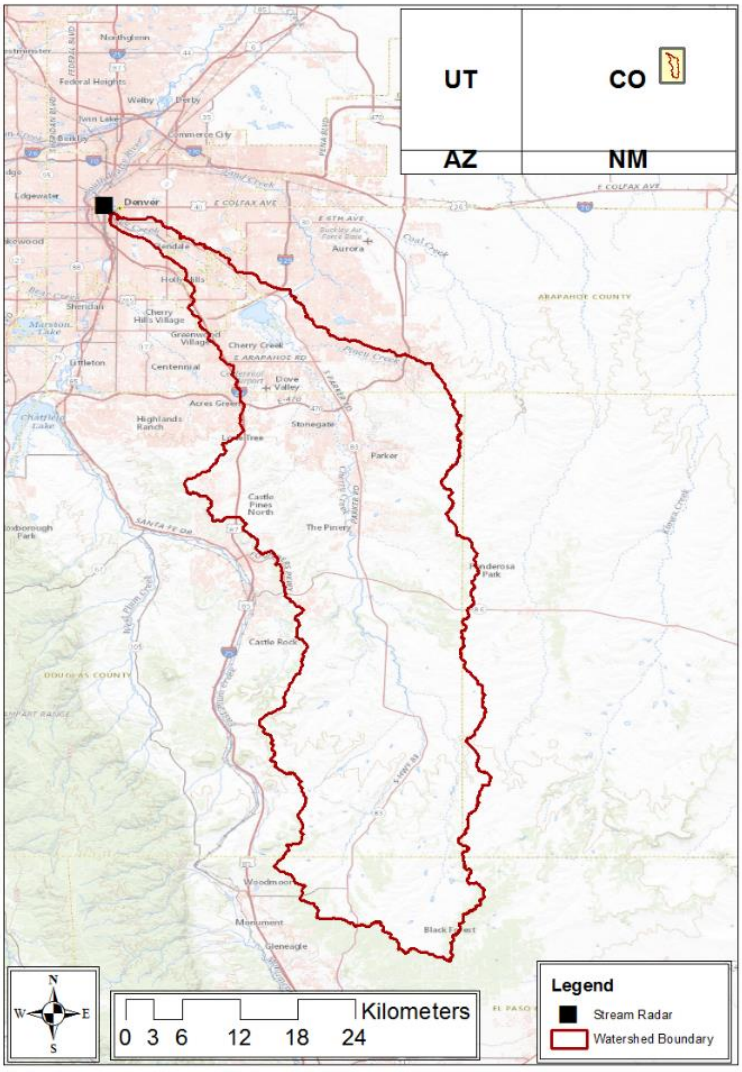

Figure 2: Delineated watershed for stream radar at Cherry Creek

Figure 3: Stream radar mounted on bridge at Cherry creek

3.1.2 Mill Creek

Mill Creek runs near Mill Creek town in Johnston County, Oklahoma. The basin area is approximately 124 square kilometers (Figure 4). The NLCD land use of the area is mostly herbaceous and hay/pasture lands. The soil texture has a relative proportion of sand, silt, and clay as 27, 42.3 and 30.7% respectively. The area has a mean watershed slope of 3.23% and the mean precipitation near the radar location is 1027 millimeters for a year. The radar is cable mounted (Figure 5) and has a USGS streamgage about 100 ft upstream from its position (ID – 07331200).

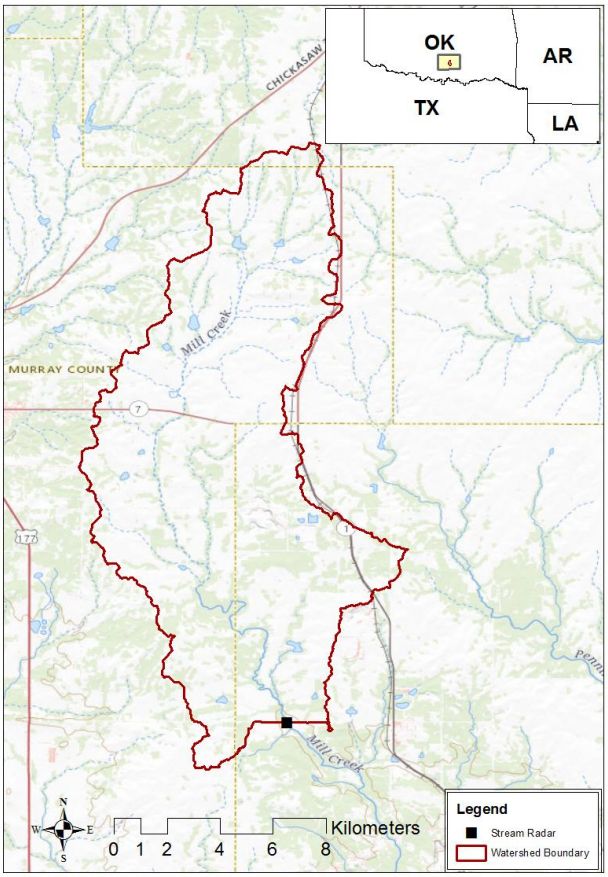

Figure 4: Delineated watershed for stream radar at Mill Creek

Figure 5: Cable mounted stream radar at Mill creek

3.1.3 Walnut Gulch

The study area is situated in the southeast corner of Arizona. Water moves through a concrete flume here and the size of the contributing area is 7.82 square kilometers (Figure 6). The primary land use type of the watershed is vegetation (e.g., shrub and herbaceous). The relative proportions of sand, silt and clay are 58, 29.6 and 12.4% respectively. The watershed has a moderately sloping mean gradient of about 12.07%. The mean annual precipitation amount is 356 millimeters. The radar is mounted on a bridge (Figure 7) here and collocated with a conventional United States Department of Agriculture (USDA) stream gauge.

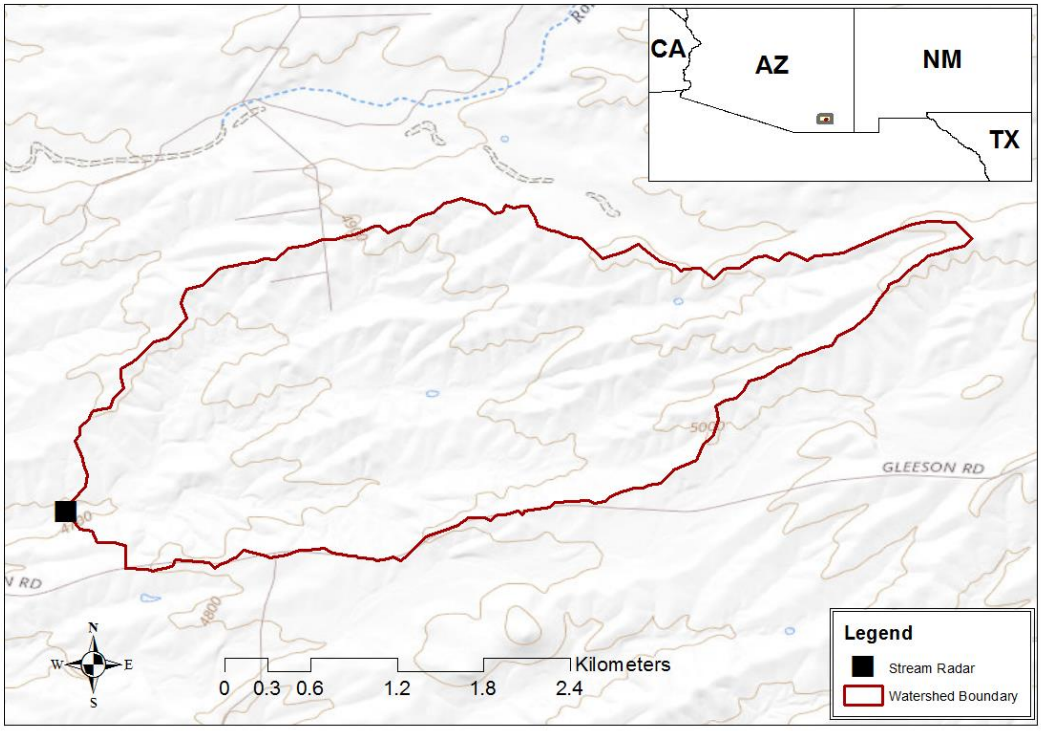

Figure 6: Delineated watershed for stream radar at Walnut Gulch

Figure 7: Stream radar mounted on bridge at Walnut Gulch

3.1.4 Paria River

Paria River is a tributary of the Colorado River that runs from southern Utah towards northern Arizona. It has a very large watershed area of approximately 3676 square kilometers for the radar location (Figure 8). The upper part of the basin has some vegetation land usages, but the rest of the area is mostly barren land. For soil texture, the relative proportions of sand, silt and clay are 56, 23.3 and 14.7%, respectively. The watershed has a high mean slope of 20.89% . The area near the radar has a very low average annual precipitation of 185 millimeters. The radar is mounted on a bridge (Figure 9) and has a USGS streamgage (ID – 09382000) about 1.2 kilometers upstream from its position.

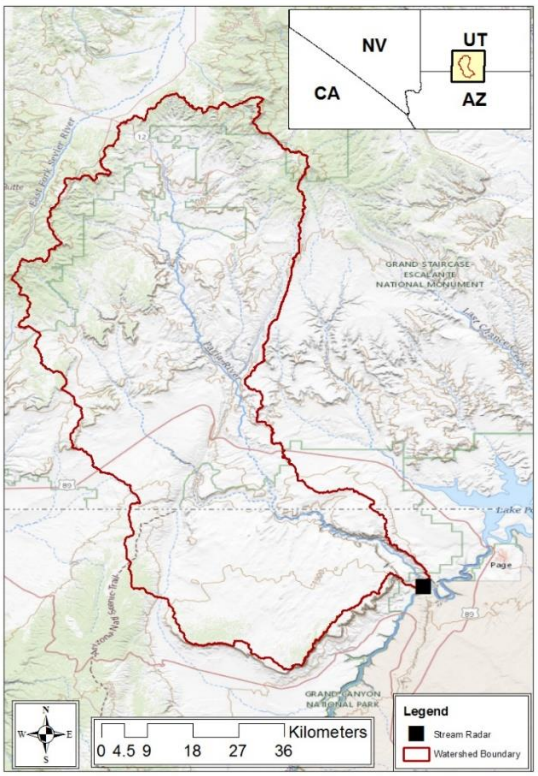

Figure 8: Delineated watershed for stream radar at Paria River

Figure 9: Stream radar mounted on bridge at Paria River

3.1.5 Falls Creek

Falls creek originates from the springs of the Arbuckle aquifer and flows towards the northeast into the Washita River in Oklahoma. The size of the watershed area for the stream radar location is 15.12 square kilometers (Figure 10). The land uses mostly include grassland and different types of forest (e.g., evergreen, and deciduous). The relative proportions of sand, silt and clay are 23, 63 and 14% respectively. The mean watershed slope is 7% and annual precipitation is approximately 1000 millimeters. The radar is cable mounted (Figure 11) and not collocated with any other streamgage.

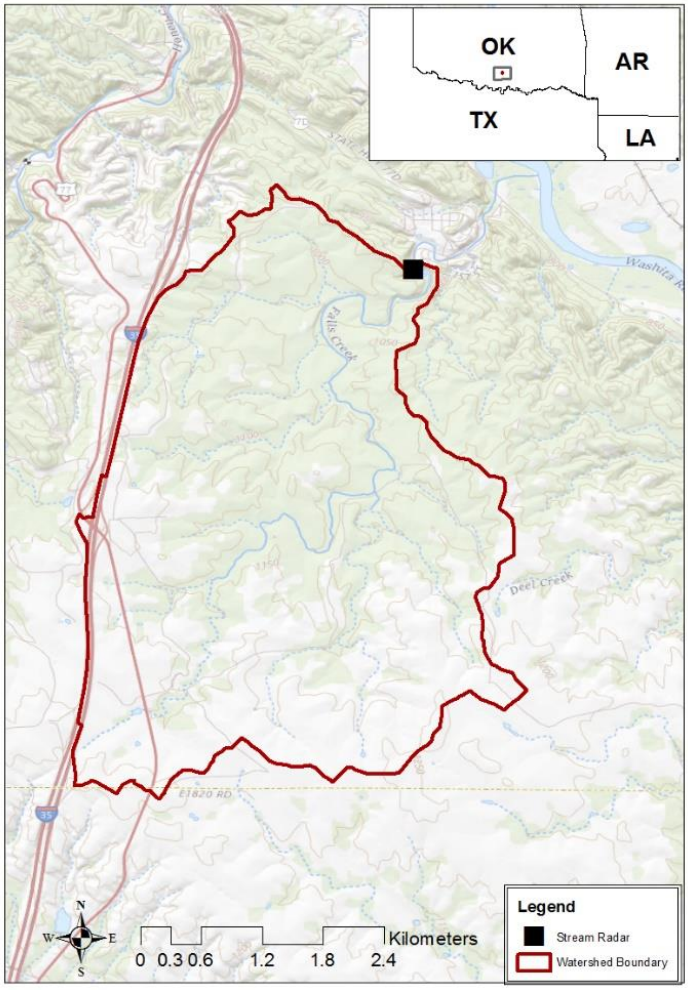

Figure 10: Delineated watershed area for stream radar at Falls Creek

Figure 11: Cable mounted stream radar at Falls Creek

3.1.6 Sessom Creek

Sessom creek is a spring creek that runs into the San Marcos River in Texas. Water moves through a concrete channel here. The contributing area at stream radar's location is only 1.56 square kilometers (Figure 12). Land uses involve mostly development, open space, and evergreen forest. The soil texture has a relative proportion of sand, silt, and clay as 24.5, 25.5 and 50% respectively. The mean watershed slope is 11.56% and annual precipitation near the radar location is about 861 millimeters. The radar is mounted on a culvert as shown in Figure 13 and there is no other streamgage here.

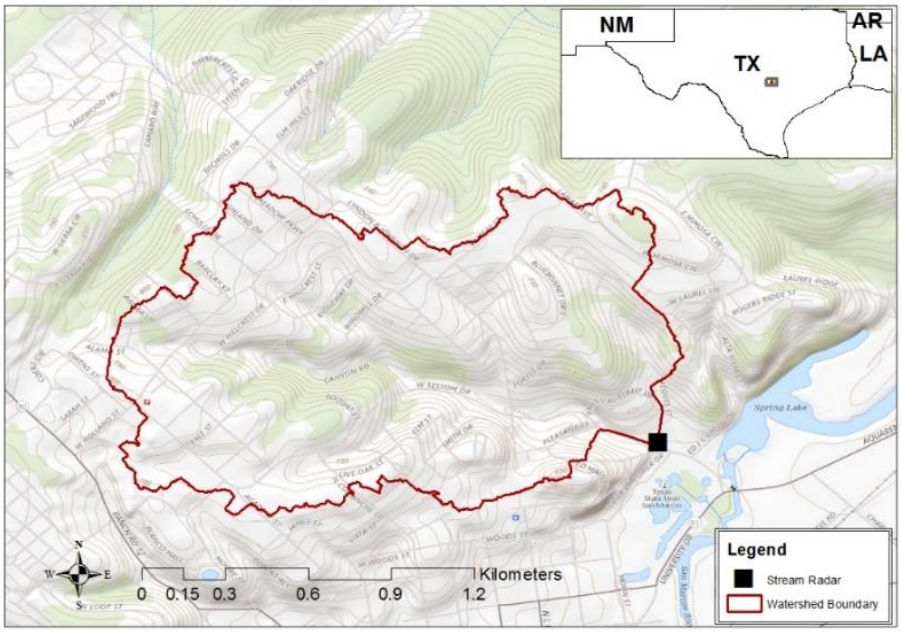

Figure 12: Delineated watershed for stream radar at Sessom Creek

Figure 13: Stream radar mounted on culvert at Sessom Creek

3.1.7 Austin North

West Fork Walnut Creek is the channel that receives the runoff from this study area. It is a tributary of Walnut Creek, which further runs southeast into the Colorado River in Austin, Texas. The watershed area for the stream radar location is 4.32 square kilometers (Figure 14). The land uses of the area involves open space and some degrees of development. The relative proportions of sand, silt and clay are 22.85, 26.15 and 51% respectively. The mean watershed slope is 5% and the mean annual precipitation is about 862 millimeters. The stream radar is mounted on a culvert, which is below a train bridge (Figure 15) and it is not collocated with any other streamgage.

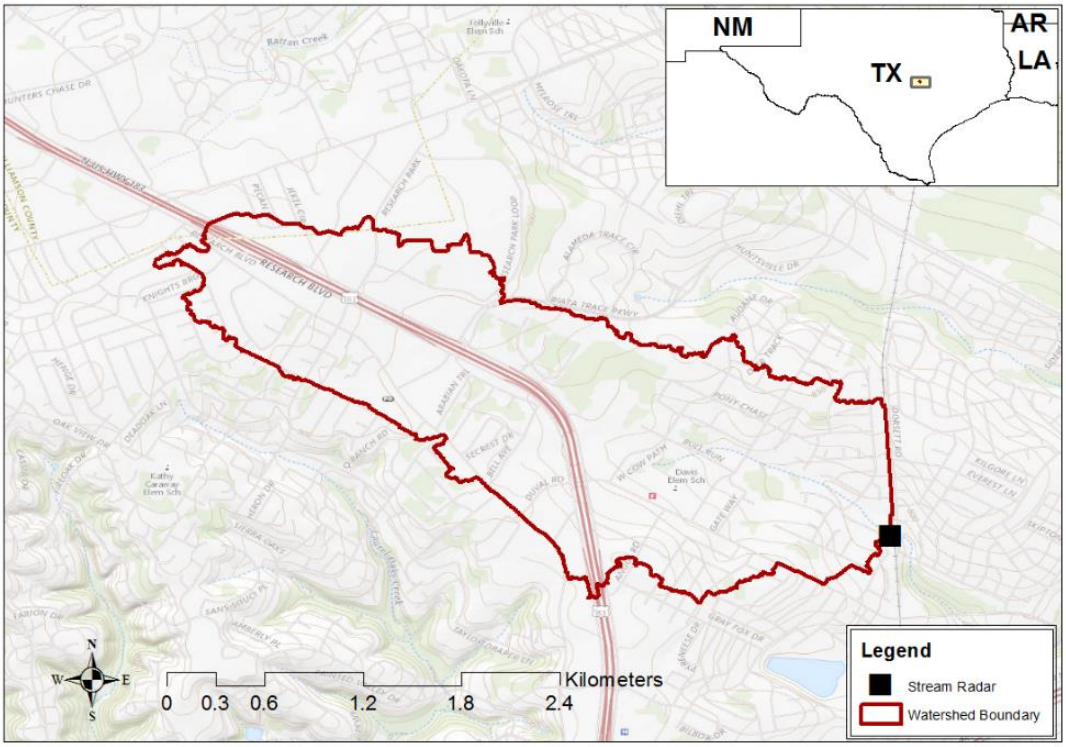

Figure 14: Delineated watershed for stream radar at Austin North

Figure 15: Stream radar mounted on culvert at Austin North (source: Google Earth Pro)

3.1.8 Austin South

The channel that receives runoff for this study area is West Bouldin Creek, which further runs northeast, and it reaches the Colorado River in Austin, Texas. The radar location has a watershed of 4.61 square kilometers (Figure 16). The area is a developed one that involves both open space and intense development. Soil texture has a relative proportion of sand, silt, and clay as 17.75, 32.5 and 49.75% respectively. The watershed has a mean slope of 7.7% and mean annual precipitation is 856 millimeters near the radar location. The radar is mounted on a train bridge (Figure 17) and there is no other streamgage here.

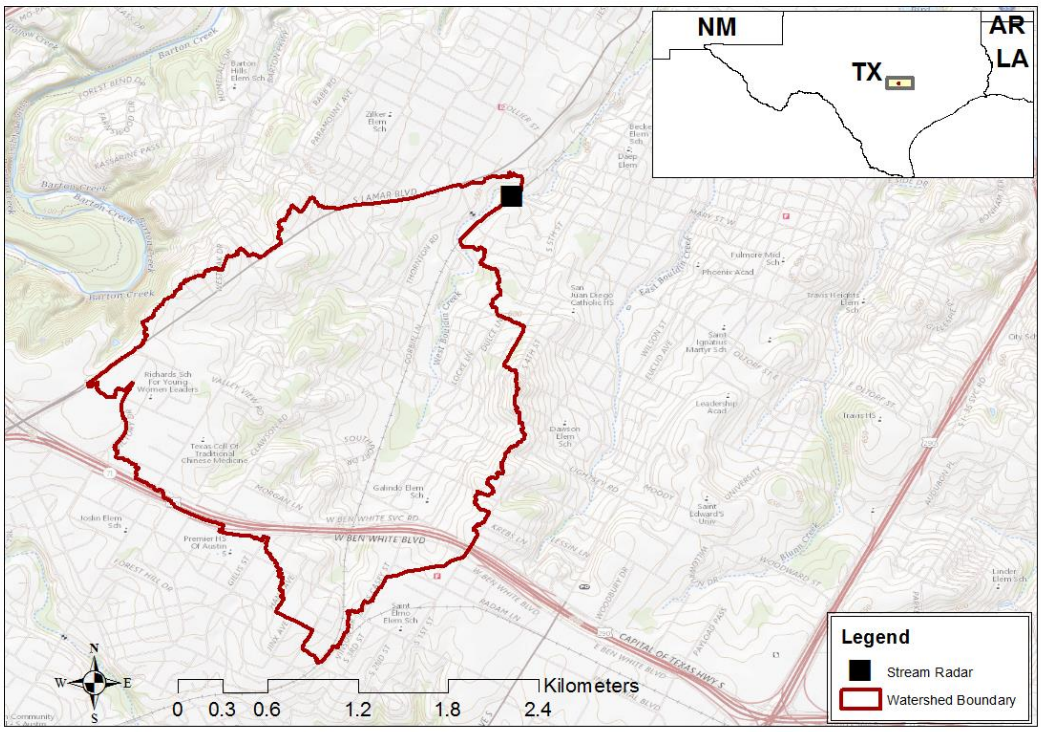

Figure 16: Delineated watershed for stream radar at Austin South

Figure 17: Stream radar mounted on bridge at Austin South

A summary of watershed characteristics and data measurement records for all the radar stations are provided in Table 1.

Table 1: Summary of radar measurements and watershed characteristics for all the stations

Station	Basin area (km^2)	Setting	Status	Data Period		Data Resolution (minutes)
				Start	End	
Cherry Creek	1059	Urban	Collocated	Aug 2017	Apr 2019	5
Mill Creek	124	Vegetation	Collocated	Sep 2017	Sep 2018	10
Walnut Gulch	7.82	Desert	Collocated	Jul 2018	Nov 2019	10
Paria River	3676	Desert	Semi-collocated	Jul 2018	Oct 2019	10
Falls Creek	15.12	Forest	Not collocated	Mar 2017	Jun 2019	10
Sessom Creek	1.56	Urban	Not collocated	Nov 2017	Jun 2019	10
Austin North	4.32	Urban	Not collocated	Jul 2018	May 2019	5
Austin South	4.61	Urban	Not collocated	Jul 2018	Sep 2018	5

3.2 REMOTE SENSING BY STREAM RADAR

This study uses short range radars that directly measure the water level and surface velocity of streams (hence, called a stream radar). The units evaluated in this study are manufactured by SOMMER Messtechnik and alternatively known by their trade name – RQ_30. The radar is generally installed on bridges, culverts, or cables and look either in the upstream or downstream direction of the channel. Figure 18 shows the basic operational setting of measurement by the stream radar.

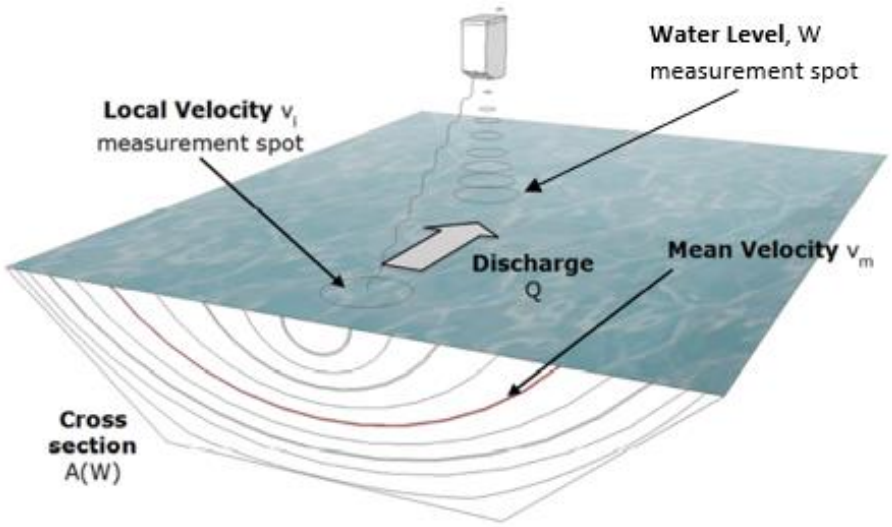

Figure 18: General measurement technique by stream radar (modified from Sommer, 2014)

3.2.1 Water Level Measurement Principle

For water level measurement, the radar sensor passes a short micro-wave pulse to the stream and receives its echo as the pulse reflects on the water surface. The time lag between sending and receiving the signal is directly proportional to the distance between the sensor and water surface and is determined as below,

$$h = \frac{ct}{2} \qquad \text{Equation (3)}$$

where, h is the distance between water surface to sensor (ft), c is the speed of light (ft/s) and t is the time of pulse interval (sec).

To retrieve water level, a reference level or Gauge Zero (GZ) needs to be defined first. When the distance between the sensor and GZ (E in Figure 19) is set into the sensor, the sensor automatically determines the water level (W) from the difference between E and h.

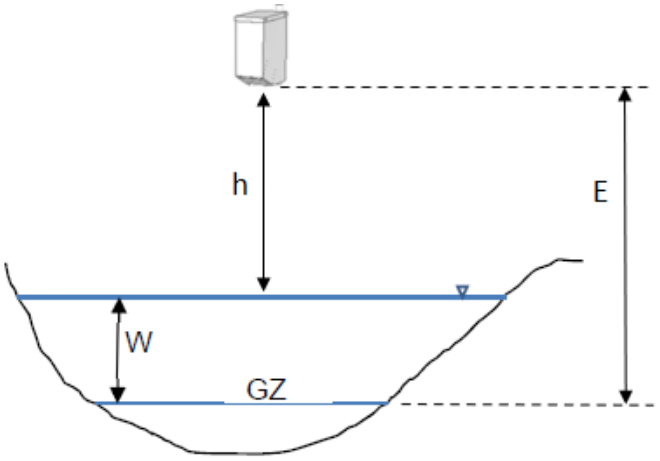

Figure 19: Retrieval of water level information (modified from Sommer, 2014)

3.2.2 Surface Velocity Measurement Principle

The surface velocity measurement is based on the principle of surface scattering and "Doppler Shift". The radar sensor transmits a signal to the stream with a specific angle and a known frequency. This signal is backscattered by the movement of the ripples on the water surface. The lengths of these short waves are determined by the Bragg resonance condition as below (Plant et al., 2005):

$$\lambda_b = \frac{\lambda}{2sin\theta} \qquad \text{Equation (4)}$$

where, λ_b is the wavelength of the resonant water wave (i.e., the Bragg wave) (ft), λ is the wavelength of the radar beam (ft) and θ is incidence angle (degree).

When the transmitted signal returns to the sensor, there is a shift in its frequency due to the Doppler effect. By calculating the shift in frequency, the surface velocity is computed as follows (Fulton & Ostrowski, 2008):

$$v = f_d\lambda_b \pm c \qquad \text{Equation (5)}$$

where, v is the surface velocity (ft/s), f_d is the Doppler shift in frequency (Hz or s^{-1}), λ_b is the wavelength of the resonant water wave (ft) and c is the phase speed of the Bragg wave (ft/s). For a λ_b= 0.056 ft, c has a value of 0.75 ft/s.

The radar sensor basically measures surface velocity for an area since it has a 12-degree beamwidth. The dimension of the area depends on the inclination angle and the distance between the water surface and sensor. From the velocity distribution of the defined area, the dominant one is reported (Sommer, 2014). The sensor can detect movement both towards and away from the sensor and the magnitude of shift in frequency depends on this direction. For better detection, the water body requires observable disturbances at the surface. These minimum disturbances are generally produced by wind, or rain (Costa et al., 2006).

Some general specifications of water level and surface velocity measurements by the stream radar are provided in Table 2.

Table 2: Specifications of water level and velocity measurement by RQ_30 (Sommer, 2014)

Property	**Water level measurement**	**Surface velocity measurement**
Measurement range	0-15 m	0.10-15 m/s
Resolution	1 mm	1 mm/s
Accuracy	± 2 mm; ± 0.025 %	± 0.01 m/s; ± 1 %
Radar Band	K-Band	K-Band
Radar frequency	26 GHz	24 GHz
Radar opening angle	10 °	12 °

3.2.3 Data Acquisition

The radar sensor allows option for serial and analog data output of the measured variables (Sommer, 2014). It uses interfaces (e.g., RS-485 and SDI-12) for serial data output and analog

outputs for analog data. Any selected option (e.g., the interfaces, or, analog outputs) is connected to a datalogger (e.g., HyQuest iRIS 350FX), which has a web configuration and data are transmitted at an adaptable interval via a local 3G cell network.

3.2.4 Data Quality

Along with water level and surface velocity, RQ_30 provides an additional measurement (e.g., Quality) that validates the radar observations at each time step. Following criteria are considered for data validity:

- Maximum Opposite Direction: The relation of velocity distributions between the analysis direction and opposite direction is defined as the opposite direction content. This parameter defines an upper limit for the opposite direction content and when the measurements go beyond that limit, the measurements are defined as invalid (Sommer, 2014). A negative sign is put in the "Quality" value when measurements are invalid due to this consideration.
- Signal to Noise Ratio: When the ripples on the surface are not detectable due to tidal influences, or back-water effect, the signal to noise ratio (SNR) becomes very low. Velocity measurements with a SNR < 30 are considered to be insufficient.
- Amplification: The strength of the returned radar signal can vary due to the condition of water surface, presence of waves and the distance between the surface and the receiver (Sommer, 2014). For any returned signal, the amplification of the radar sensor is automatically adjusted between 0 to 9. High amplification (e.g.,9) denotes weak radar signal and are considered as bad, whereas low amplification (e.g., 0) is considered optimal signal.

The radar observations that do not meet the above criteria are ignored for any type of analysis in this study.

3.3 CORRECTION FOR WIND DRIFT

3.3.1 Principle of Drift Computation

Since stream radar measures velocity at the surface of water, this measurement can be affected by wind. If the wind blows in the same direction as the radar measures velocity, it can create an additional drift to the actual measurement resulting in an overestimation of the variable; while if it blows in the opposite direction, velocity can be underestimated due to the resistance caused by the drift. Now, the stream radar uses microwave frequencies (24 GHz) and for a microwave measurement, the velocity is actually measured at a depth of $0.044\lambda_b$ rather than at the water surface (Plant et al., 2005); where λ_b is the wavelength of Bragg wave (Equation 4). On the other hand, the magnitude of the wind drift at the water surface is about 2% of the speed measured 10 m above the surface (Costa et al., 2006). If it is assumed that the effective depth of microwave measurement follows a logarithmic decay, the wind drift at the effective measurement depth can be estimated combining the work of Shemdin (1972) and Ha (1979) as below:

$$U_w(z) = U_w(0) - \frac{U_{*w}}{K} ln\left(\frac{z}{z_{0w}}\right) \quad \text{Equation (6)}$$

$$U_{*_w} = \sqrt{C_D \left(\frac{\rho_a}{\rho_w}\right)} * V \quad \text{Equation (7)}$$

where, $U_w(z)$ is the wind drift at elevation *z* ft below the surface (ft/s), $U_w(0)$ is the wind velocity at surface (ft/s), U_{*_w} is the friction (shear) velocity at the water surface (ft/s), *K* is the universal Von Karmann's constant (0.41), z_{0w} is the roughness height [3.28 x 10^{-4} ft, Chow et al. (1988)], C_D is the drag coefficient [1.3 x 10^{-3}, Ha (1979)], ρ_a and ρ_w are the densities of air and water in (lb/ft^3), respectively, and *V* is the wind speed (ft/s) measured at an anemometer height of 10 m.

3.3.2 Drift Computation for Study Streams

To compute the wind drift at the radar locations, wind speed data are collected from the "Local Climatological Data (LCD)" database of National Oceanic and Atmospheric Administration (NOAA) (NOAA, 2019), which typically measures wind speed at 10 m height from ground at the airports. It is assumed that wind pattern of each radar location should not be significantly different than its closest airport. Now, the 2%-wind drift at the water surface prevails only when wind blows in the same, or opposite direction of the streamflow and for other direction, the drift is negligible (Plant et al., 2005). The direction of wind is measured in degrees clockwise from north. Following this convention, the angle of flow direction is determined manually from the streamline (Flow Accumulation Raster, FAC) of each channel in ArcMap, which eventually determines the angle of the opposite direction too. To minimize the uncertainty in angle measurements, additional ±10 – 20 degrees are also added to the determined angle for each station leading to a range of angles for both directions. Then wind velocities corresponding to these specified angles are only used for wind drift computation. Table 3 provides the airport names and characteristics of wind speed data.

Table 3: Summary on wind speed data

Station	Airport Name	Data Resolution (minutes)	Data Period		Direction Angle (degree)	
			Start	End	Same	Opposite
Cherry Creek	Denver centennial airport, CO	60	Jul 2018	Aug 2019	320 - 340	140 - 160
Mill Creek	Ardmore municipal airport, OK	60	Mar 2017	Jun 2019	150 - 170	330 - 350
Walnut Gulch	Douglas bisbee international airport, AZ	60	Aug 2017	July 2019	260 – 280	80 – 100
Paria River	Page municipal airport, AZ	60	Jul 2018	Jul 2019	220 – 240	40 - 60
Falls Creek	Ardmore municipal airport, OK	60	Mar 2017	Jun 2019	310 – 330	130 – 150
Sessom Creek	San marcos municipal airport, TX	60	Nov 2017	Jun 2019	130 – 150	310 – 330
Austin North	Austin bergstrom international airport, TX	60	Jun 2018	May 2019	130 – 150	310 – 330
Austin South	Austin bergstrom international airport, TX	60	Jun 2018	May 2019	110 - 130	290 – 310

3.4 DISCHARGE COMPUTATION

From the conservation of mass theory, volumetric discharge is computed as below:

$$Q = \bar{v}A \qquad \text{Equation (8)}$$

where, Q is the discharge (ft^3/s), $\bar{v}$ is the mean channel velocity (ft/s) and A is the wetted cross-sectional area (ft^2).

Multiple field experiments show that the velocity distribution in the vertical in natural channels consists of a logarithmic form with depth from the bottom of the channel (Smart, 1999). Quick changes of velocity are mainly observed near the riverbed and banks, whereas the changes in the middle is quite slow that eventually forms eddies (Costa et al., 2006). From this behavior, it is generally assumed that the mean channel velocity of a channel can be found at 0.6 times depth below the water surface for relatively shallow channels, or, from the mean of the velocities found at 0.2 and 0.8 times depth below the surface for deep channels. For example, if a channel has a total water depth of 10 ft, then the mean velocity can be found at a depth of 6 ft below from the surface, or, from the average of the velocities at depths of 2 and 8 ft below from the surface. However, for the same channel, mean channel velocity for a natural channel can be obtained from the surface velocity by multiplying it by a constant (Rantz, 1982). Therefore, discharge from radar observations at any time step i is computed as below:

$$Q_i = kv_iA_i \qquad \text{Equation (9)}$$

where, Q_i is the discharge (ft^3/s), k is a constant, v_i is the surface velocity (ft/s) and A_i is the wetted cross-sectional area (ft^2).

3.4.1 Determination of k-value

The constant "k" is referred to as the ratio of mean channel velocity to surface velocity; alternatively known as velocity coefficient or velocity index. In general, it has a value less than

1.0 and the default one is taken as 0.85 (Rantz, 1982). Although multiple studies accept the validity of the default value for natural channels (Costa et al., 2000; Melcher et al., 2002; Costa et al., 2006; Hauet et al., 2008; Le Coz et al., 2012; Welber et al., 2016), from recent experiments it is found that the actual value of k depends on the roughness of the bed material, the place where the measurement is taken, and Reynolds number. Also, secondary currents, presence of vegetation, or tidal fluctuations can affect it (Johnson & Cowen, 2017). Considering different criteria, numerous k-values have been recommended so far such as, 0.85 and 0.93 for base flow and high flow condition, respectively (Harpold et al., 2006); 0.79 to 0.93 depending on the roughness condition of the channel bed (Polatel, 2006); 0.75 to 0.83 for high flow situations in mountain channels (Jodeau et al., 2008); 0.79 to 1.72 in compound or irregular channels (Sun et al., 2010); 0.72 to 0.79 for channel bed consisting of gravel (Dramais et al., 2011); 0.86 to 1.18 due to secondary currents (Gunawan et al., 2012); 0.82 to 0.93 for varying Reynolds number (Johnson & Cowen, 2016); and so on. However, this study does not involve any field experiments to obtain the appropriate k-value based on channel condition and considers the default value (0.85) for discharge computation.

3.4.2 Calculation of Wetted Cross-Sectional Area

Discharge estimates using the stage-velocity radar data assume that there is a stable cross-section. Changes to the bathymetry can have a negative impact on the discharge estimates. Therefore, at first, surveys are conducted to find a stable streambed for each site and then the cross-sections are established at the selected location of the channel. Cross-section of any channel is measured by the conventional surveying method. The vertical elevations along the line where the radar takes stage measurements are recorded by a total-station survey relative to the reference level (e.g., GZ if known, otherwise taken as the channel bottom). However, in case of Mill Creek, the

floodplain at its left bank dramatically extends away from the channel with a very flat slope. As a result, the total-station measurement is carried out up to the left bank (Figure 20-a). To solve the issue, a cross-section is developed from Digital Elevation Model (DEM) (USGS, 2020c) along the same line where the actual survey is done (Figure 20-b). The data points of the floodplain from the DEM-produced cross-section are separated at the elevation where the surveyed profile ends at the left bank and then merged with the surveyed datapoints to get the complete as shown in Figure (Figure 20-c) . The cross-section profiles for rest of the channels are provided in Figure 21.

Cross-section data (e.g., station and elevation) of a channel are further loaded into an online calculator (NWS, 2020) that gives the corresponding wetted area for any water depth. For each radar station, wetted areas corresponding to a range of water depths are determined, where the range varies from the minimum recorded stage value for that station to the maximum one with an increment of 0.1-0.2 ft. Finally, an equation is developed from the best fit of these data points and for any *i*th stage value, A_i is derived from the equation. However, only for Cherry Creek, stage-area rating curve is provided by USGS. Figure 22 shows the stage-area curves for each channel.

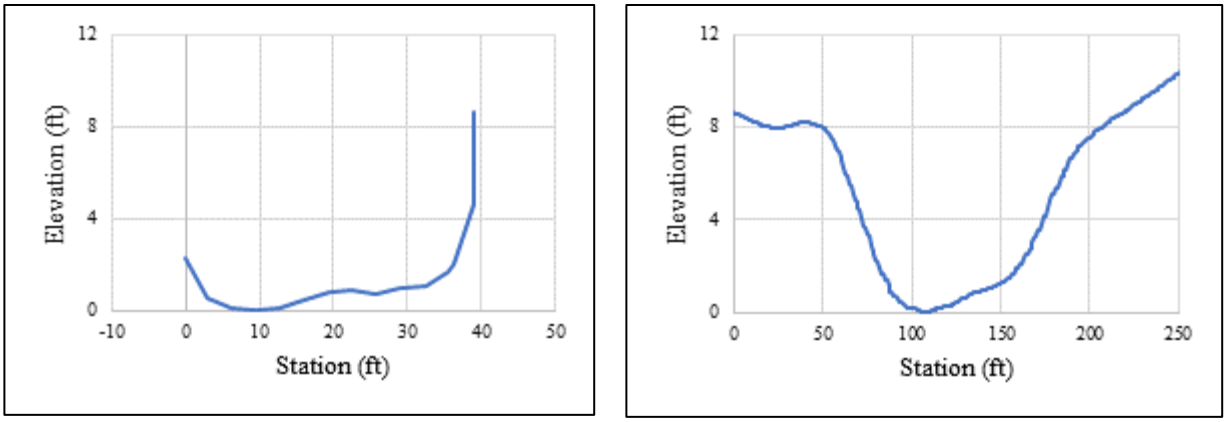

(a) (b)

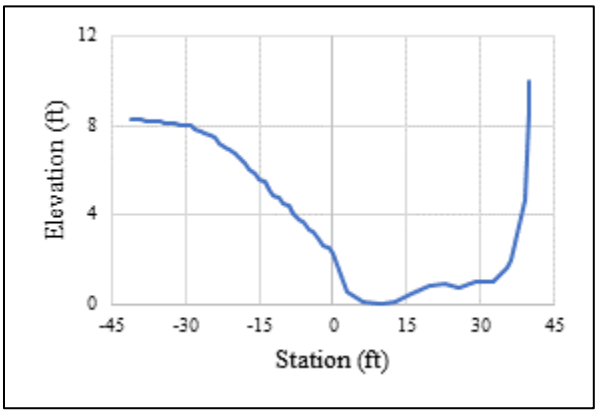

(c)

Figure 20: Cross-section profile at Mill Creek (a) from survey (b) from DEM (c) final

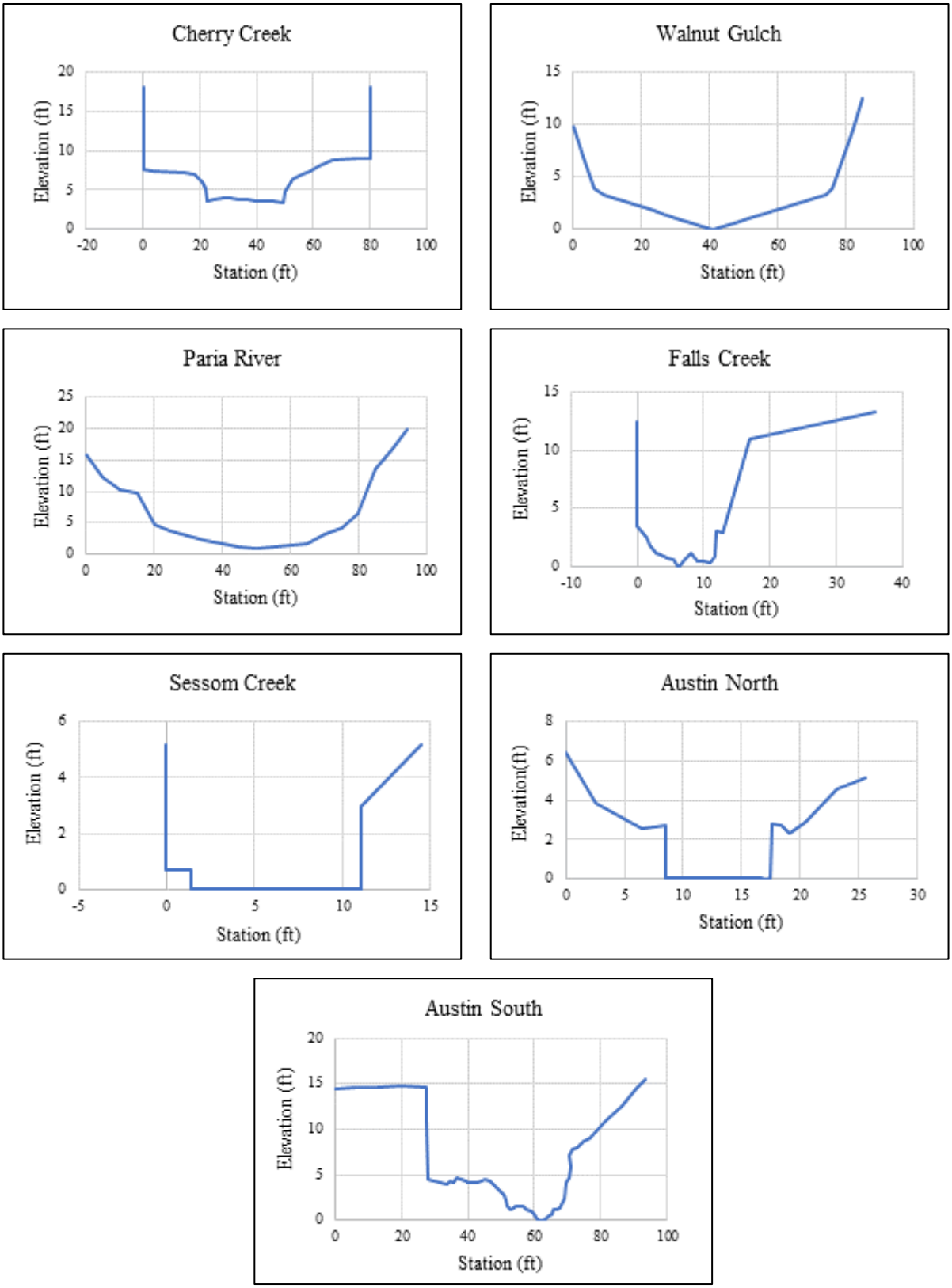

Figure 21: Cross-section profile for all the channels (except Mill Creek)

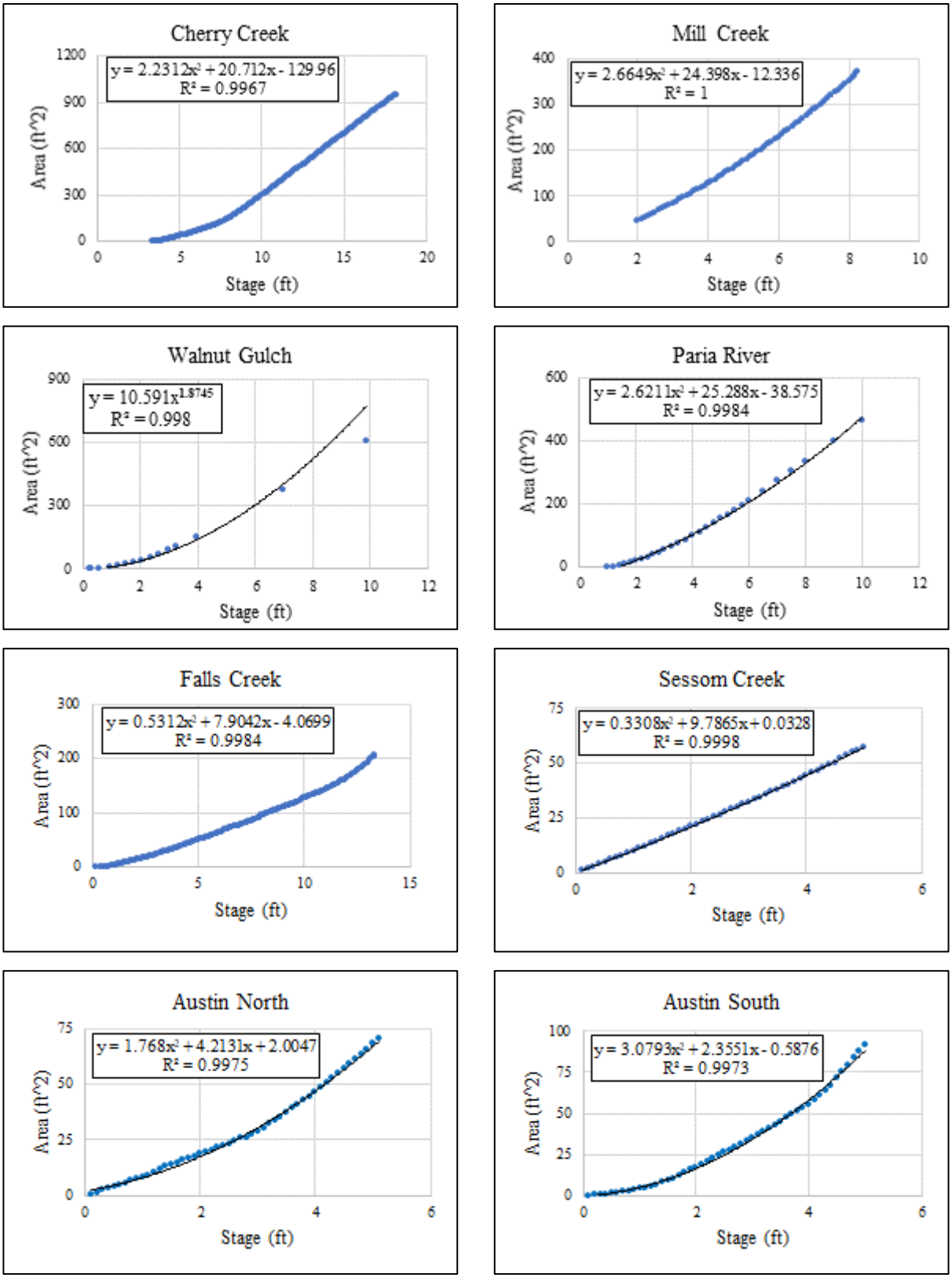

Figure 22: Stage-area curve for all the channels

3.5 STATISTICAL SCORES FOR COMPARISON

For both stage and discharge comparison, the following statistical measurements are considered:

i. Nash-Sutcliffe Efficiency (NSE): The residual variance of the radar observations is compared to the variance of the streamgage data by the NSE coefficient (Nash & Sutcliffe 1970). When the radar observations accurately match the streamgage data, NSE is equal to 1. NSE > 0 means that the stream radar data matches the streamgage observations better than the mean of the streamgage observations., while NSE < 0 indicates the radar data are worse than the mean value of the streamgage data. It is calculated as follows,

$$NSE = 1 - \frac{\sum_{i=1}^{n}(O_i - P_i)^2}{\sum_{i=1}^{n}(O_i - \bar{O})^2} \quad \text{Equation (10)}$$

where, O_i is the ith streamgage value, P_i is the ith stream radar value and $\bar{O}$ is the arithmetic average of the streamgage values. The streamgage data are collected from the respective websites of USGS (USGS, 2018) and USDA (USDA, 2019).

ii. Correlation Coefficient (CC): Correlation coefficient provides the measurement of how well the streamgage and radar stage data are related to each other. CC has a value between -1.0 to 1.0; where -1.0 means the variables are perfectly correlated but in a negative fashion, while 1.0 indicates there is a perfect positive correlation between them. CC = 0 mean no correlation between the variables. It is computed as below:

$$CC = \frac{n\sum_{i=1}^{n}(O_i P_i) - [\sum_{i=1}^{n}(O_i))(\sum_{i=1}^{n}(P_i)]}{\sqrt{[n\sum_{i=1}^{n} O_i^2 - (\sum_{i=1}^{n} O_i)^2] * [n\sum_{i=1}^{n} P_i^2 - (\sum_{i=1}^{n} P_i)^2]}} \quad \text{(Equation 11)}$$

where, O_i is the ith streamgage value, P_i is the ith stream radar value.

iii. Normalized Bias (NB): Normalized bias quantifies the radar measurements' performance in terms of total depth of water. It is estimated as,

$$NB = \frac{\sum_{i=1}^{n}(P_i - O_i)}{\sum_{i=1}^{n} O_i} \quad \text{(Equation 12)}$$

where, O_i is the *i*th streamgage value, P_i is the *i*th stream radar value.

iv. Root Mean Square Error (RMSE): Root mean square error accumulates the residuals (i.e., difference between streamgage and radar data) and determines the overall error between the two datasets. It is computed like below:

$$RMSE = \sqrt{\frac{\sum_{i=1}^{n}(O_i - P_i)^2}{n}} \quad \text{(Equation 13)}$$

where, O_i is the *i*th streamgage value, P_i is the *i*th stream radar value.

3.6 CONSTRUCTION OF FLOW DURATION CURVES

Flow duration curve for any channel is simply a plot of discharge that shows the percent of time any specific discharge is equaled or exceeded. To construct the flow duration curve, at first, the discharge values for the analyzed time periods are sorted in a descending order and then each value is assigned a rank like the maximum streamflow is ranked as 1. Then the exceedance probability (E) is computed as follows:

$$P = \left(\frac{M}{n+1}\right) * 100 \quad \text{Equation (14)}$$

where, *P* is the probability for a given flow to be equaled or exceeded (%), *M* is the rank of a discharge quantity, and n is the total number of discharge quantity.

Finally, the discharge values are plotted in the y-axis, while the probabilities are in the x-axis.

Chapter 4

RESULTS AND DISCUSSIONS

4.1 ARTIFACTS ANALYSIS

To get accurate discharge estimates by remote sensing, it is important to identify the artifacts and remove them if significant. The observations can be subjected to error due to the vertical movement of the stream radar in stage measurement, while due to disturbances at the water surface for velocity measurement. The vertical movement can be induced by expansion and contraction of the supporting structures (e.g., bridges or cables) due to variation in temperature, or by deflection of bridges due to vehicle load. In contrast, excessive interference at the water surface can be primarily produced by high turbulent flow conditions or wind drift. This study evaluates the effect of temperature and wind in remote sensing measurement by stream radars.

4.1.1 Temperature Effect

4.1.1.1 Observation of Temperature Effect

Bridge, culverts, and cables experience expansion and contraction throughout a day as they heat up and cool down due to temperature variation, which can cause the radar to move from its original position leading to an error in stage measurements. To evaluate this effect, stage data are selected for a period with stable water surface and two such “quiet periods” (QP) are chosen to confirm the consistency of the behavior throughout the whole timeseries. For each station, temperature data are collected from the same database as provided in Table 3. It is assumed that temperature behavior should not change drastically between each radar location and its closest airport. Finally, stage and temperature data are plotted as shown in Figure 23 - Figure 30.

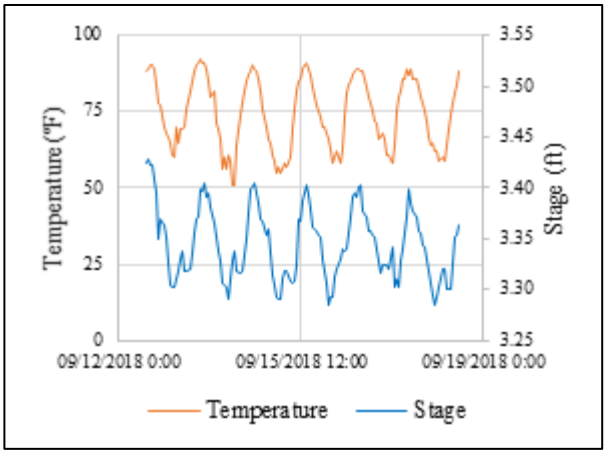

(a)

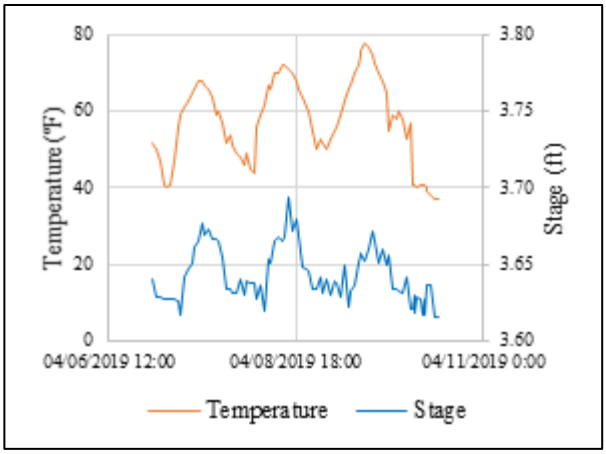

(b)

Figure 23: Stage vs temperature plot of Cherry creek for (a) QP1 (b) QP2

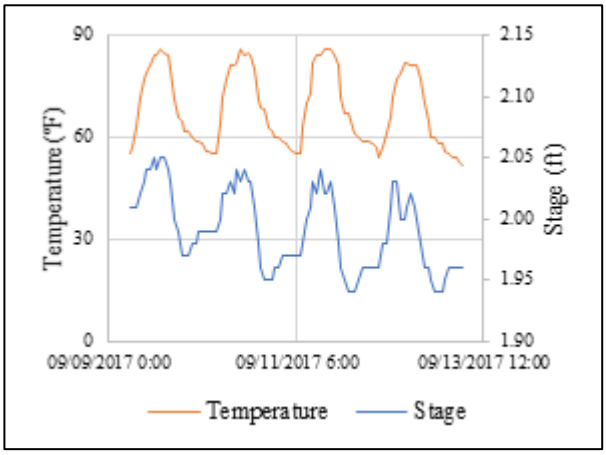

(a)

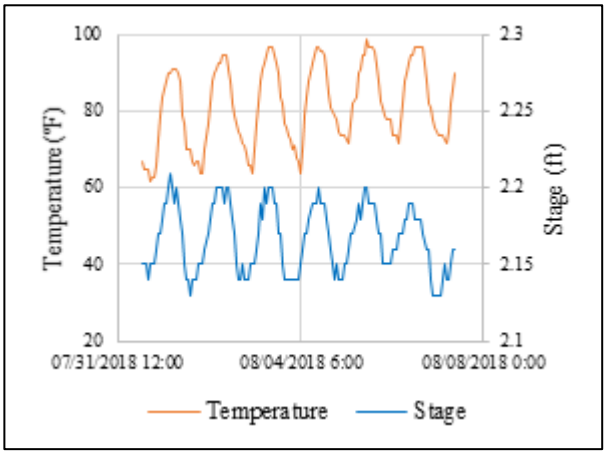

(b)

Figure 24: Stage vs temperature plot of Mill creek for (a) QP1 (b) QP2

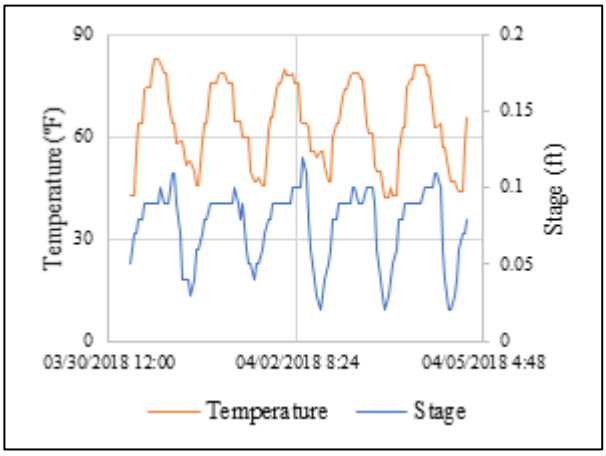

(a)

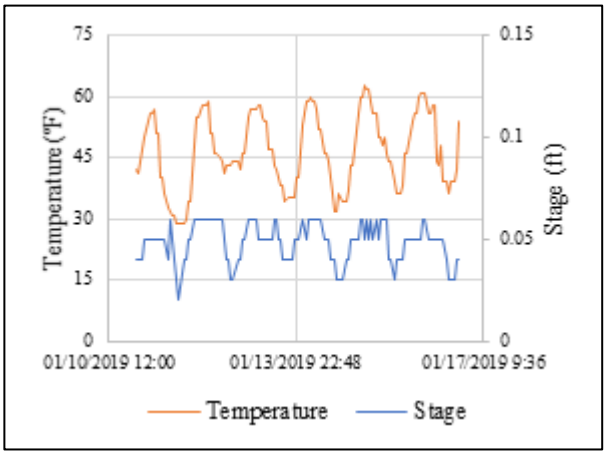

(b)

Figure 25: Stage vs temperature plot of Walnut Gulch for (a) QP1 (b) QP2

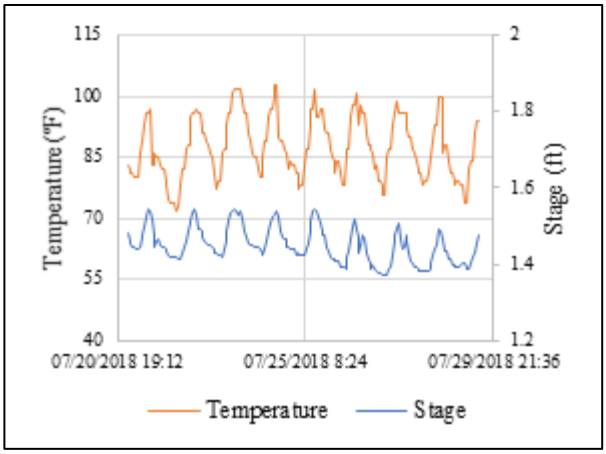

(a)

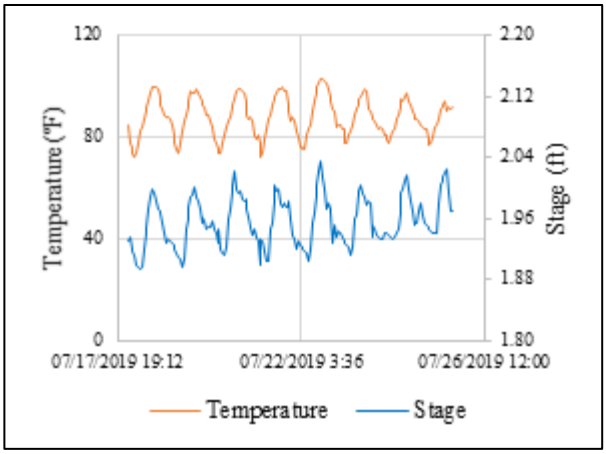

(b)

Figure 26: Stage vs temperature plot of Paria River for (a) QP1 (b) QP2

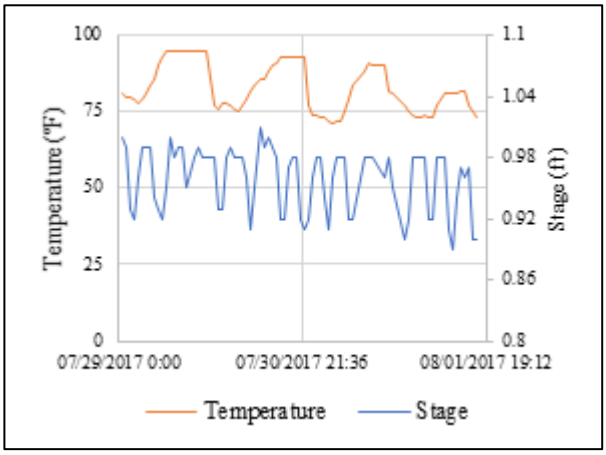

(a)

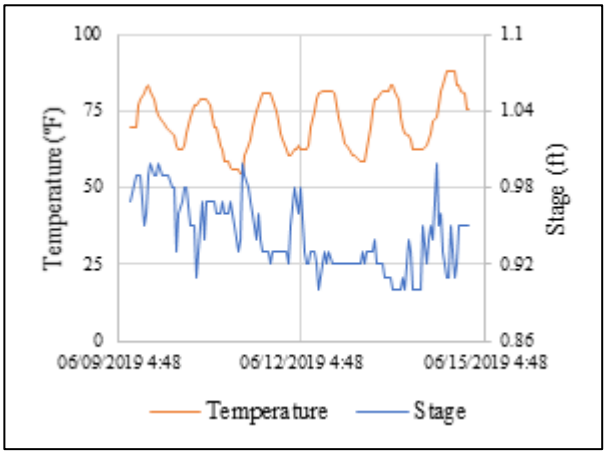

(b)

Figure 27: Stage vs temperature plot of Falls creek for (a) QP1 (b) QP2

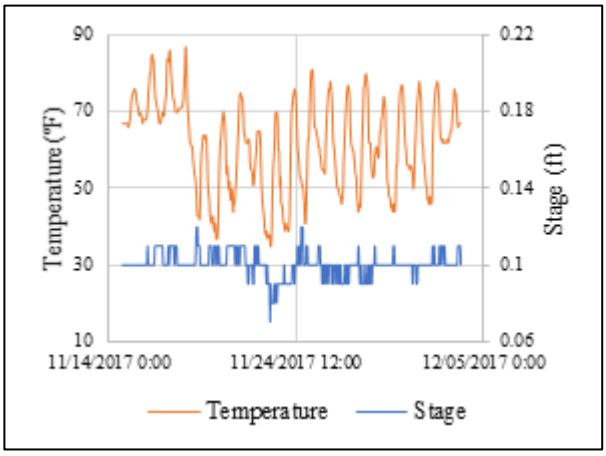

(a)

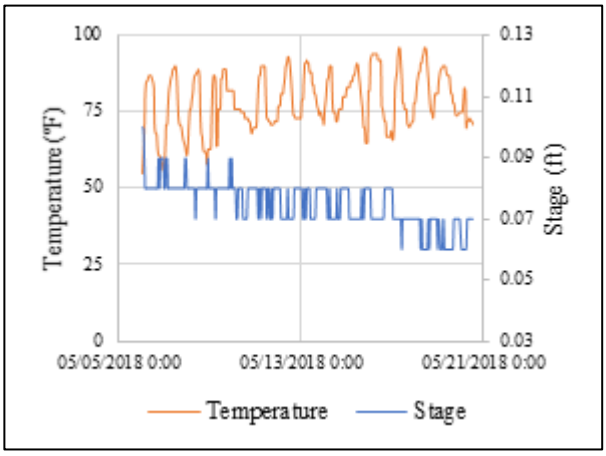

(b)

Figure 28: Stage vs temperature plot for Sessom Creek for (a) QP1 (b) QP2

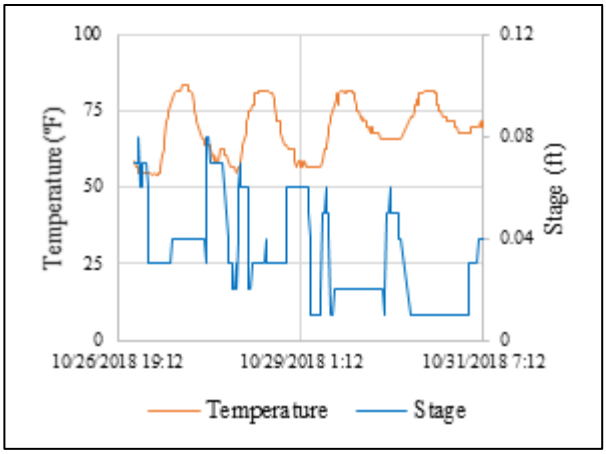

(a)

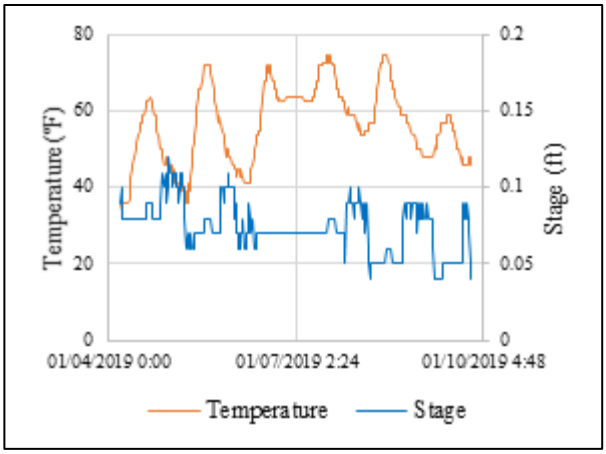

(b)

Figure 29: Stage vs temperature plot of Austin North for (a) QP1 (b) QP2

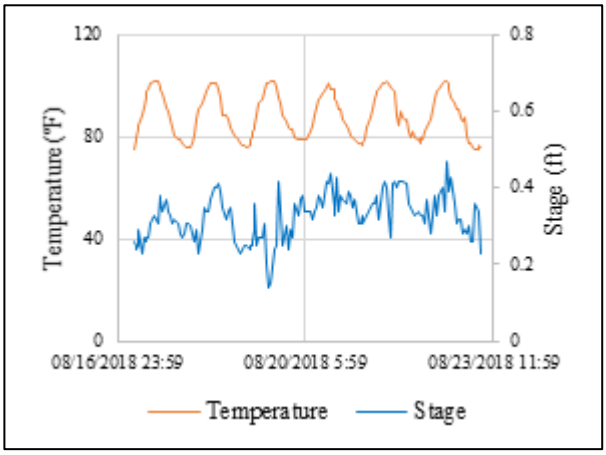

(a)

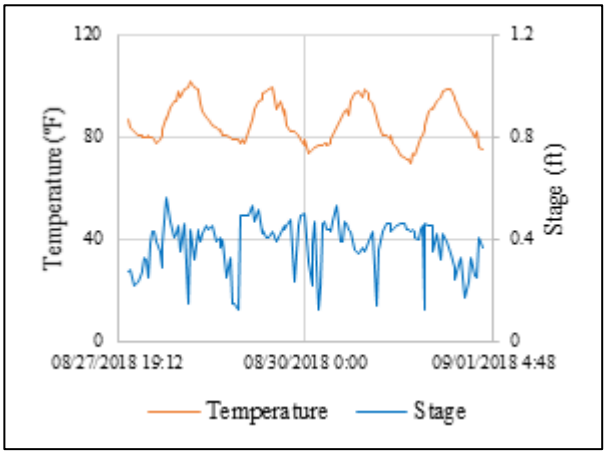

(b)

Figure 30: Stage vs temperature plot of Austin South for (a) QP1 (b) QP2

The graphs show that the stage records of Cherry Creek, Mill Creek, Walnut Gulch and Paria River are positively correlated with temperature. With the increase of temperature, both bridge (for Cherry Creek, Walnut Gulch and Paria River) and cables (for Mill Creek) expand that causes the radar to move down from its original position. Since the water surface remains steady (as assumed for a quiet period), the distance between the radar and water surface (h in Figure 19) decreases that results in an overestimation of stage. Therefore, when the temperature increases, the stage also increases. In contrast, when temperature decreases, a contraction occurs in the

supporting structures causing an increase in h by the upward movement of the radar. It eventually results in an underestimation of the water level and hence, the stage decreases with the decrease of temperature. .

In case of Falls creek, there is a water treatment plant nearby that pumps water from the creek at 6-hour intervals. The 6-hour period between two consecutive crests in Figure 27-a indicates that this discharge system may affect the steady state of the quiet periods. For Sessom Creek and Austin North, the radars are mounted on a culvert and with the increase of temperature, it expands as a whole that causes the radar to go up and hence, the stage decreases (Figure 28 and 29). Similarly, with a decrease in temperature, the whole culvert contracts and causes the stage to be increased by the descending of the radar. .On the other hand, radar at Austin South is mounted on a wooden train bridge that produces intense vibration due to frequent trains crossing the bridge. As a result, the stage records become very noisy for this station (Figure 30) and similarity with temperature cannot be readily observed.

Table 4 shows the correlation coefficient (CC) between stage and temperature timeseries of both quiet periods for all the stations. For Cherry Creek, Mill Creek, Walnut Gulch and Paria River, the CC varies between 0.526 to 0.804, which indicates a strong, positive correlation between stage and temperature data and confirms the temperature effect in stage measurements for these stations. Although Falls Creek has a cable mounted radar, QP1 has a positive CC (0.155), while QP2 shows a negative CC (-0.139) and they both are very weak. Therefore, it indicates the stage behavior at Falls Creek is random in the quiet periods, possibly, due to the pumping system. As for Sessom Creek and Austin North, they both show negative correlations since the radars are mounted on culverts here. However, very low CC values for both QPs (-0.129 to -0.441) indicate the temperature effect is not strong in the stage measurements for these channels. On the other hand,

due to the vibration, the stage records at Austin South have poor correlation with the temperature (CC = 0.023 and 0.330) in both quiet periods.

Table 4: Coefficient of correlation between stage and temperature for the selected data periods

Station	Data Period of QP1		CC	Data Period of QP2		CC
	Start	End		Start	End	
Cherry Creek	Sep 9 2018	Sep 18 2018	0.563	Apr 7 2019	Apr 10 2019	0.729
Mill Creek	Sep 9 2017	Sep 13 2017	0.772	Jul 31 2018	Aug 8 2018	0.526
Walnut Gulch	Mar 30 2018	Apr 10 2018	0.742	Jan 10 2019	Jan 18 2019	0.639
Paria River	Jul 20 2018	Jul 30 2018	0.779	Jul 17 2019	Jul 26 2019	0.804
Falls Creek	Jul 22 2017	Aug 2 2017	0.155	Jun 9 2019	Jun 18 2019	-0.139
Sessom Creek	Oct 12 2017	Dec 6 2017	-0.258	May 5 2018	May 21 2018	-0.441
Austin North	Oct 23 2018	Nov 2 2018	-0.475	Jan 2 2019	Jan 12 2019	-0.129
Austin South	Aug 15 2018	Aug 23 2018	0.330	Aug 27 2018	Sep 5 2018	0.023

4.1.1.2 Error Quantification due to Temperature Effect

To correct stage measurement for temperature effect, it is important to quantify the error and compare with the measured stage record to evaluate if significant or not. The stage – temperature curves show the hourly variation of the variables throughout a day. To quantify the error, it is assumed that the first stage value of each rising and receding part is the initial water level before temperature starts to increase and decrease ($W_{0,rise}$ and $W_{0,recede}$), respectively. Similarly, the initial temperatures $T_{0,rise}$ and $T_{0,recede}$ are defined. For each rising part of both stage and temperature curves, $W_{0,rise}$ and $T_{0,rise}$ are subtracted from *i*th stage and temperature value to get the overestimation respective to the hourly temperature increase. In contrast, for each receding part, *i*th stage and temperature value are subtracted from $W_{0,recede}$ and $T_{0,recede}$ to get the underestimation

respective to the hourly temperature decrease. Then the difference of stage (ΔW) and temperature (ΔT) of all the rising and receding parts are plotted together in separate plots for each station as shown in Figure 31 – Figure 34.

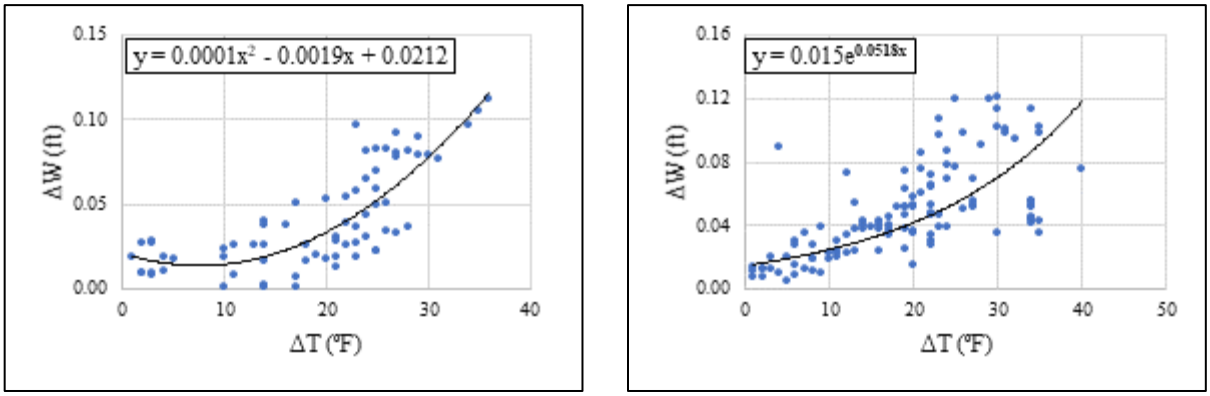

(a) (b)

Figure 31: Error in stage measurement at Cherry creek (a) overestimation (b) underestimation

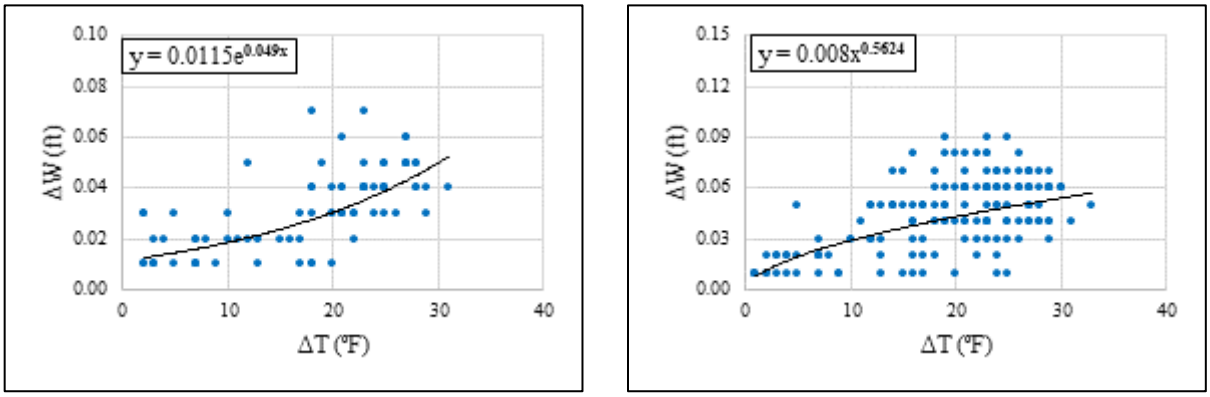

(a) (b)

Figure 32: Error in stage measurement at Mill creek (a) overestimation (b) underestimation

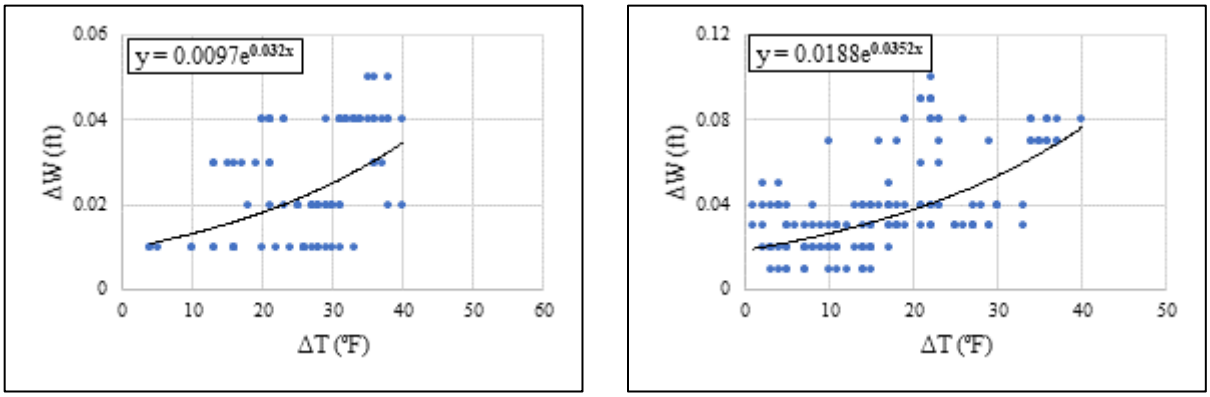

(a) (b)

Figure 33: Error in stage measurement at Walnut Gulch (a) overestimation (b) underestimation

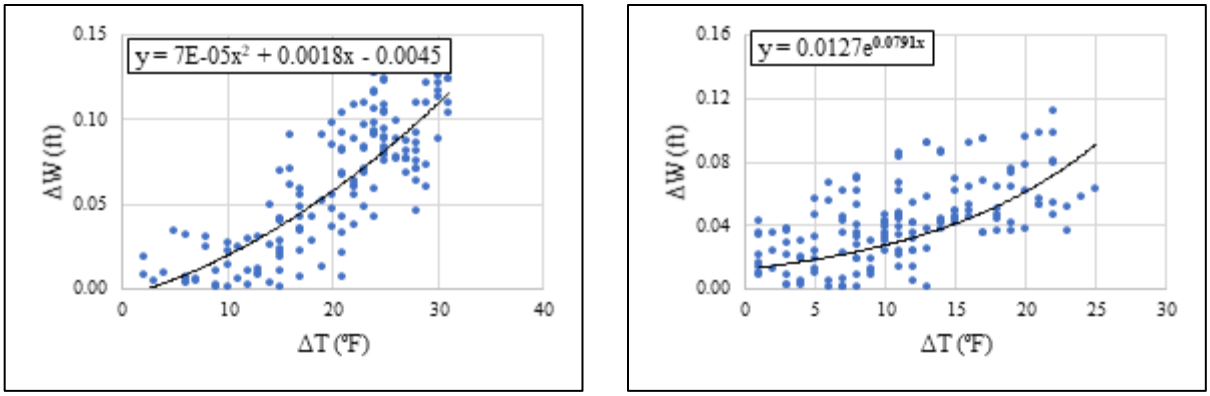

Figure 34: Error in stage measurement at Paria River (a) overestimation (b) underestimation

The graphs show that the error in stage measurement follows the same trend during both heating, or cooling phase (underestimation or overestimation) for a specific station. The amount of error has a proportional relation with the difference in temperature as can be observed form the fitted equations. Therefore, for a single day, the maximum overestimation or underestimation of stage (ΔW_{max}) occurs when the temperature reaches its maximum or minimum (ΔT_{max}). The higher the ΔT_{max}, the higher the ΔW_{max}.

The objective of this analysis is to determine if the daily temperature variation produces significant error in stage measurements. To get the highest ΔW_{max} of the two datasets (e.g., QP1 and QP2 in Figure 23 – Figure 30) for any station, it is important to determine the highest ΔT_{max} value as ΔT_{max} can vary on each day. On the other hand, to get the maximum error that occurs, on average, each day of these datasets, the average of ΔT_{max} and ΔW_{max} are computed as shown in Table 5. Finally, to evaluate the significance of these maximum errors (ΔW_{max}), the overall magnitudes of stage measurement considering both event and base-flow conditions for the concerned four stations are provided in Table 6.

Table 5: Maximum daily error for stage measurement due to temperature in the quiet periods

Station	$\Delta T_{max, most}$ (°F)		$\Delta W_{max, most}$ (ft)		$\Delta T_{max, avg}$ (°F)		$\Delta W_{max, avg}$ (ft)	
	Heating	Cooling	Heating	Cooling	Heating	Cooling	Heating	Cooling
Cherry Creek	38	36	0.112	0.120	30.45	27.55	0.056	0.062
Mill Creek	33	33	0.070	0.090	28.63	29.13	0.047	0.053
Walnut Gulch	30	28	0.020	0.080	25.4	24.67	0.022	0.045
Paria River	28	27	0.128	0.122	24.0	23.29	0.079	0.080

Table 6: Maximum, modal, average, and minimum stage value of the affected stations

Station	Recorded Stage (ft)			
	Maximum	Modal	Average	Minimum
Cherry Creek	8.54	4.47	4.47	4.01
Mill Creek	7.60	2.67	3.37	2.01
Walnut Gulch	3.36	0.04	0.12	0.01
Paria River	8.14	2.39	2.38	1.30

Table 5 shows that the highest stage-errors for both quiet periods vary between 0.025 – 0.107 ft, where the greatest of them occurs to Paria River. Although it is possible that there may be larger stage-error for days that have larger temperature swings than the days in the quiet periods, this study assumes that the maximum diurnal temperature difference (e.g., ΔT_{max}) should not be abnormally higher than the ones provided in Table 5 and hence, the highest stage-errors (ΔW_{max}) should be similar too. Based on this, the maximum errors for the quiet periods are compared to the typical stage records of these four stations that are provided in Table 6. Now, Table 6 indicates except Walnut Gulch, for rest of the stations these values are very negligible since the highest error (0.107 ft) is still less than 10% in magnitude from the minimum recorded stage (1.30 ft) of the

respective station (Paria River). Therefore, they should not have any significant impact in wetted perimeter, or area calculation of a channel. However, caution should be followed for Walnut Gulch since the highest or average ΔW_{max} is greater than the modal, or minimum stage value. Therefore, anything less than the $\Delta W_{max,\ most}$ for this site (0.08 ft) should be ignored. On the other hand, since the $\Delta T_{max,\ avg}$ values conform to the average diurnal temperature variation range of 20 - 30 ºF (Means, 2019), the $\Delta W_{max,\ avg}$ values in Table 5 show that the average daily-maximum-error for any station is always less than 1 inch throughout the whole year. Therefore, the error in stage measurements due to temperature can be ignored.

4.1.2 Wind Effect

Adjusting radar observations for wind drift requires a timeseries of wind speed with uniform temporal resolution similar to radar observations and a constant direction angle (e.g., exact or opposite to streamflow direction). Since wind data (Table 3) are not available in the required format, the objective of this analysis is to observe if wind produces significant drift in the channel locations instead correcting for each timestep. Therefore, this study computes the highest wind drift for each channel, which occurs when the wind speed (V) is maximum in Equation 6 and 7 Again, for an overall assessment it is important to evaluate the drift for normal weather conditionsthat can be represented by the modal and average wind speed data (Table 7). On the other hand, heavy rainfall typically occurs with strong wind (Johansson & Chen, 2003; Back & Bretherton, 2005; Swarno et al., 2020). This concept is utilized to compare the maximum drift with the event velocities (maximum velocity). Another evaluation criterion is to observe the minimum surface velocity that should have a magnitude of 0.49 ft/s (0.15 m/s) or greater to be reliable (i.e., surface-water scatters are well-defined and wind drift is not dominant) (Fulton et al., 2020). Hence, to evaluate the significance of the wind drifts, the maximum and minimum recorded surface

velocity by stream radar for the data time period provided in Table 3 are also determined for each station (Table 8). To keep consistency with the wind drift computations, the modal and average surface velocities are also presented in Table 8.

Table 7: Wind drift at channel locations for all the station

Station	Direction	Wind Speed (ft/s)			Wind Drift (ft/s)		
		Maximum	Modal	Average	Maximum	Modal	Average
Cherry Creek	Same	47.26	10.13	13.22	0.28	0.06	0.08
	Opposite	57.39	10.13	16.05	0.34	0.06	0.09
Mill Creek	Same	57.39	11.81	16.67	0.34	0.07	0.10
	Opposite	50.63	15.19	19.63	0.30	0.09	0.12
Walnut Gulch	Same	55.70	8.44	15.08	0.33	0.05	0.09
	Opposite	54.01	15.19	20.90	0.32	0.09	0.13
Paria River	Same	28.69	8.44	10.58	0.17	0.05	0.06
	Opposite	35.44	5.06	10.73	0.21	0.03	0.06
Falls Creek	Same	38.82	5.06	9.18	0.23	0.03	0.06
	Opposite	69.20	5.06	17.29	0.41	0.03	0.10
Sessom Creek	Same	48.95	5.06	12.50	0.29	0.03	0.07
	Opposite	37.13	5.06	12.55	0.22	0.03	0.08
Austin North	Same	38.82	5.06	13.70	0.23	0.03	0.08
	Opposite	35.44	5.06	11.21	0.21	0.03	0.07
Austin South	Same	33.76	5.06	9.80	0.20	0.03	0.06
	Opposite	30.38	5.06	11.29	0.18	0.03	0.07

Table 8: Maximum, modal, average, and minimum recorded surface velocity for each station

Station	Measured Surface Velocity (ft/s)			
	Maximum	Modal	Average	Minimum
Cherry Creek	10.91	1.92	2.10	1.04
Mill Creek	3.82	0.75	1.44	0.71
Walnut Gulch	19.47	0.96	2.63	0.96
Paria River	19.95	18.82	1.85	0.71
Falls Creek	10.44	1.13	1.50	0.49
Sessom Creek	9.39	1.58	3.16	0.79
Austin North	24.02	9.06	10.0	7.12
Austin South	3.77	0.57	1.28	0.36

From Table 7, the highest wind drift among all the stations is found as 0.41 ft/s for Falls Creek when wind blows in the opposite direction to the streamflow. For rest of the stations, the maximum wind drift varies between 0.17 – 0.34 ft/s. These drifts are quite insignificant in comparison to the event surface velocities (Table 8). Although in case of Mill Creek and Austin South, the maximum measured surface velocities are low, their corresponding drifts are still less than 10%, which is not significant. On the other hand, the modal and average drifts vary between 0.06 - 0.13 ft/s, which are also quite insignificant comparing with that of the surface velocities. However, caution should be needed in case of Austin South as the minimum measured-surface velocity is less than the threshold of reliable surface velocity (0.49 ft/s). Therefore, since wind does not blow along a direction constantly and when it does, the magnitude of drift is insignificant, wind effect in surface velocity measurement are neglected in this study.

4.2 STAGE COMPARISON

For the collocated stations (e.g., Mill Creek, Walnut Gulch and Paria River), stage data are compared to that of the streamgage data. As for Cherry Creek, USGS has no "approved" gage height (stage) data for the analyzed period (Table 1) and stage comparison is not made for this station. The input data preparations and the result of comparison are provided below.

4.2.1 Datum Correction

The streamgage stage data (gage height) are generally expressed as the distance of water surface from a defined datum, or reference level (USGS, 2019). So, gage height is an integration of distances of datum to channel bottom and channel bottom to the water surface. To compare the radar stage data to the gage height for any station, it is imperative that the stream radar data also has the same datum as its reference level (GZ in Figure 19). But, except for Cherry Creek, the information on datum of any USGS streamgage is not available. Therefore, for stage comparison, a datum correction is applied to the water level data of Mill Creek, Walnut Gulch and Paria River.

Since the GZs of these three stations are set as their channel bottoms while taking measurements, the radar stage data represent the actual water depth in these channels. Since radars at each station are installed in a dry period, and after installation, there is no vertical shifting of the radar, the first radar observation represents the true base flow condition of a channel and subtracting them from the corresponding gage height data gives the distance between the existing datum and channel bottom. Finally, this distance is added to the existing radar data and compared to the gage height data. Table 9 shows the details on datum corrections.

Table 9: Details of datum correction for the collocated stations

Station	Streamgage Datum	Radar Reference Level	Datum Correction (ft)
Mill Creek	978.08 feet above NAVD88	Channel bottom	4.00
Walnut Gulch	Channel bottom	Channel bottom	0.00
Paria River	3,123.68 feet above NGVD29	Channel bottom	3.40

4.2.2 Results of Comparison

The overall statistical performances of stage comparison are provided in Table 10, while Figure 35 – 37 show the plots of stage comparisons during rainfall events for all the stations.

Table 10: Statistical scores of stage comparison for the collocated stations

Station	NSE	CC	NB (%)	RMSE (ft)
Mill Creek	0.959	0.981	0.390	0.083
Walnut Gulch	0.982	0.992	-6.33	0.074
Paria River	0.176	0.718	5.679	0.430

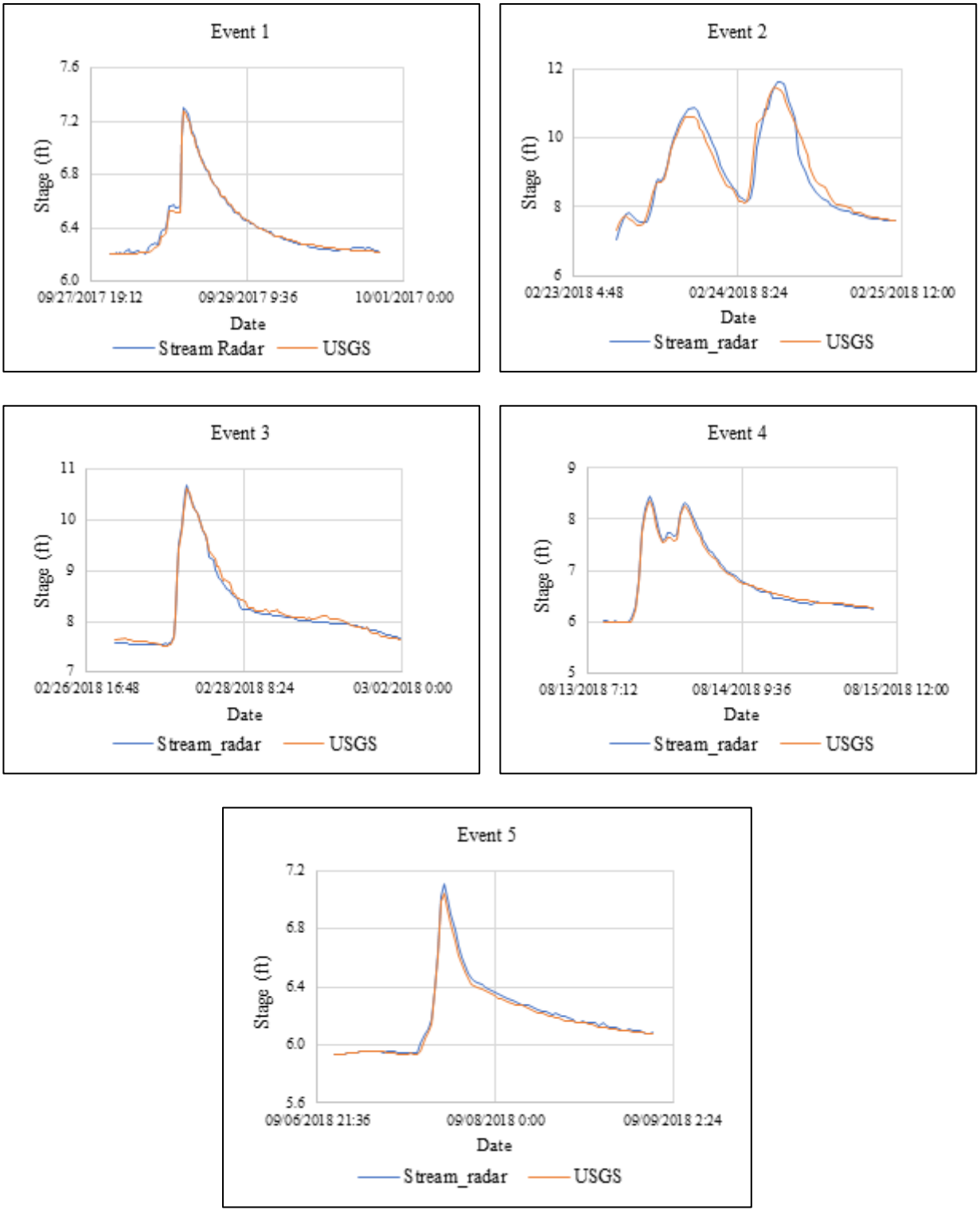

Figure 35: Stage comparison during rainfall events for Mill Creek

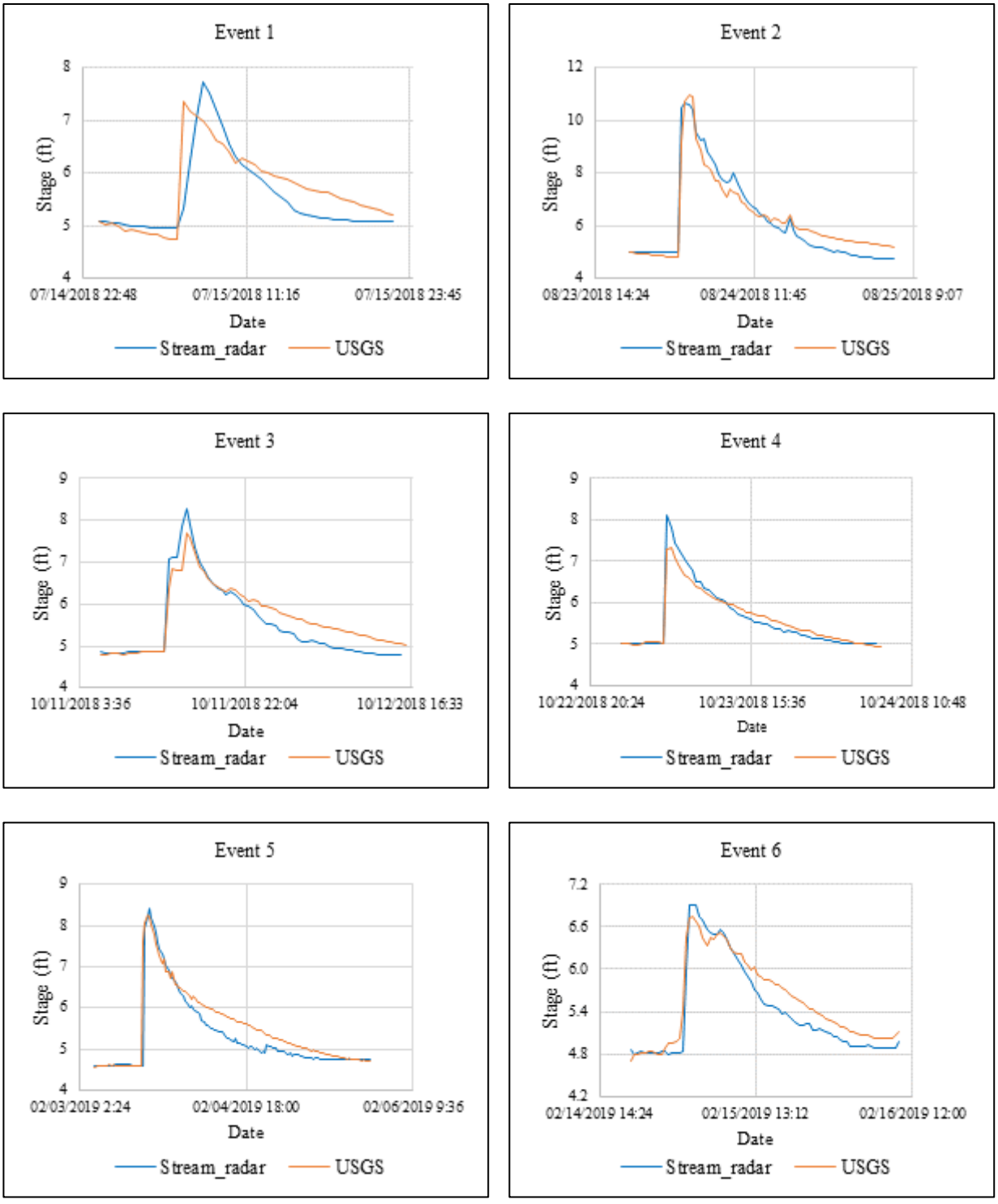

Figure 36: Stage comparison during rainfall events for Paria River

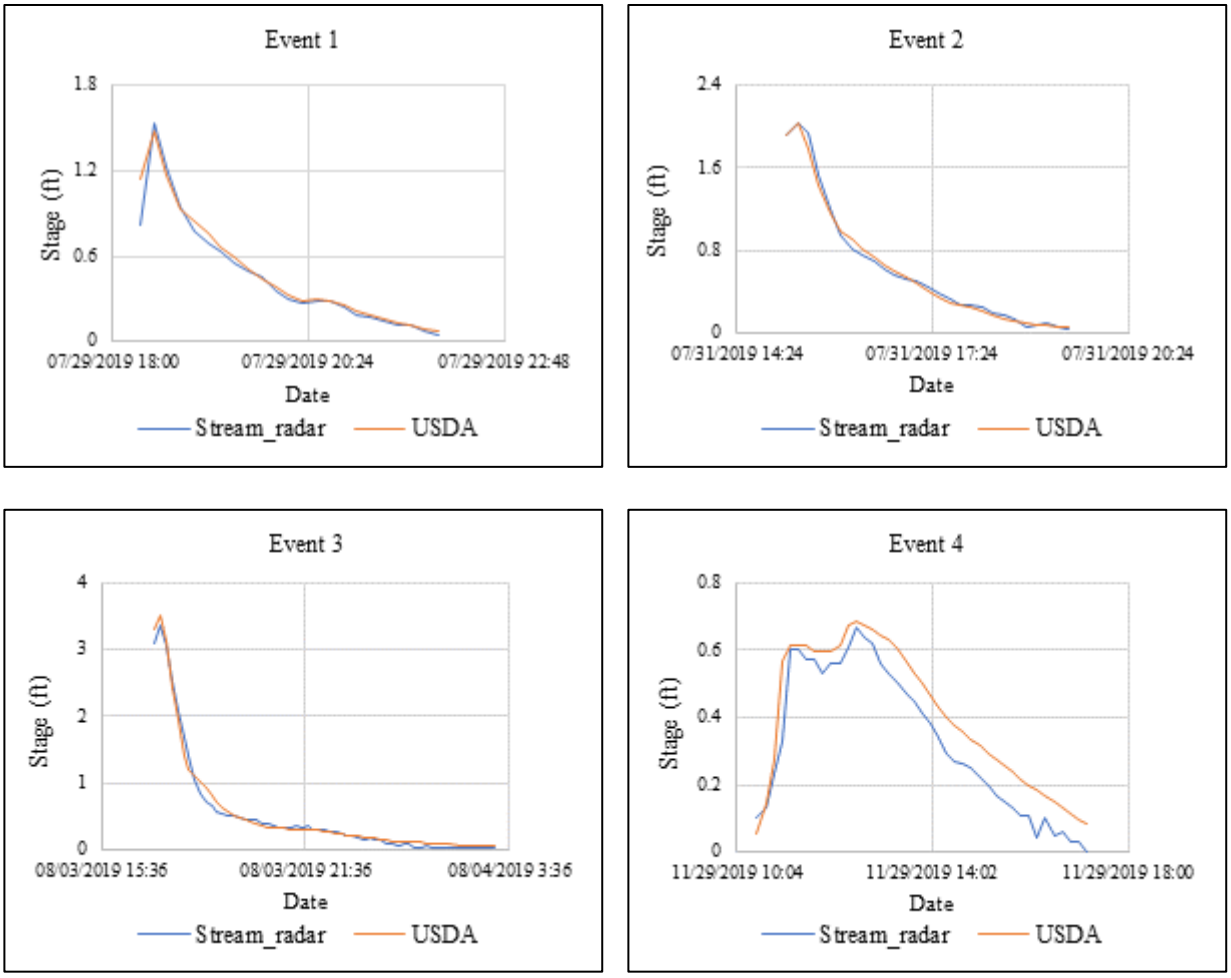

Figure 37: Stage Comparison during rainfall events for Walnut Gulch

Table 10 shows that the water level measurements at Mill Creek and Walnut Gulch are quite good. For both stations, NSE and CC scores are close to 1.0 that indicate that the stage observations at these stations are almost as accurate as the streamgage data and perfectly correlated. As shown by RMSE, the radar measurements at these stations, overall, vary by less than 1 inch from the streamgage data. The event graphs (Figure 35 and 37) also show that the measurements in the rainfall events also quite similar at these stations. The radar observations at Mill Creek are not significantly biased (e.g., NB ~ 0.4%), but for Walnut Gulch, the measurements are negatively biased by about 6% that indicates that stream radar slightly underestimates water level at this site.

This underestimation can be mostly observed in Figure 37 – Event 4 where the radar observations consistently tend to underestimate by 0.05 – 0.1 ft in the receding phase.

On the other hand, for Paria River, the statistical scores are not as good as for Mill Creek and Walnut Gulch. It has a relatively low NSE score of 0.176, whereas the CC score does not depict the best correlation either. The radar tends to overestimate than USGS measurements as indicated by the NB score and overall, it has a difference of about 5 inches (RMSE = 0.43 ft) with streamgage data. The event graphs (Figure 36) also show that the stream radar records higher stage values especially the peak depths than the USGS, although they both have the similar trend in water level. As previously mentioned, the stream radar at Paria River cannot be collocated since the USGS streamgage is about 1.2 kilometers upstream from it. It is possible that within this distance the river has some morphological changes such as variation in channel width, or bed. Also, this long distance provides slight offset in the timing of hydrograph that significantly affects the NSE and CC scores. Therefore, comparing with streamgage data should not be a good choice to decide on radar measurement accuracy for Paria River.

4.3 DISCHARGE COMPARISON

For all the collocated stations, the estimated discharge data are compared to that of the streamgage data. The discharge computation and discussion on result of each station are discussed below.

4.3.1 Results of Comparison

Like stage comparison the radar discharge estimates are also compared to streamgage discharge data statistically for whole timeseries and graphically for the rainfall events only. Table 11 provides the results of overall statistical analysis of the discharge comparison, while Figure 38 - 41 represent the hydrographs of the respective stations.

Table 11: Statistical scores of stage comparison for the collocated stations

Station	NSE	CC	NB (%)	RMSE (ft^3/s)
Cherry Creek	0.925	0.972	13.556	9.717
Mill Creek	0.948	0.975	1.84	41.078
Walnut Gulch	0.989	0.996	-2.279	32.724
Paria River	0.776	0.905	45.54	51.819

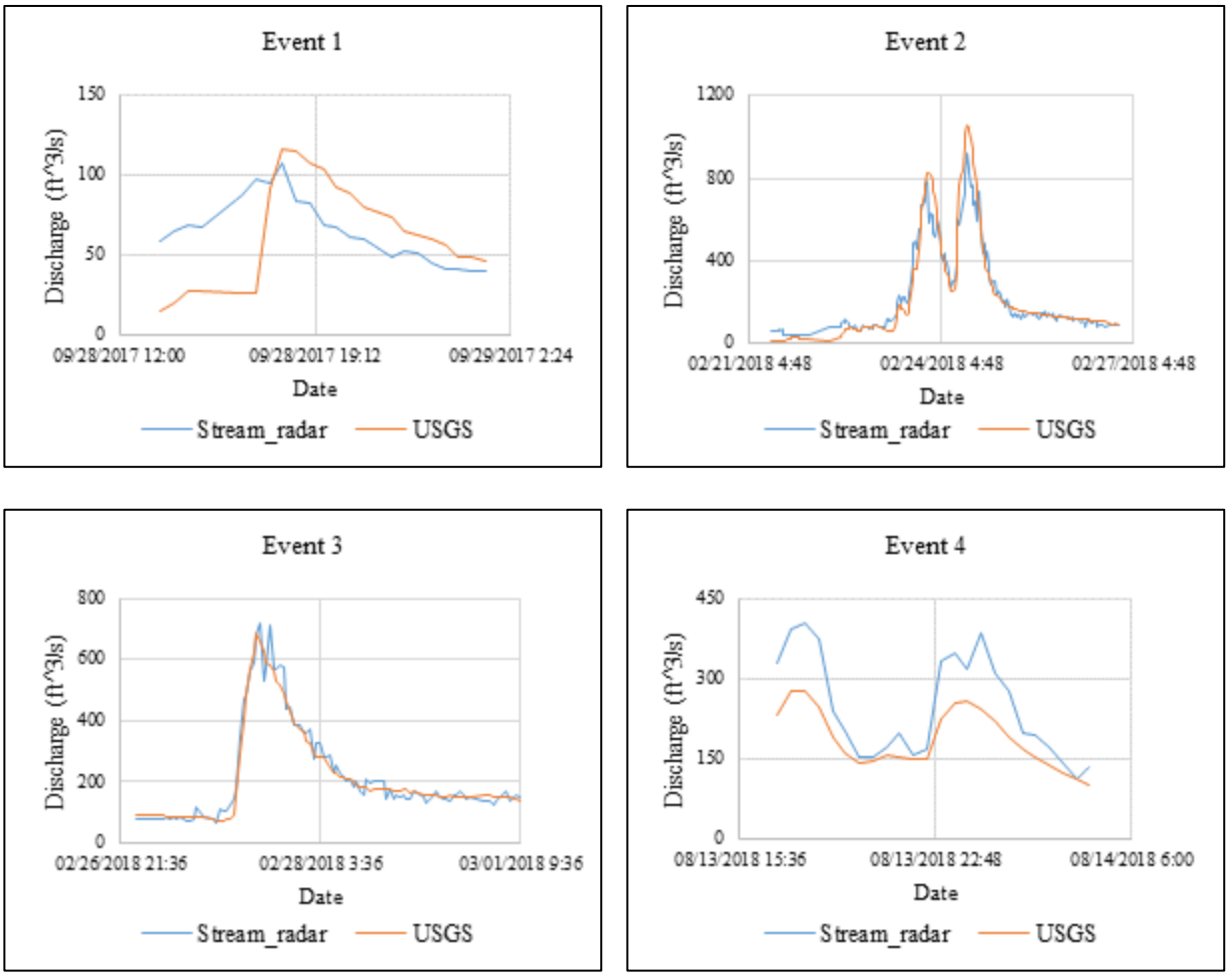

Figure 38: Discharge comparison during rainfall events for Mill Creek

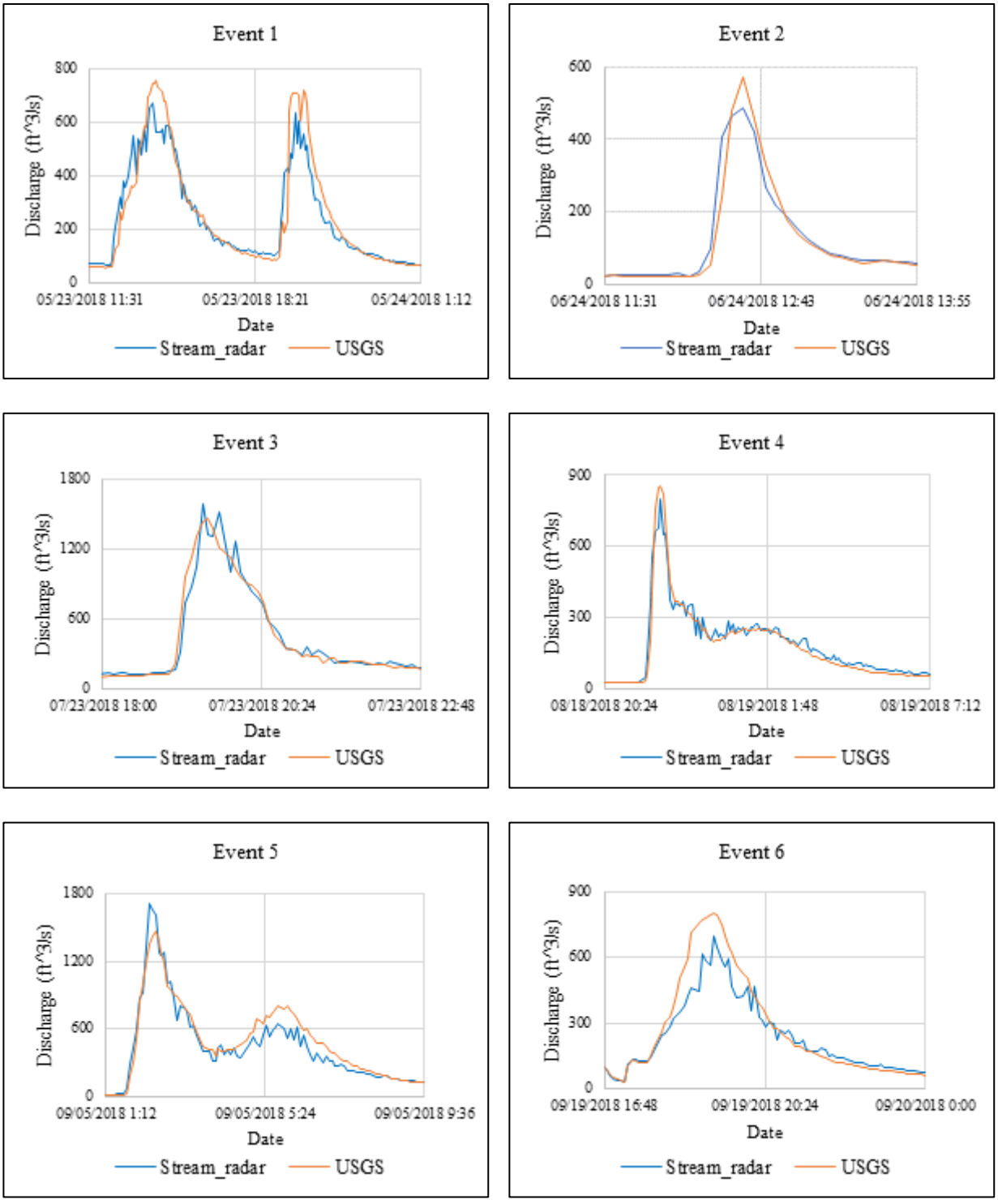

Figure 39: Discharge comparison during rainfall events for Cherry Creek

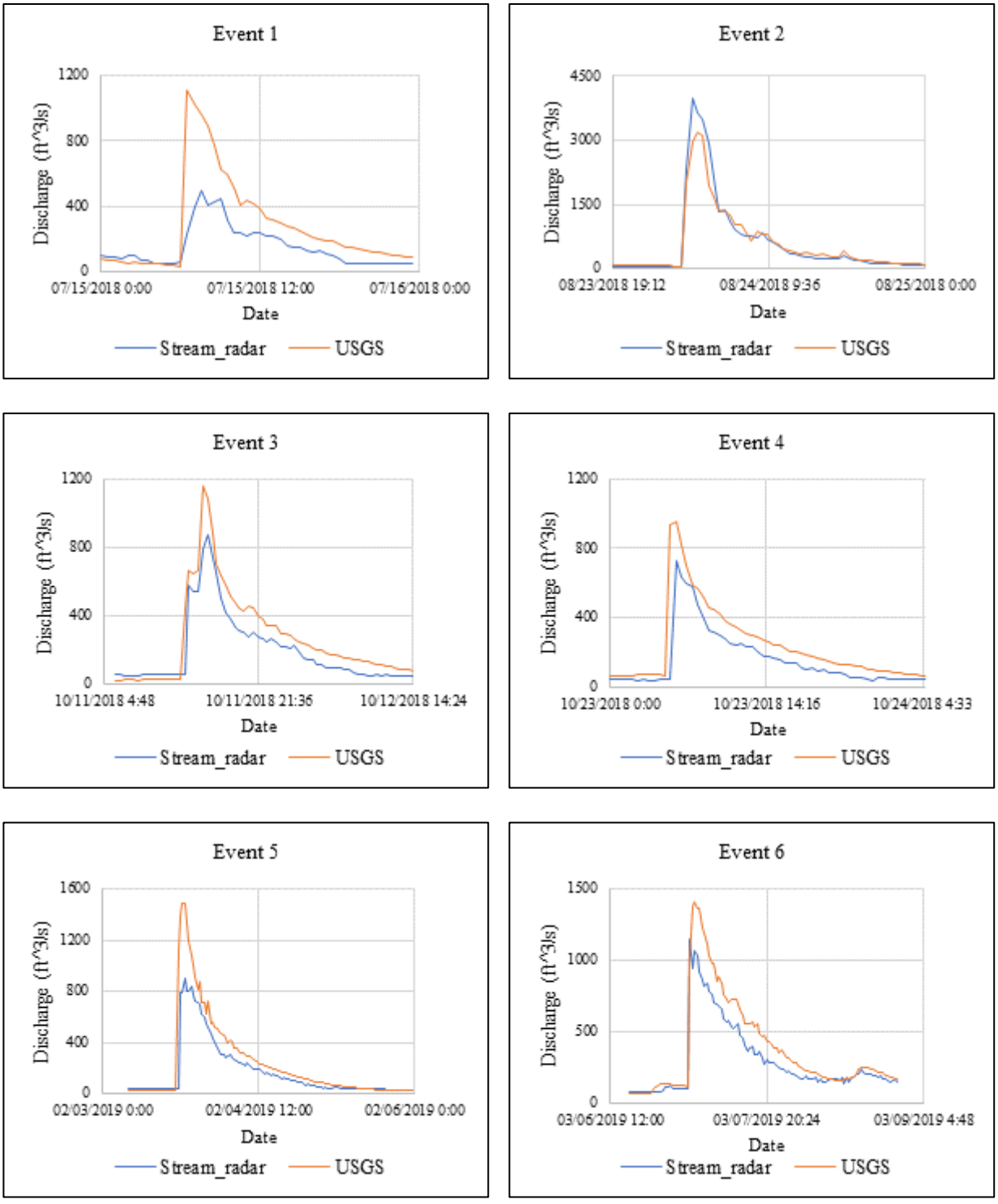

Figure 40: Discharge comparison during rainfall events for Paria River

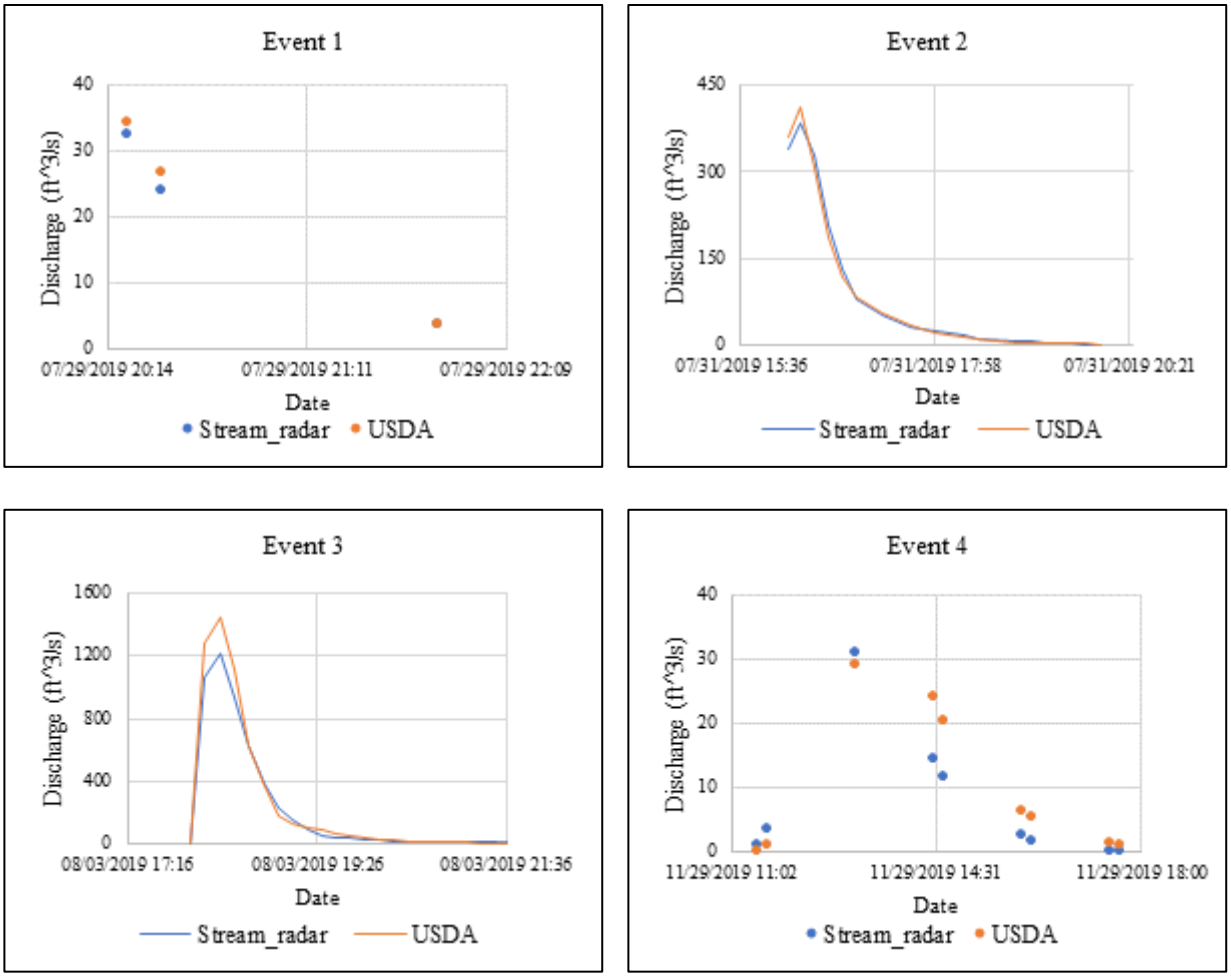

Figure 41: Discharge comparison during rainfall events for Walnut Gulch

Table 11 shows that the radar observations of all the collocated stations are quite accurate in providing the discharge estimates when compared to their respective streamgage data. Except Paria River, all the station has NSE and CC values close to 1.0, which is a good indicator of their accurate measurements and perfect correlation to that of the streamgages. In case of Paria River, although both the data are well correlated, NSE score denotes a lower inaccuracy with respect to USGS data. As indicated by the bias scores, overall, the discharge estimates at Walnut Gulch are lower than the streamgage data, whereas for rest of the stations the estimates are higher.

On the other hand, the hydrographs primarily show two types of anomalies: i) error in event-peak value, and ii) error in the total volume under a hydrograph. For example, in case of Mill Creek (Figure 38), peak-value error can be observed for events 2 and 3, whereas events 1 and 4 show the volumetric error. For Cherry Creek (Figure 39), Event 6 shows volumetric error and all the other events represent the peak-value error. On the other hand, almost all the events of Paria River (Figure 40) show peak-value error, and volumetric error while receding. As for Walnut Gulch (Figure 41), some events (Event 1 and 4) have discrete timeseries due to discontinuity in discharge records by USDA. Therefore, only errors in event-point value can be considered for these events. The events that have continuous data entries (e.g., event 2 and 3) indicate peak-value error.

4.3.2 Sensitivity Analysis for k-value

Since k-value is only assumed for discharge computation in this study, it is possible to reduce the hydrograph errors (volumetric and peak-value) by optimizing it. A higher k-value will yield higher discharge estimates that can reduce the errors when the radar-driven estimates are lower than the streamgage value, but it can produce high bias for the base flows that will eventually affect the overall accuracy, and vice versa. Therefore, it is important to simultaneously quantify the hydrograph errors, and check the overall accuracy of the discharge estimates due to the different k-values. To do so, the following multi-objective function is developed:

$$\Psi = \frac{1}{3} NSE + \frac{1}{3}\left(1 - \frac{VE}{100}\right) + \frac{1}{3}\left(1 - \frac{PE}{100}\right) \quad \text{(Equation 15)}$$

where, Ψ is a dimensionless quantity that should vary between 0 to 1, *NSE* is the Nash-Sutcliffe Efficiency for whole timeseries, *VE* is the average volumetric error of an event (%) and *PE* is the average error in peak-value of an event (%).

NSE demonstrates how well a plot of observed (streamgage) and simulated (radar) data fits the 1:1 line (Equation 9) and is the best objective function for this type of fit (Sevat & Dezetter, 1991; Legates & McCabe, 1999). It is also recommended by ASCE (1993) and chosen to represent the overall accuracy level of the measurements in this study. On the other hand, the average volumetric and peak-value error are computed as below:

$$VE = \frac{1}{n}\left(\sum_{i=1}^{n} abs\left(\frac{(V_{P,i} - V_{O,i})}{V_{O,i}}\right)\right) \quad \text{Equation (16)}$$

where, $V_{P,i}$ is the volume of *i*th event under the hydrograph of radar discharge data (ft^3), $V_{O,i}$ is the volume of *i*th event under the hydrograph of streamgage discharge data (ft^3), *n* is the total number of events, and *abs* operator implies the absolute value of the variables within the bracket.

$$PE = \frac{1}{n}\left(\sum_{i=1}^{n} abs\left(\frac{(P_{P,i} - P_{O,i})}{P_{O,i}}\right)\right) \quad \text{Equation (17)}$$

where, $P_{P,i}$ is the peak value of *i*th event for radar discharge data (ft^3/s), $P_{O,i}$ is the peak value of *i*th event for streamgage discharge data (ft^3/s).

Since VE and PE are calculated as average, it is important to have a greater number of event-hydrographs. The more the number of hydrographs, the better the optimization of the function. The appropriate k-value should provide the lowest volumetric and peak-value error, at the same time the highest NSE value. Therefore, the objective function in Equation 15 is optimized, when the Ψ value is maximum.

4.3.2.1 Consideration on k-value

The previous studies show that k-value can vary roughly from 0.7 to 1.0, even greater than 1.0, based on the channel and flow conditions (section 3.4.1). On the other hand, some studies recommend using two k-values for a specific channel depending on its base flow and high flow

condition (Harpold et al., 2006; Hauet et al., 2018). The event hydrographs show that except Walnut Gulch, all the other stations individually have both types of hydrograph errors (i.e., underestimating or overestimating). It means if a single k-value is used, then increasing the k-value from 0.85 will improve the condition only for the underestimating events; while the events that are already overestimating, the error will be more due to the multiplicative nature of the k-value, and vice versa. It strengthens the idea of using two k-values for these stations too. Therefore, this study computes the multi-objective function for both "single k-value" and "double k-value" for these four stations and determines the k-value(s) that produces the maximum Ψ. The following methods are considered during computation:

- For single-k optimization, k-value is varied from 0.7 to 1.0 with an increment of 0.001 and the corresponding Ψ is computed
- For double-k optimization, based on the work of Hauet et al. (2018), the threshold for water depth limit is varied from 6.0 to 7.0 ft in case of Cherry Creek, Mill Creek and Paria River since they are natural channels. Under each threshold of depth, lower k-value (for depth lower than the threshold) is varied from 0.75 to 0.85, while higher k-value (for depth higher than the threshold) is varied from 0.9 to 1.0. The increments for depth threshold and k-value are 0.01 ft and 0.001, respectively.
- Since Walnut Gulch has an artificial concrete channel, following the work of Hauet et al. (2018) k-value is varied from 0.85 to 1.0 with an increment of 0.001 for single-k optimization. On the other hand, this study utilizes the double k-value concept for Walnut Gulch too assuming the bed roughness decreases as the water level increases. Considering the lower event stage values, depth limit is varied from 3 – 3.5 ft, while the range for lower and higher k-values are kept same as for the other channels.

A code is developed in python to run the trials, which is provided in the Appendix – A.

4.3.2.2 Multi-objective Function Optimization

Table 12 shows the k-values that maximize the multi-objective function for each collocated station. Except Paria River the results are improved for all the stations due to k-value optimization. For single-k optimization, it varies from 0.78 – 0.91 while for double-k, it varies from 0.746 – 0.963. In general, the highest Ψ values are obtained for double-k optimization, although the relative differences between the results for two different k-values are very low. In case of Paria River, a k-value of 1.0 optimizes the multi-objective function eliminating the need for double-k optimization.

Table 12: Results on multi-objective function optimization for all station

Station	**Number of hydrographs**	**k-value**	**Ψ**	**NSE**	**VE (%)**	**PE (%)**
Cherry Creek	26	0.85 (default)	0.883	0.925	13.221	14.291
		0.780	0.912	0.939	9.566	10.879
		0.893 for stage > 6.2 ft and 0.746 for stage ≤ 6.2 ft	0.923	0.949	7.561	10.426
Mill Creek	4	0.85 (default)	0.878	0.938	9.630	20.732
		0.828	0.884	0.936	8.107	20.196
		0.963 for stage > 6.2 ft and 0.810 for stage ≤ 6.2 ft	0.906	0.965	7.517	17.165
Walnut Gulch	4	0.85 (default)	0.943	0.976	5.784	9.043
		0.911	0.954	0.989	6.200	6.578
		1.00 for stage > 3 ft and 0.848 for stage ≤ 3 ft	0.979	0.998	0.704	5.399
Paria River	7	0.85 (default)	0.743	0.776	27.909	26.947
		1.00	0.780	0.734	20.230	19.135

In case of Cherry Creek, the optimized single k-value is found to be less (0.78) than the default one and it reduced the VE and PE error by almost 4 % with an increase in NSE score. On the other hand, for double-k optimization, the threshold of depth limit differs by about 0.4 ft than the recommended value (2 m or 6.56 ft) by Hauet et al., (2018). For the k-values, the higher one (0.893) is very close to their recommended value of 0.9, whereas the lower one (0.746) slightly deviates from 0.8 (recommended). However, the VE error is almost halved and PE is also reduced by 4%. Since the total number of events is 26 for Cherry Creek (the event hydrographs are provided in Appendix – B), this is significant improvement in hydrograph errors and therefore, these k-values can represent the whole timeseries well.

As for Mill Creek, the single k-value (0.828) is slightly lower than 0.85 and the NSE, VE and PE scores do not change that much from the results found with default-k. However, the double k-value provides higher NSE score as well as lower VE and PE scores. The threshold of depth limit (6.2 ft) also varies for Mill creek from 6.56 ft. The lower k-value is very close to 0.8, while the higher k-value is 0.963 which is higher than 0.9. However, it is still less than 1.0 and multiple studies confirm that k-value can be higher than 0.9 (Harpold et al., 2006; Polatel, 2006; Johnson and Cowen, 2016); so, this is acceptable.

For Walnut gulch, the optimized single-k value (0.911) is similar to the recommended value (0.9) by Hauet et al., (2018). However, the hydrograph errors do not change that much from the default k-derived errors. On other hand, for double-k optimization, the k-value is quite similar (0.848) to the default one when depth is less than 3.00 ft, and for greater depth the optimized k-value is found as 1.00. With the use of these two k-values, VE becomes less than 1%, PE is almost halved and NSE gets close to 1.0 (0.979). Now with the increase of water level, channel bed

roughness should have less effect on mean channel velocity and therefore, k-value as 1.00 for depth above 3 ft is physical.

Although the USGS streamgage is located 1.2 km upstream of Paria River, the discharge should be similar. However, despite using the maximum k-value (1.0), the NSE score is still low (0.780) and the VE, and PE remain high (20.23 and 19.14, respectively). As previously mentioned, the 1.2 km-distance from the USGS creates a time lag in the hydrographs (Figure 40), that eventually hurts all these parameters. On the other hand, from field observation it is found that the radar is installed on the downstream side of the bridge and a series of upstream bridge piers as shown in Figure 42 creates obstacles in flow direction. As a result, the surface velocity is exhausted where the stream radar takes measurement that eventually lead to low discharge estimates as can be observed for the all the events (except Event 2) in Figure 40.

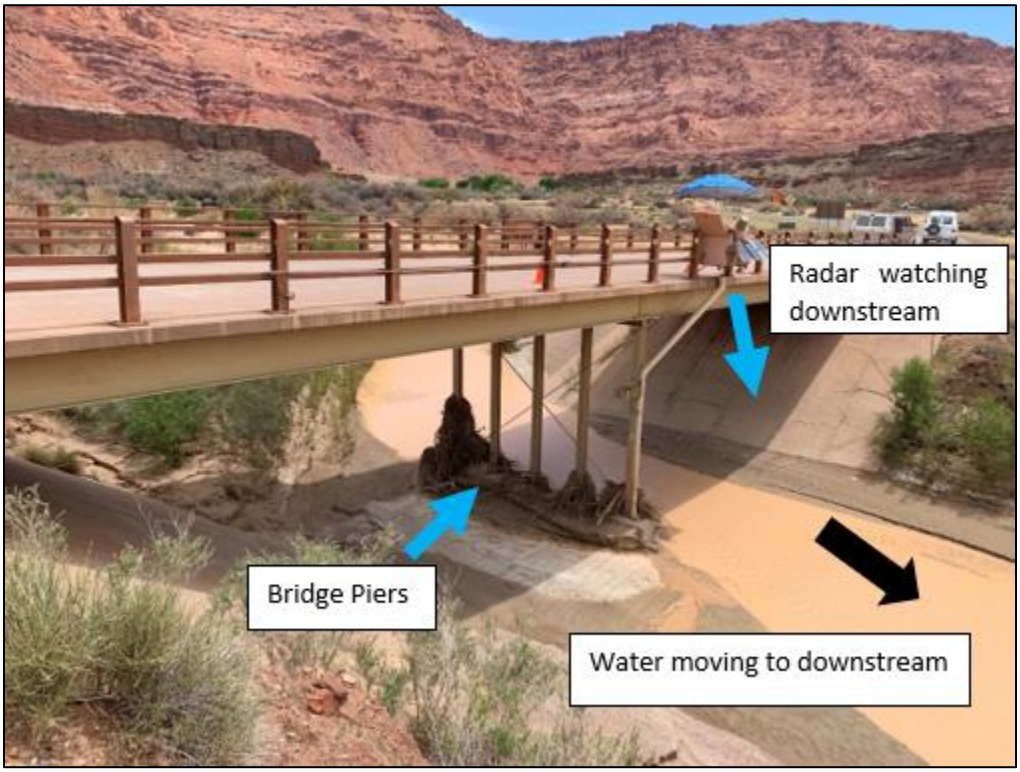

Figure 42: External complication in surface velocity measurements at Paria River

4.3.3 Equation for k-value

4.3.3.1 Assumption and Principle

This study develops an equation for k-value as a function of stage. It assumes streamgage data as the true discharge estimates and wetted area obtained from radar stage data are the true cross-sectional area for each channel. Therefore, the required (true) mean channel velocity for stream radar can be derived by dividing the streamgage discharge data with the radar wetted area. The idea is if this required mean velocity can be predicted well from the measured stage data, k-value can be well-predicted too from the stage data since it is the ratio of required mean velocity and radar surface velocity.

For this analysis, a sufficiently large sample size of observed data, especially for rainfall events, should be available so that it represents the year-round behavior of a channel. As mentioned before, Cherry Creek has a good number of events (26), whereas for both Mill Creek and Walnut Gulch, the number is only 4. On the other hand, the streamflow data for Paria River are not reliable due to the long inter-distance and external complication (bridge piers). Therefore, this study only develops equation of k-value for Cherry Creek. The required mean channel velocities are computed using Equation 17 and then plotted against the corresponding radar stage data as shown in Figure 43.

$$V_{req,i} = \frac{Q_{o,i}}{A_i} \qquad \text{Equation (18)}$$

where, $V_{req,i}$ is the *i*th required mean channel velocity, $Q_{o,i}$ is the *i*th observed streamgage discharge value and A_i is the *i*th cross-sectional area obtained using RQ_30 stage data.

The density plot in Figure 43 shows that there is a hotspot between the required mean velocity and measured stage values, and the required velocity can be well-predicted from the stage

observations as indicated by the high coefficient of determination (R^2 = 0.89). It means k-value can be predicted well from stage data. However, the data points corresponding to stage value 7 ft or more do not tend to increase with higher stage values. This can be attributed to the change in cross-section as water moves to the floodplain from the main channel at the same elevation (~ 7.1 ft) (Figure 21-a). It can be confirmed qualitatively by using Manning's velocity formula (Equation 1), since it addresses the wetted perimeter (hydraulic radius) and area in the computation.

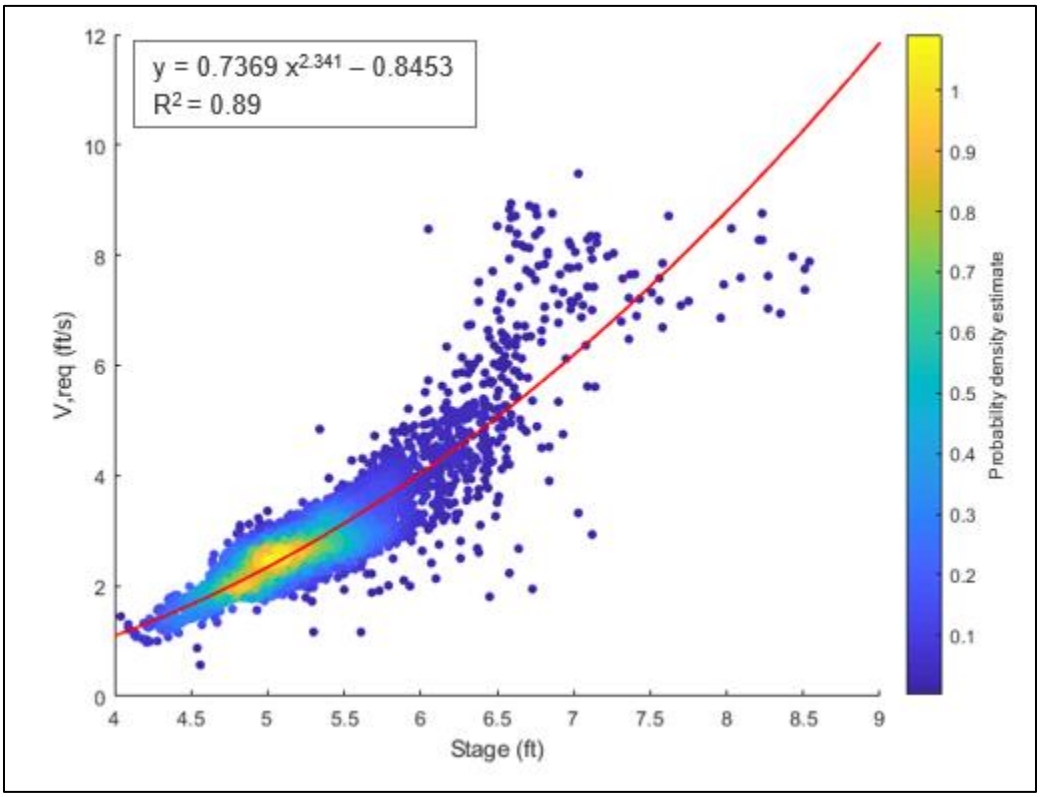

Figure 43: Density plot for required mean velocity vs stage at Cherry Creek

For a specific channel, Manning's roughness coefficient and friction slope remain constant. The velocity becomes a function of wetted area and hydraulic radius (Equation 1). The same online calculator that is previously used for computing wetted area provides the hydraulic radius for the same range of water depth. Assuming reasonable roughness coefficient and friction slope for the

channel, the mean channel velocities are obtained. These velocities are then plotted against the input water depth as shown in Figure 44.

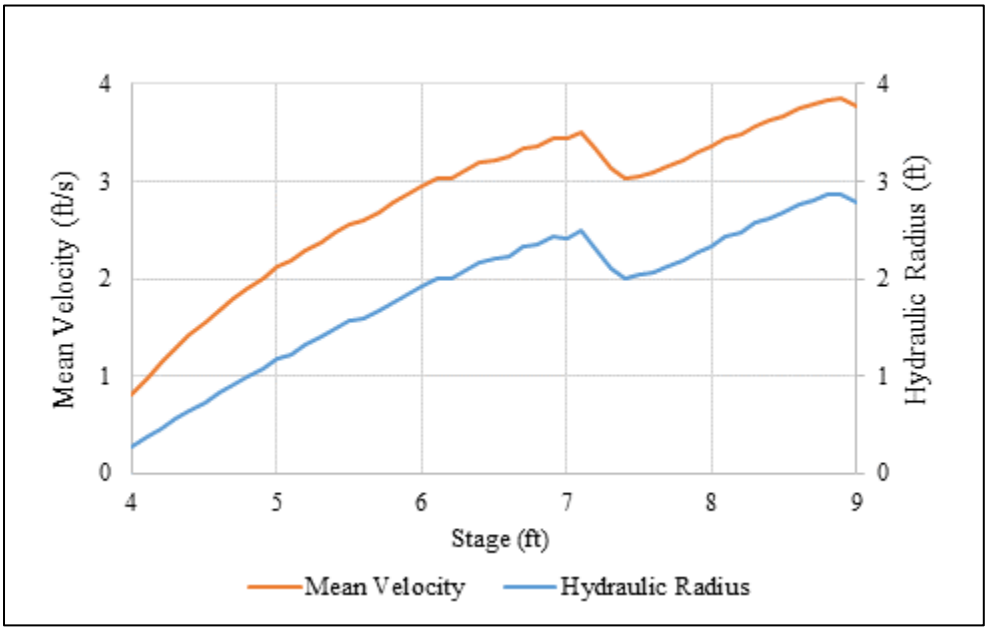

Figure 44: Behavior of mean channel velocity and hydraulic radius at Cherry Creek

As shown in Figure 44, when water moves to the floodplain at an elevation of 7.1 ft, the hydraulic radius starts to decrease and returns to this same position at 8.3 ft of stage. Since, in Manning's equation, velocity is proportional to the two-third power of hydraulic radius, it follows the same decreasing trend of hydraulic radius and starts to increase again after 8.3 ft. This behavior confirms the deviation of V_{req} in Figure 43 and leads to the decision that there should two equations of k-value: one corresponding up to an elevation of 7.1 ft and the other for stage values above 7.1 ft. The required k-values are computed by using Equation 18 and following the above criteria, they are plotted against the corresponding stage values as shown in Figure 45 and 46.

$$k_{req,i} = \frac{V_{m,i}}{v_i} \qquad \text{Equation (19)}$$

where, $k_{req,i}$ is the *i*th required k-value and v_i is the ith surface velocity measured by the radar.

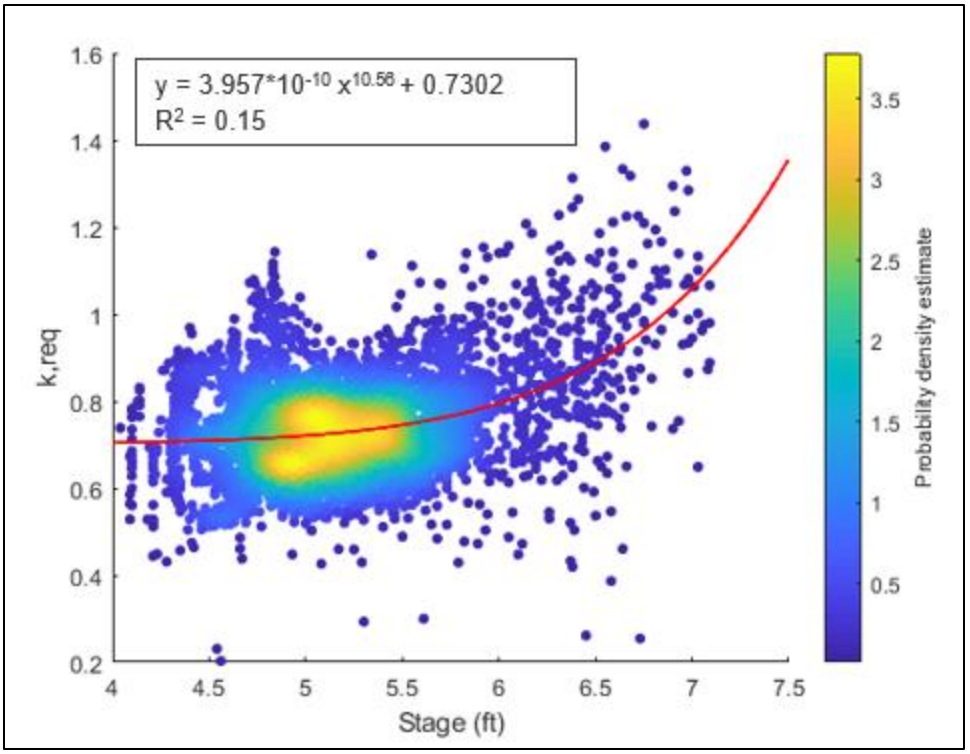

Figure 45: Density plot of k_req vs stage for stage up to 7.1 ft

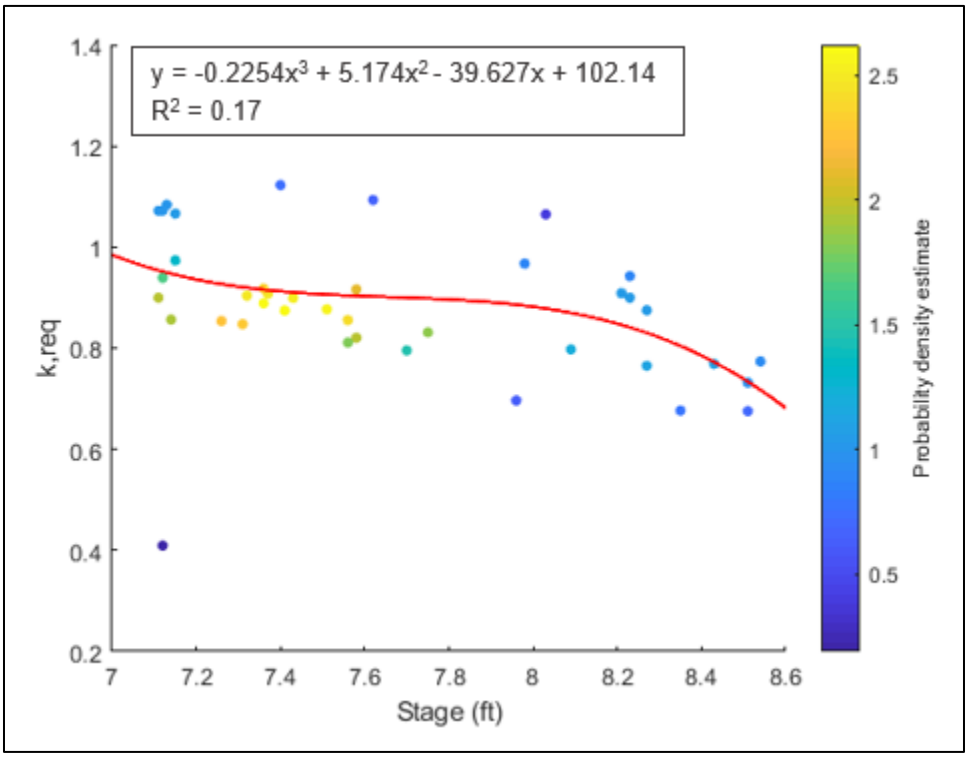

Figure 46: Density plot of k_req vs stage for stage above 7.1 ft

The scatter density plot in Figure 45 shows that the regression may not be able to describe k-value well for all the surface velocity measurements (i.e., $R^2 = 0.15$), however, there is a hot spot in the plot that can be well-predicted by the equation. On the contrary, Figure 46 indicates that water moves to the floodplain for a very few numbers of events and the regression may not approximate k_{req} well from those stage measurements (i.e., $R^2 = 0.17$).

4.3.3.2 Result with k-value Equation

The equation for depth up to 7.1 ft, provides k-value more than 1.0 after a stage value of 6.89 ft. Therefore, for stage between 6.89 – 7.1 ft, the k-values are assumed as 1.0. To evaluate the result with equation, multi-objective function is optimized and compared with that of double-k. The results are provided in Table 13.

Table 13: Result comparison of multi-objective function optimization for double-k and k-equation for Cherry Creek

k-value	**Ψ**	**NSE**	**VE (%)**	**PE (%)**
From equation	0.927	0.954	7.406	9.792
Double-k	0.923	0.949	7.561	10.426

With the use of equations, NSE score has improved from to 0.949 to 0.954 that indicates the radar-driven discharge data match the streamgage data more than the estimates provided by the double-k. On the other hand, both VE and PE have been improved by almost 0.2 and 0.6 %, respectively indicating average hydrograph errors are reduced too. Therefore, it can be said that the equation for k-value provides the most accurate discharge estimates for Cherry Creek.

4.3.3.3 Applicability of k-equation to Other Natural Streams

Since all the natural channels have a logarithmic profile for vertical distribution of velocity (Rantz, 1982), this study assumes that the equation of k developed for Cherry Creek can be applied

for other natural channels too. The channel at Walnut Gulch is an artificial concrete channel and velocity measurements at Paria River are affected, hence, the applicability of the equation is evaluated for Mill Creek only. Figure 20 (c) already shows that the channel cross-section at Mill Creek does not have water moved from main channel to floodplain on both sides, however, this is qualitatively confirmed by the use of Manning's equation as shown in Figure 47 following the same procedure utilized with Cherry Creek. Therefore, the equation that corresponds to stage value up to 7.1 ft at Cherry Creek is used here and the result of multi-objective function optimization is provided in Table 14.

Table 14: Result comparison of multi-objective function optimization for double-k and k-equation for Mill Creek

k-value	**Ψ**	**NSE**	**VE (%)**	**PE (%)**
From equation	0.908	0.967	10.418	13.960
Double-k	0.906	0.965	7.517	17.165

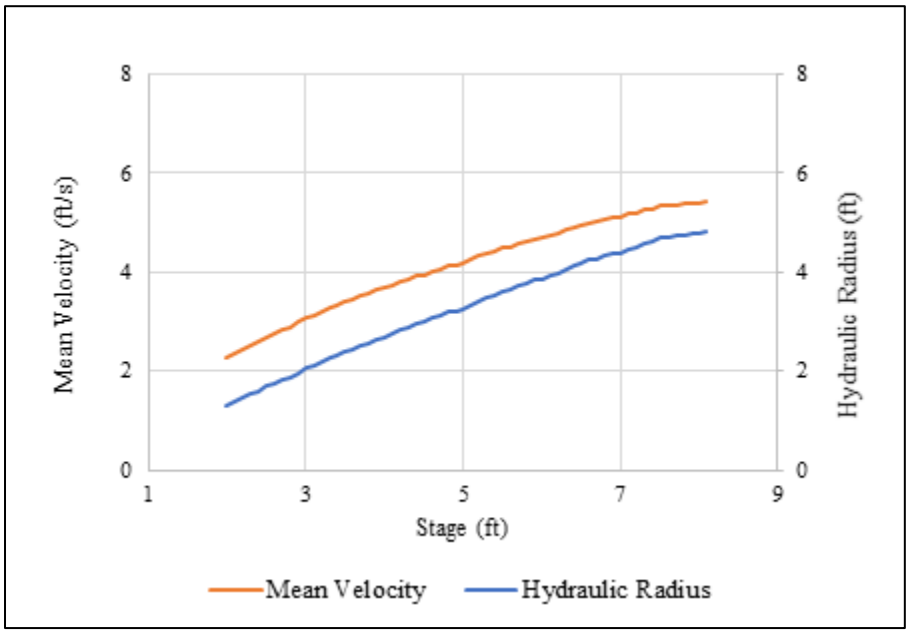

Figure 47: Behavior of mean channel velocity and hydraulic radius at Mill Creek

Table 14 shows that the equation derived discharge estimates provide higher Ψ value than that of double k-values, which means the multi-objective function at Mill Creek is best optimized for the equation-derived k-values. It gives the highest NSE score and lowest PE for Mill Creek, while the lowest VE is still achieved by the double-k driven discharge estimates. Therefore, this result proves the applicability of the k-equation for any natural channel as long as water remains in the main channel.

4.4 UNDERSTANDING VELOCITY CONTENTS

Since the stream radar simultaneously provides stage and surface velocity measurements for any specific channel and there are radar observations for eight different channels, this study attempts to understand the contents of velocity measurement such as how do they evolve with stage, do they differ in time while evolving, does the evolution depend on the magnitude of event, or the topography of the basin, etc. The analyses are discussed below.

4.4.1 Rising and Receding Behavior During Events

Estimating discharge from the "rating curve" method involves extracting the corresponding amount of streamflow for a determined stage (water level) value. On the other hand, during a rainfall event, the water level (stage) can rise quickly, but recede slowly. Now, if the velocity does not follow the same trend of its corresponding stage during both rising and receding phases, it is possible that a specific water level can have two different discharge quantities since discharge is computed from velocity. But the rating curve method will only provide one estimate in this case leading to a possible source of error. Therefore, it is important to evaluate the behavior of stage-velocity evolution in both phases. For this purpose, all the event-hydrographs of any channel are divided according to the rising and receding phases and then the surface velocities are plotted against the corresponding stage values as shown in Figure 48.

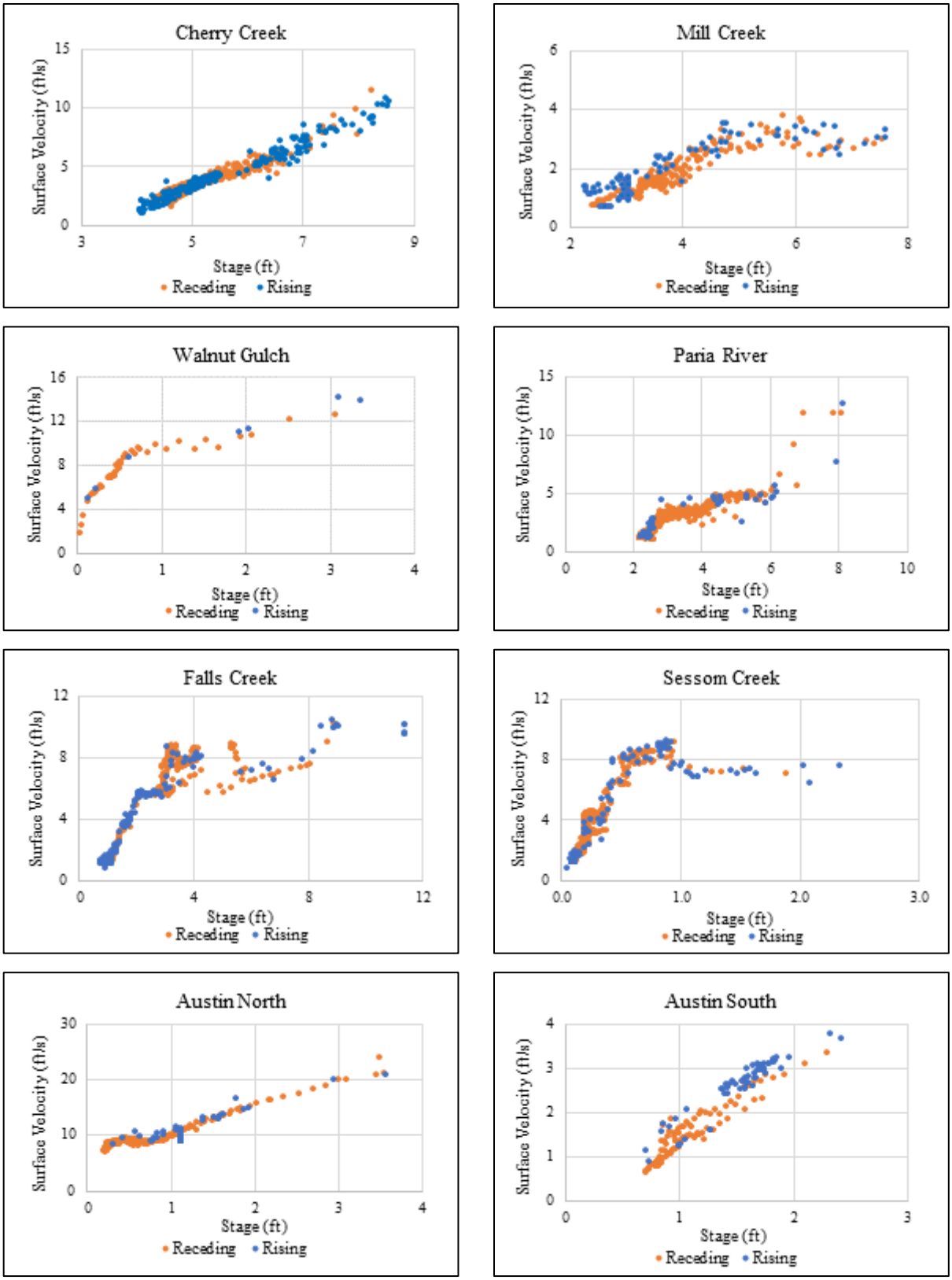

Figure 48: Rising and receding behavior during rainfall events for all the station

Figure 48 shows that the behavior of stage-velocity evolution follow the same trend in both rising and receding phases. Although the number of rising points are lower for each channel complying to the assumption that the variables reach their peak values quickly, it does not create any contrast in the stage-velocity behavior while they recede slowly.

4.4.2 Time Lag Between Stage and Velocity

Ideally, stage and surface velocity should start to increase at the same time during any rainfall event. However, an abrupt change of water level can create a celerity in the water wave that works as an additional speed to normal water velocity of the channel (Pandey, 2015). This celerity can cause the surface velocity to rise more quickly than the stage resulting in a time lag between stage and velocity. Now, this time-lag may not occur for each event of a specific channel. Therefore, to understand if this time-lag only occurs with big floods, or if it occurs frequently due to channel slope, this study attempts to identify such events for all the stations and explain their behavior.

4.4.2.1 Identifying Events with Time-Lag

To identify the events that have time-lag, at first the time difference between the hydrograph of stage and velocity is determined manually for each of the events of a single station. The time-lag can be created within a very short time after the variables start to rise and can continue until their recession. To compute the time-lag, it is assumed that during a rainfall event, both the variables start to increase at the same time, then the celerity drives the surface velocity ahead of stage and hence, surface velocity reaches its peak earlier than stage. Therefore, the time difference between the peak stage and surface velocity in a hydrograph provides the time-lag for the respective event. Table 15 represents the number of events where surface velocity leads the stage for all the stations and the respective time differences.

Table 15: Velocity-leading events for all the stations

Station	Number of events showing time-lag	Data reporting interval (minutes)	Time-lag of the events (minutes)
Cherry Creek	4	5	5, 5, 5, 5
Mill Creek	7	10	70, 140, 60, 140, 70, 70, 40
Walnut Gulch	1	10	10
Paria River	7	10	70, 100, 100, 70, 30, 20, 30
Falls Creek	5	10	80, 40, 40, 70, 40
Sessom Creek	9	10	10, 10, 20, 10, 20, 20, 10, 10, 10
Austin North	2	5	5, 5
Austin South	3	5	5, 5, 5

Table 15 shows that Mill Creek, Paria River, Falls Creek, and Sessom Creek have good number of events where surface velocity leads the stage significantly. The number of such events vary from 5 - 9, whereas the time-lag varies from 10 – 140 minutes for these stations. On the other hand, in case of Cherry Creek, Austin North, and Austin South, the events that show time-lag have a constant magnitude for all the events (5 minutes). Since the time for data reporting interval is also the same for these stations, it is possible that some events may have time-lag less than 5 minutes. However, considering insignificant time difference, these events are ignored. There is only one event at Walnut Gulch that shows time-lag, which is not sufficient to represent a channel's overall behavior, hence, these data are not analyzed further. Therefore, events of Mill Creek, Paria River, Falls Creek, and Sessom Creek are only considered for behavioral analysis.

Figure 49 shows a single event for each of the four stations where velocity leads the stage as pointed out by an arrow (→) sign. The rest of events of the respective stations are provided in

Appendix – C. The plots also show that the velocity not only leads the stage, it also remains noisy until the stage recedes.

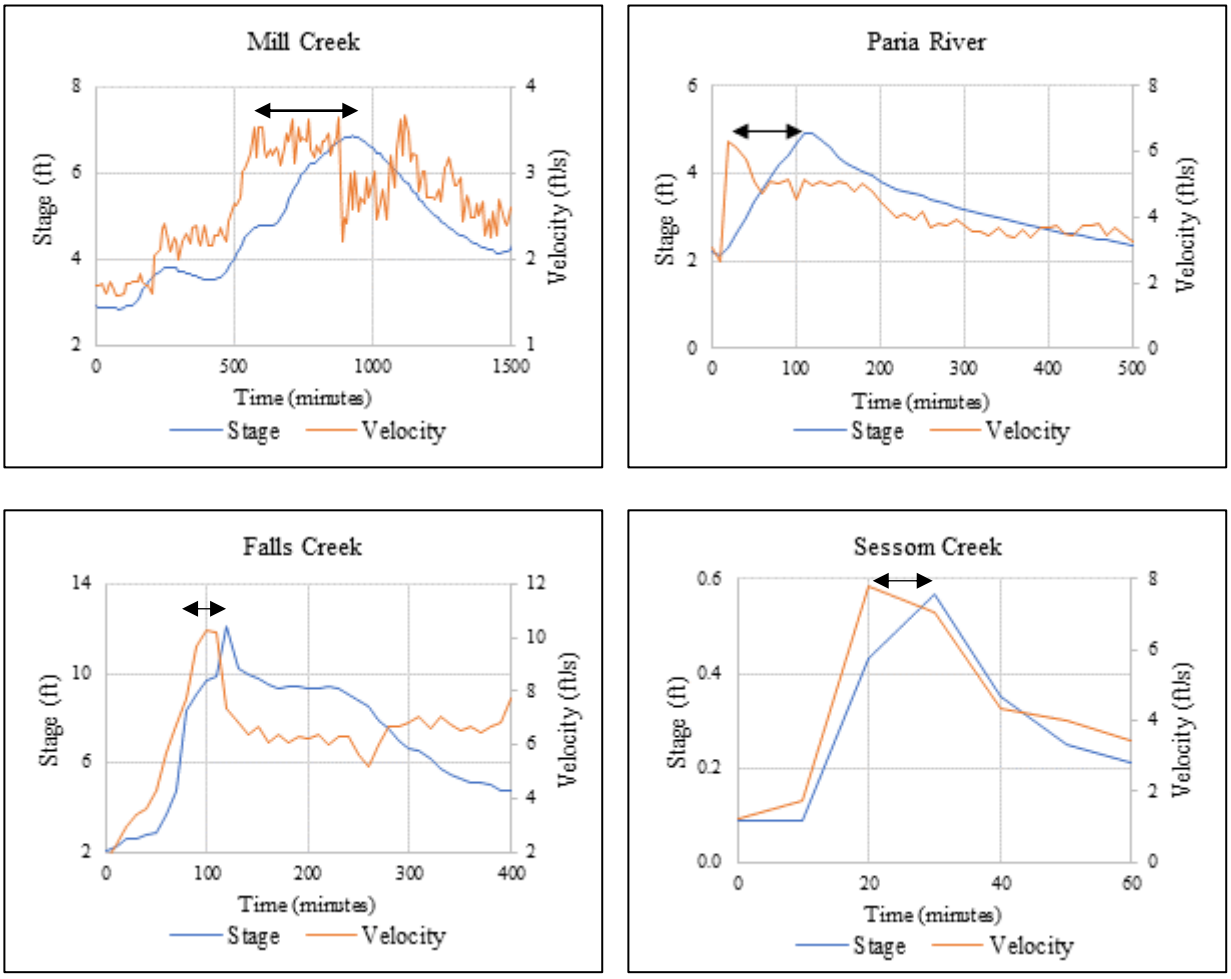

Figure 49: Event for each channel having stage led by surface velocity

4.4.2.2 Analyzing Time-Lag Behavior

To evaluate the impact of big events, the peak event-depths (h_{max}) of the selected four stations are plotted against the corresponding time-lag (ΔT) as shown in Figure 50. On the other hand, for checking the channel steepness effect, first the % slope is computed for the above channels. It is computed by using DEM in ArcGIS. After identifying the main channel for each study area, multiple points are generated on the channel line with a 10 ft equal spacing (run) and the elevation

of each point is determined by a spatial analyst tool of ArcMap. Then the elevation difference between two consecutive points in an upstream direction (rise) is computed and divided by the run length (10 ft). Finally, the % slope is determined by taking the average of the above quotients multiplied by 100 as presented in Table 16. Then the maximum time-lag for each channel (ΔT_{max}) and the 50th percentile surface velocity are plotted against the corresponding channel slope as shown in Figure 51.

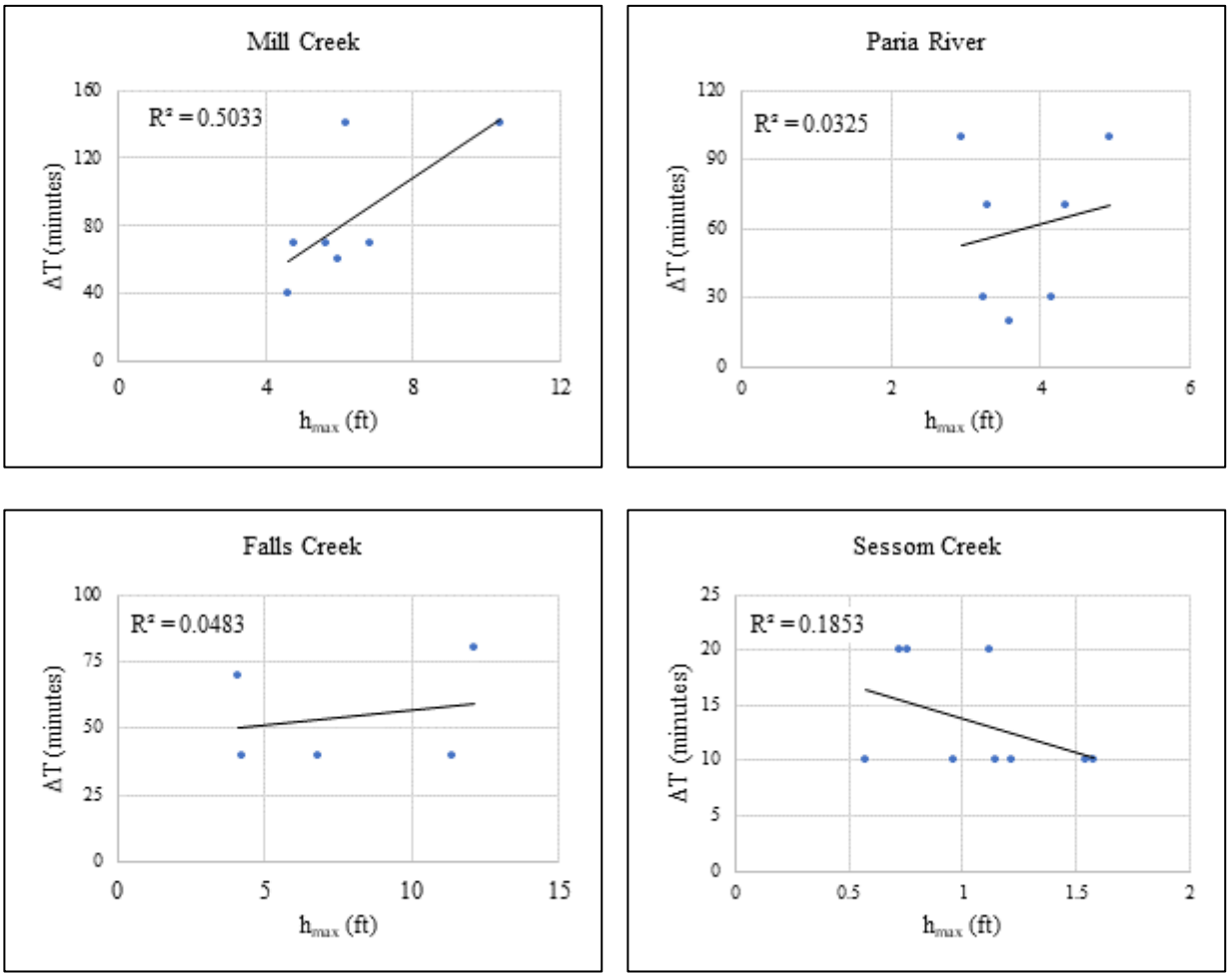

Figure 50: Event time-lag vs peak depth for the selected streams

Table 16: Length of main channel and average channel slope for the selected four stations

Station	Main channel length (ft)	% channel slope
Mill Creek	96048.8	0.24
Paria River	155176.1	1.01
Falls Creek	22268.8	1.19
Sessom Creek	3362.5	2.10

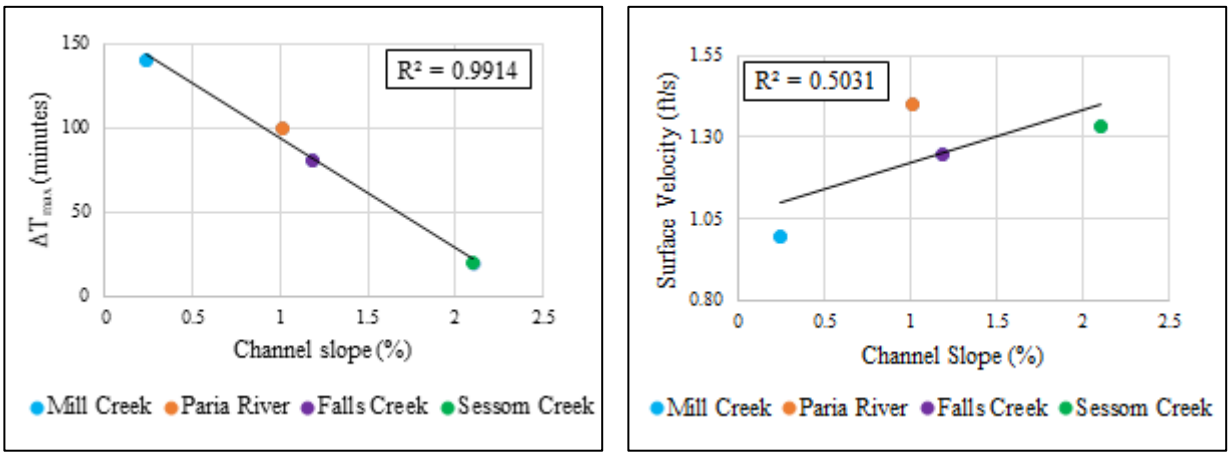

(a) (b)

Figure 51: Scatter plots for the selected four stations – (a) maximum time-lag and channel slope (b) 50th percentile surface velocity and channel slope

The objective of the above two analyses is to identify if there is any correlation between the event time-lag with the magnitude of event depth and channel bed slope. Figure 50 shows that except Sessom Creek, all the other three stations show some degrees of positive correlation between the time-lag of an event and the maximum event depth. However, only Mill Creek has a good coefficient of determination ($R^2 > 0.5$), while for Paria River and Falls Creek, they are quite weak. It indicates that the time-lag of an event can be influenced by the event size at Mill Creek.

On the other hand, Figure 51(a) shows a perfect, negative correlation between the ΔT_{max} and channel slope meaning the time lag increases when the channel bottom gets flatter and Figure 52(b) shows a good, positive correlation between the 50^{th} percentile surface velocity and channel slope indicating steeper channel has higher velocity. Now, the findings of maximum time-lag and channel slope can be explained considering an ideal situation. If there is celerity in reaches of two channel, having similar channel morphology and flow conditions except one is steep and the other one is flat, the surface velocities will reach their peaks earlier than the stage in both of the channels. Due to slope difference, there will be an offset in the timing of peak velocities for these channels and the flat channel will achieve its peak velocity later than the steep one. Since, the celerity effect is gone or reduced now, the next accumulation of water at the downstream points of the reaches will be at a slower rate for both channels and the flat channel will achieve its peak depth later than the steep one like peak velocities. However, the offset in the timing of peak depths will be higher than that of the peak velocities due to absence of celerity. As a result, the overall time-lag between stage and velocity for the flat channel will be higher than steep one.

4.5 DISCHARGE COMPUTATION FOR NON-COLLOCATED STATIONS

The sensitivity analysis for k-value of the collocated stations shows that appropriate selection of k-value is of paramount importance for estimating discharge of any channel. As for the non-collocated stations, there is no streamgage data to compare the discharge estimates and therefore, k-value optimization is not possible. However, this study already finds that the concept of double k-value by Hauet et al., (2018) provides the best results for all the collocated stations of all types (e.g., natural, and artificial concrete). Therefore, this study utilizes this theory for the non-collocated stations too. On the other hand, cross-section analysis of Cherry Creek also shows that before selecting the k-values, the flow behavior should also be evaluated due to channel geometry.

Based on Manning's formula, the same qualitative analysis is done for each of the non-collocated stations. While selecting the appropriate k-value, the maximum recorded stage value and channel condition are also considered. The results are provided below.

4.5.1 Falls Creek

Figure 52 shows the mean channel velocity behavior at Falls Creek. It shows that after an elevation of 11 ft, water moves to the floodplain at the right bank (Figure 21) that decreases the hydraulic radius and consequently, the mean velocity. On the other hand, the analyzed time period of Falls Creek is more than 2 years (Table 1) and should be sufficient to describe the year-round behavior of the channel. The maximum recorded stage for this period is 12.09 ft. It shows that for big events, water level crosses the 11 ft benchmark. Therefore, following the work of Hauet et al., (2018), the recommended k-value for Falls Creek is as follows:

- For stage $\leq$ 6.5 ft, use k = 0.8, while for 6.5 ft $\leq$ stage $\leq$ 11.1 ft, use k = 0.9
- For stage > 11.1 ft, use k = 0.85 to address the decrease in mean velocity and avoid high bias in discharge estimates

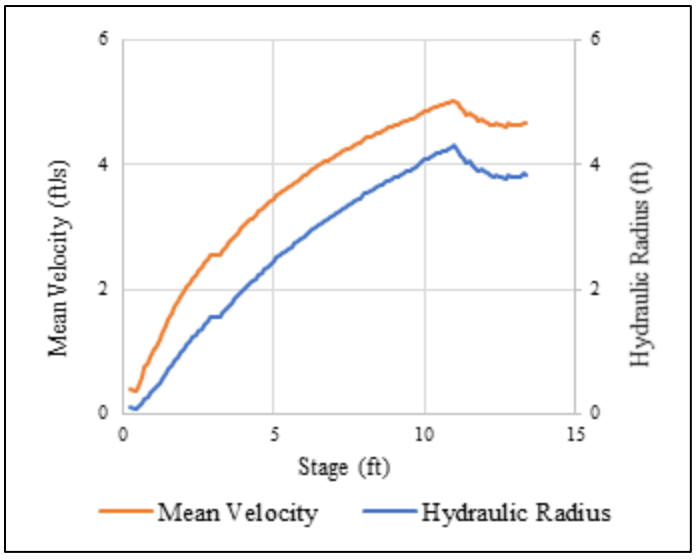

Figure 52: Mean channel velocity behavior for Channel at Falls Creek

4.5.2 Sessom Creek

The behavior of mean channel velocity at Sessom Creek is presented in Figure 53. It does not have any floodplain and therefore, no significant change (decrease) occurs to the hydraulic radius and mean channel velocity at any level of water depth. On the other hand, Sessom Creek has a data period of almost two years (Table 1) and the maximum recorded stage is 2.34 ft. Since it has an artificial concrete channel and the water level rise much, following Hauet et al., (2018), this study recommends using a k-value of 0.9 for the whole timeseries.

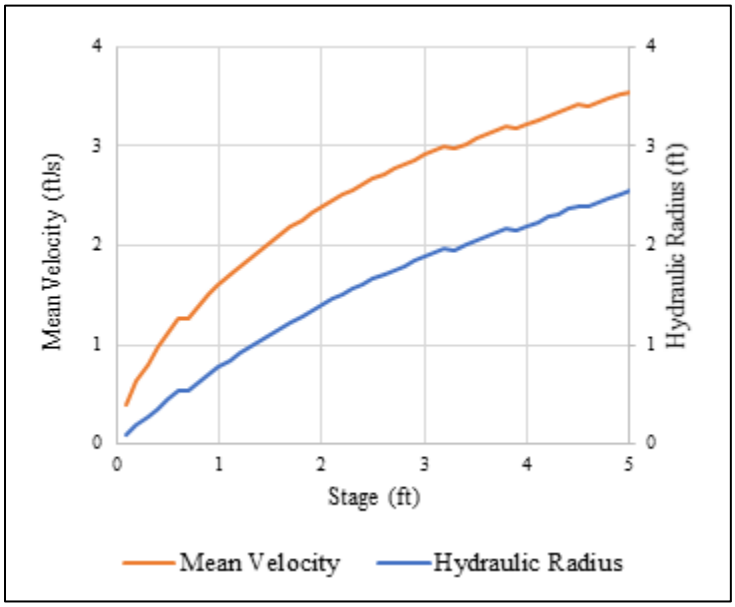

Figure 53: Mean channel velocity behavior for Channel at Sessom Creek

4.5.3 Austin North

Figure 54 illustrates the behavior of mean velocity for the channel at Austin North. It shows at elevation 2.7 ft, there is a decrease in hydraulic radius and mean velocity that happens due to the water crossing the wing wall on the both sides of the culvert along the line where the radar takes measurements and moving to the embankment of the railway track (Figure 15 and Figure 21) . On the other hand, the maximum recorded depth is 3.57 ft for the analyzed time period that indicates

there are events where water level moves to the embankment. Since this is a concrete channel, this study recommends using a k-value of 0.9 for stage below 2.5 ft, while for higher depth, a k-value 0.85 should address the decrease in mean velocity.

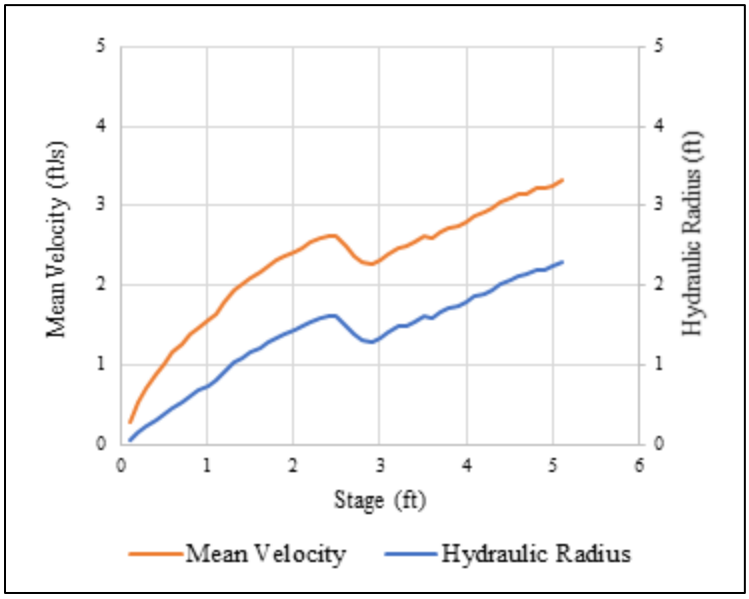

Figure 54: Mean channel velocity behavior for Channel at Austin North

4.5.4 Austin South

Due to the geometry of the channel at Austin South, shown in Figure 21, the hydraulic radius and mean velocity reduce at an elevation of 4 ft and from 4.5 ft they start to increase again. Austin South has a data period of only two and half months (Table 1) as the stream radar experienced vandalism several times and is no longer working. The maximum stage record within these two months is 3.47 ft. Now, following Hauet et al., (2018), a k-value of 0.9 cannot be used for depth above 6.5 ft since after 4 ft, the water experiences a decrease in hydraulic radius, while between 4.0 – 6.5 ft, another k-value (lower than 0.8) is required to address the decrease within this depth range. To avoid complication, this study recommends using k-value as 0.85 for the whole timeseries.

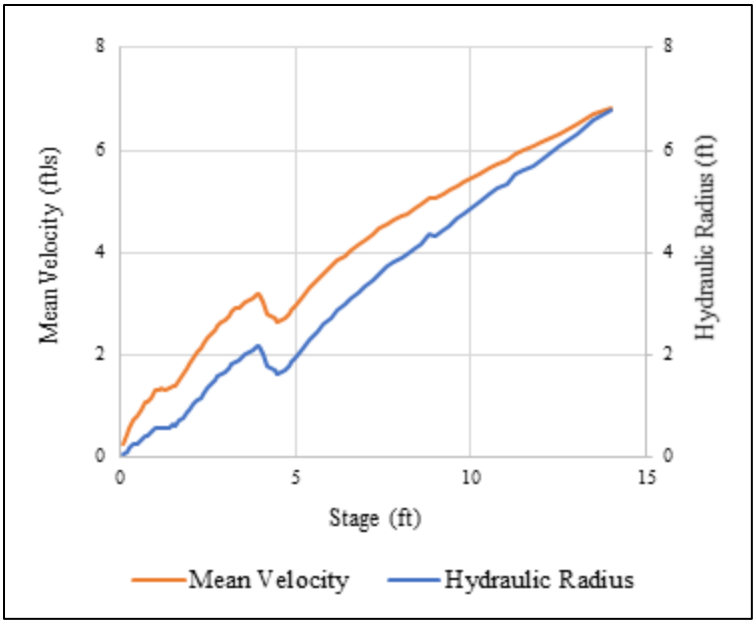

Figure 55: Mean channel velocity behavior for Channel at Austin South

4.6 FLOW CHARACTERISTICS OF THE STREAMS

To evaluate the potential of future flows for hydropower, water supply, and other water resource management, designing drainage structures, and flood control and pollution studies, it is important to know the flow characteristics of a stream. This study constructs flow duration curve to observe and understand the year-round streamflow variability of all the channels as shown in Figure 56.

While computing discharge, double-k and the recommended k-values are used for the collocated and non-collocated stations, respectively. For the collocated stations, curves for streamgage discharge data are also plotted.

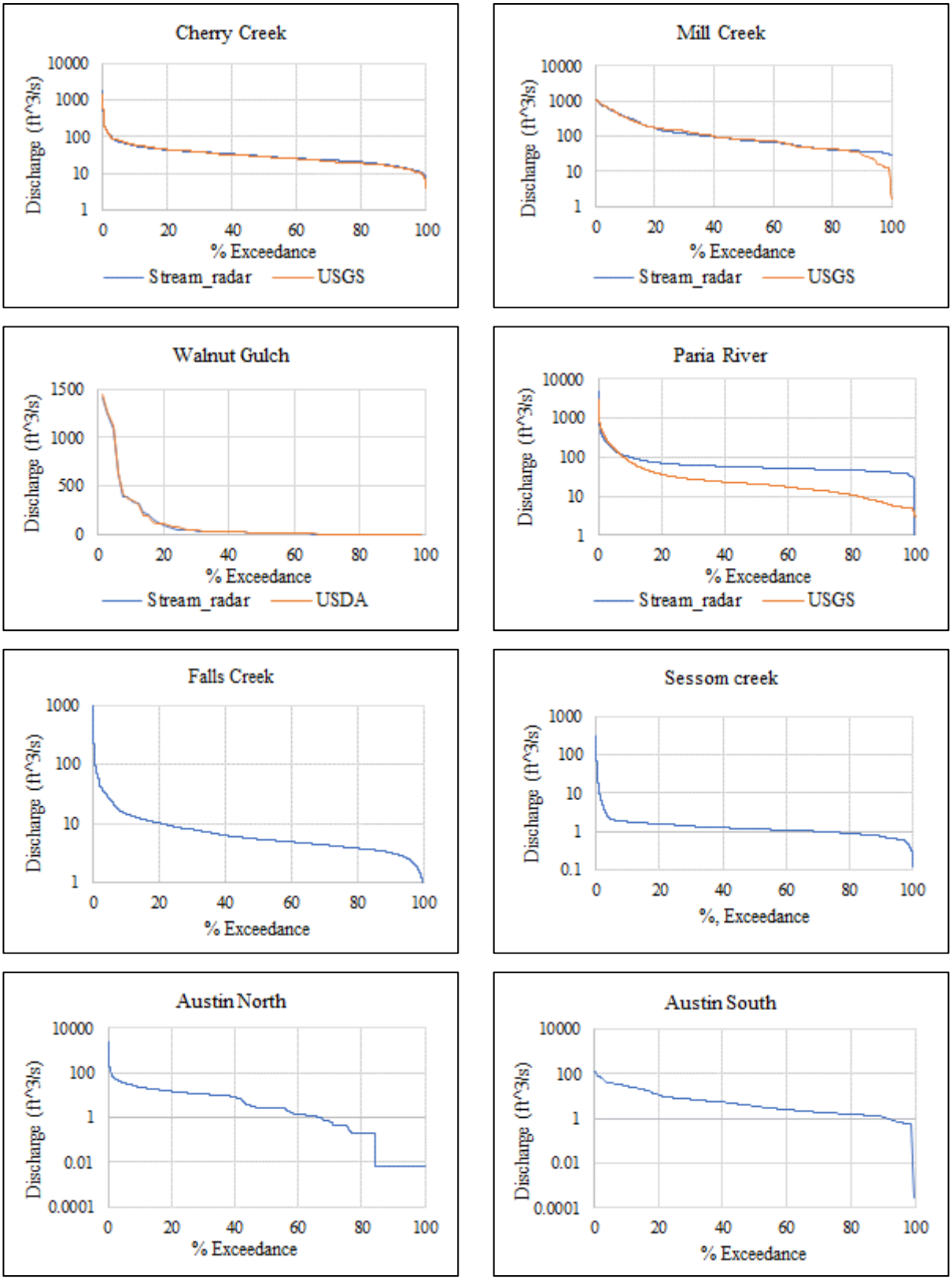

Figure 56: Flow duration curve for all the stations

Cherry Creek has a nice, smooth flow duration curve that indicates it has streamflow all the year round. The step upper region curve indicates it has high flows for a short period of time meaning big events seldom occurs. A perfect match with USGS curve shows the estimate accuracy. As for Mill Creek, the upper region curve is flat indicating the channel experience big events frequently. It has a good match with the USGS-curve except in the lower region curve, where USGS-curve is quite steeper than the radar-driven curve. This means according to USGS record, streamflow disappears quickly in the dry period, while stream radar shows it does not. On the other hand, Walnut Gulch has a perfectly matching with USDA, very steep high region curve that indicates big events are rare in this area. However, after 50%-exceedance limit, the curves get aligned with the x-axis, which indicates during half time of the year there is no flow in the channel. A steep curve can be observed in the high region for Paria River too, however, during low flow (flow < 100 ft^3/s), it always overestimates from the USGS, whereas during event times, it mostly underestimates.

Among the non-collocated stations, both Falls Creek and Sessom Creek have streamflow throughout the year. The base flow for Sessom Creek comes from the spring of San Marcos that sustain some endangered species there (TSU, 2020). On the other hand, their high region curves are also steep indicating the channels rarely receive floods. The channel at Austin North also seldom experiences big events; while the quantized nature at the low region indicates 50% of the time, the flow is so insignificant that the stream radar cannot accurately detect it and hence, converts it to the nearest whole number. For Austin South, the overall flat curve points out that the stream frequently has flow of 50-100 ft^3/s in those two-month time period and most of the values are above 1 ft^3/s.

Chapter 5

CONCLUSIONS AND RECOMMENDATIONS

5.1 CONCLUSIONS

To evaluate the effectiveness of remote sensing technologies in non-contact, direct measurement of stream variables (water level and surface velocity), eight stream radars have been installed at high-priority locations across the Unites States. The radars are mounted on bridges, culverts, and cables and almost all of them have provided measurements for at least one year with a temporal resolution of 5-10 minutes. The eight streams represent a variety of hydrologic and hydraulic characteristics and three of them have conventional gauges from USGS and USDA at the radar location. Based on the hypotheses of this study and results of different analyses, the following conclusions can be drawn:

- To determine if the stream radars can accurately measure water level, the stage data of the collocated stations are compared to the respective streamgage data. The statistical measurements show that the remote sensing observations have negligible random biases and are as accurate as the conventional streamgages. The event hydrographs also show that they have similar behavior during floods. Since it is assumed that the streamgage data represent the true measurements for any station, it can be said that the stream radars are able to measure the water level correctly. As for systematic error, this study identifies the expansion and contraction of the supporting structures due to daily temperature variation are responsible for inducing small errors in stage measurements. Although for normal measurements they can be negligible, for very low water-depth (e.g., < 0.08 ft), these errors are significant, and stage record should be avoided. As for surface velocity measurements, there is no source for direct validation and an indirect accuracy-test should be done using

the discharge estimates. For the collected wind speed data, this study finds wind drift negligible. However, a wind sensor at the radar location should provide more precise wind speed data rather than at the closest airport and the drifts can be well verified then. Based on the above evidences, the first hypothesis of this study that the stream radar will be able to accurately measure the stage and surface velocity, and the reasons for biases will be identified and quantified can therefore be accepted.

- To evaluate the accuracy of the radar-driven discharge estimates, the discharge data are compared to the streamgage data for the collocated stations. With an appropriate k-value to convert surface velocity to a mean channel velocity, the statistical measurements show that the radar-driven discharge estimates are as accurate as in-situ, conventional streamgages, and have acceptable event-based hydrograph errors (less than 10% volumetric and peak-value error) during floods. It also verifies the accuracy of the surface velocity measurements by the stream radar. Therefore, the second hypothesis of this study that discharge can accurately be estimated from the remote-sensing observations are acceptable. In this regard, this study finds the utilization of a double-k application following Hauet et al. (2018) provides better estimates of discharge than the use of the default one (0.85) for the three collocated stations. Using the streamgage discharge data of Cherry Creek, this study develops an equation of k-value as a function of stage that provides the best discharge estimates not only for Cherry Creek, but for another natural channels too (i.e., Mill Creek).
- In examining the time series of river stage and velocity, this study finds events at four streams where surface velocity leads the stage due to an apparent wave celerity effect. The time-lag that is created between stage and velocity has a positive correlation with the

magnitude of the event, while it is negatively correlated with channel slope. Hence, these observations give acceptance to the third hypothesis of this study that there will be specific sites and events that show offset between the evolution of stage and velocity. However, during rainfall events, there is no observed hysteresis behavior for stage and surface velocity while they rise and fall.

5.2 RECOMMENDATIONS

To get more accurate real-time discharge data with the use of stream radars and expand the study, the following recommendations can be helpful:

1. Deploy a wind sensor at the radar location that can record wind speed along the channel direction with a temporal resolution similar to the radar and use the methods described in this study to compute the drift.
2. Pay careful attention to the siting of a stream radar that should include but not limited to a straight channel having uniform flow, adequate cell coverage for transmitting the data, sufficient visibility to the south for the solar panel, smooth access to the site and permission to mount, and lack of potential vandalism.

REFERENCES

Adrian, R. J. (1991). Particle-imaging techniques for experimental fluid mechanics. *Annual Review of Fluid Mechanics*, *23*(1), 261-304.

ASCE (American Society of Civil Engineers) (1993). Criteria for evaluation of watershed models. *Journal of Irrigation and Drainage Engineering*, *119*(3), 429-442.

Aya, S., Fujita, I., & Yagyu, M. (1995). Field-observation of flood in a river by video image analysis. *Proceedings of Hydraulic Engineering*, *39*, 447-452.

Back, L. E., & Bretherton, C. S. (2005). The relationship between wind speed and precipitation in the Pacific ITCZ. *Journal of Climate*, *18*(20), 4317-4328.

Benson, M. A., & Dalrymple, T. (1967). *General field and office procedures for indirect discharge measurements* (No. 03-A1). U.S. Government Printing Office.

Bolognesi, M., Farina, G., Alvisi, S., Franchini, M., Pellegrinelli, A., & Russo, P. (2017). Measurement of surface velocity in open channels using a lightweight remotely piloted aircraft system. *Geomatics, Natural Hazards and Risk*, *8*(1), 73-86.

Bradley, A. A., Kruger, A., Meselhe, E. A., & Muste, M. V. (2002). Flow measurement in streams using video imagery. *Water Resources Research*, *38*(12), 51-1.

Capesius, J. P., Sullivan, J. R., O'Neill, G. B., & Williams, C. A. (2004). Using the tracer-dilution discharge method to develop streamflow records for ice-affected streams in Colorado. *U.S. Geological Survey Scientific Investigations Report-5164*, 14.

Chow, V. T., Maidment, D. R., & Mays, L. W. (1988). Applied Hydrology. *McGraw-Hill Series in Water Resources and Environmental Engineering*.

Clow, D. W., & Fleming, A. C. (2008). Tracer gauge: An automated dye dilution gauging system for ice-affected streams. *Water Resources Research*, *44*(12).

Costa, J. E., Cheng, R. T., Haeni, F. P., Melcher, N., Spicer, K. R., Hayes, E., ... & Barrick, D. (2006). Use of radars to monitor stream discharge by noncontact methods. *Water Resources Research*, *42*(7).

Costa, J. E., Spicer, K. R., Cheng, R. T., Haeni, F. P., Melcher, N. B., Thurman, E. M., ... & Keller, W. C. (2000). Measuring stream discharge by non-contact methods: A proof-of-concept experiment. *Geophysical Research Letters*, *27*(4), 553-556.

Creëlle, S., Roldan, R., Herremans, A., Meire, D., Buis, K., Meire, P., ... & Troch, P. (2018). Validation of large-scale particle image velocimetry to acquire free-surface flow fields in vegetated rivers. *Journal of Applied Water Engineering and Research*, *6*(3), 171-182.

Creutin, J. D., Muste, M., Bradley, A. A., Kim, S. C., & Kruger, A. (2003). River gauging using PIV techniques: a proof of concept experiment on the Iowa River. *Journal of Hydrology*, *277*(3-4), 182-194.

Dalrymple, T., & Benson, M. A. (1984). *Measurement of peak discharge by the slope-area method* (No. 03-A2). U.S. Government Printing Office.

Di Baldassarre, G., & Montanari, A. (2009). Uncertainty in river discharge observations: a quantitative analysis. *Hydrology & Earth System Sciences*, *13*(6), 913-921

Dottori, F., Martina, M. L. V., & Todini, E. (2009). A dynamic rating curve approach to indirect discharge measurement. *Hydrology & Earth System Sciences*, *13*(6), 859–896.

Dramais, G., Le Coz, J., Camenen, B., & Hauet, A. (2011). Advantages of a mobile LSPIV method for measuring flood discharges and improving stage–discharge curves. *Journal of Hydro-Environment Research*, *5*(4), 301-312.

Dramais, G., Le Coz, J., Camenen, B., & Hauet, A. (2011). Advantages of a mobile LSPIV method for measuring flood discharges and improving stage–discharge curves. *Journal of Hydro-Environment Research*, *5*(4), 301-312.

Fujita, I., & Komura, S. (1994). Application of video image analysis for measurements of river-surface flows. *Proceedings of Hydraulic Engineering*, *38*, 733-738.

Fujita, I., Muste, M., & Kruger, A. (1998). Large-scale particle image velocimetry for flow analysis in hydraulic engineering applications. *Journal of Hydraulic Research*, *36*(3), 397-414.

Fulton, J. W., Mason, C. A., Eggleston, J. R., Nicotra, M. J., Chiu, C. L., Henneberg, M. F., ... & Laveau, C. D. (2020). Near-Field Remote Sensing of Surface Velocity and River Discharge

Using Radars and the Probability Concept at 10 US Geological Survey Streamgages. *Remote Sensing*, *12*(8), 1296.

Fulton, J., & Ostrowski, J. (2008). Measuring real-time streamflow using emerging technologies: Radar, hydroacoustics, and the probability concept. *Journal of Hydrology*, *357*(1-2), 1-10.

Gunawan, B., Sun, X., Sterling, M., Shiono, K., Tsubaki, R., Rameshwaran, P., ... & Fujita, I. (2012). The application of LS-PIV to a small irregular river for inbank and overbank flows. *Flow Measurement and Instrumentation*, *24*, 1-12.

Ha, E. C. (1979). Remote Sensing of Ocean Surface Current and Current Shear by HF Backscatter Radar. *PhD Thesis, Stanford University*.

Harpold, A. A., Mostaghimi, S., Vlachos, P. P., Brannan, K., & Dillaha, T. (2006). Stream discharge measurement using a large-scale particle image velocimetry (LSPIV) prototype. *Transactions of the ASABE*, *49*(6), 1791-1805.

Hauet, A., Creutin, J. D., Belleudy, P., Muste, M., & Krajewski, W. (2006). Discharge measurements using Large Scale PIV under varied flow conditions, recent results, accuracy and perspectives. *River Flow*, 1829-1834.

Hauet, A., Kruger, A., Krajewski, W. F., Bradley, A., Muste, M., Creutin, J. D., & Wilson, M. (2008). Experimental system for real-time discharge estimation using an image-based method. *Journal of Hydrologic Engineering*, *13*(2), 105-110.

Hauet, A., Morlot, T., & Daubagnan, L. (2018). Velocity profile and depth-averaged to surface velocity in natural streams: A review over a large sample of rivers. *E3SWC*, *40*, 06015.

Homer, C., Dewitz, J., Yang, L., Jin, S., Danielson, P., Xian, G., ... & Megown, K. (2015). Completion of the 2011 National Land Cover Database for the conterminous United States–representing a decade of land cover change information. *Photogrammetric Engineering & Remote Sensing*, *81*(5), 345-354.

Jodeau, M., Hauet, A., Paquier, A., Le Coz, J., & Dramais, G. (2008). Application and evaluation of LS-PIV technique for the monitoring of river surface velocities in high flow conditions. *Flow Measurement and Instrumentation*, *19*(2), 117-127.

Johansson, B., & Chen, D. (2003). The influence of wind and topography on precipitation distribution in Sweden: Statistical analysis and modelling. *International Journal of Climatology: A Journal of the Royal Meteorological Society*, *23*(12), 1523-1535.

Johnson, E. D., & Cowen, E. A. (2016). Remote monitoring of volumetric discharge employing bathymetry determined from surface turbulence metrics. *Water Resources Research*, *52*(3), 2178-2193.

Johnson, E. D., & Cowen, E. A. (2017). Remote determination of the velocity index and mean streamwise velocity profiles. *Water Resources Research*, *53*(9), 7521-7535.

Kilpatrick, F. A., & Cobb, E. D. (1985). *Measurement of discharge using tracers* (No. 03-A16). U.S. Government Printing Office.

Kim, Y., Muste, M., Hauet, A., Bradley, A., Weber, L., & Koh, D. (2007). Uncertainty analysis for LSPIV in-situ velocity measurements. In *Proceedings of the Congress-International Association of Hydraulic Engineering and Research, 32*(1), 81.

Lang, M., Pobanz, K., Renard, B., Renouf, E., & Sauquet, E. (2010). Extrapolation of rating curves by hydraulic modelling, with application to flood frequency analysis. *Hydrological Sciences Journal*, *55*(6), 883-898.

Le Boursicaud, R., Pénard, L., Hauet, A., Thollet, F., & Le Coz, J. (2016). Gauging extreme floods on YouTube: application of LSPIV to home movies for the post-event determination of stream discharges. *Hydrological Processes*, *30*(1), 90-105.

Le Coz, J., Pobanz, K., Faure, J. B., Pierrefeu, G., Blanquart, B., & Choquette, Y. (2012). Stage-discharge hysteresis evidenced by multi-ADCP measurements. *River Flow*, 8.

Lee, M. C., Lai, C. J., Leu, J. M., Plant, W. J., Keller, W. C., & Hayes, K. (2002). Non-contact flood discharge measurements using an X-band pulse radar (I) theory. *Flow Measurement and Instrumentation*, *13*(5-6), 265-270.

Legates, D. R., & McCabe Jr, G. J. (1999). Evaluating the use of "goodness-of-fit" measures in hydrologic and hydroclimatic model validation. *Water resources research*, *35*(1), 233-241.

MacVicar, B. J., Hauet, A., Bergeron, N., Tougne, L., & Ali, I. (2012). River Monitoring with Ground-Based Videography. *Fluvial Remote Sensing for Science and Management*, 367-383.

McMillan, H., Krueger, T., & Freer, J. (2012). Benchmarking observational uncertainties for hydrology: rainfall, river discharge and water quality. *Hydrological Processes*, *26*(26), 4078-4111.

Means, T. (2019, July 24). *How the Atmosphere Heats and Cools During a 24-Hour Period*. https://www.thoughtco.com/diurnal-temperature-range-3444244.

Melcher, N. B., Costa, J. E., Haeni, F. P., Cheng, R. T., Thurman, E. M., Buursink, M., ... & Hayes, K. (2002). River discharge measurements by using helicopter-mounted radar. *Geophysical Research Letters*, *29*(22), 2084.

Miller, D. A., & White, R. A. (1998). A Conterminous United States Multilayer Soil Characteristics Dataset for Regional Climate and Hydrology Modeling. *Earth Interactions*, *2*(2), 1–26. https://doi.org/10.1175/1087-3562(1998)0022.3.co;2

Muste, M., Ettema, R., & Fujita, I. (2000). Image-based technique for monitoring ice motion in laboratory and field conditions. In *International Workshop on River Environments Considering Hydraulic and Hydrologic Phenomena in Snowy and Cold Regions*, 1-6.

Muste, M., Fujita, I., & Hauet, A. (2008). Large-scale particle image velocimetry for measurements in riverine environments. *Water Resources Research*, *44*(4).

Nash, J. E., & Sutcliffe, J. V. (1970). River flow forecasting through conceptual models part I — A discussion of principles. *Journal of hydrology*, *10*(3), 282-290.

NOAA (National Oceanic and Atmospheric Administration) (2019). *Data Tools: Local Climatological Data (LCD)*. Local Climatological Data (LCD) | Data Tools | Climate Data Online (CDO) | National Climatic Data Center (NCDC). Retrieved July 10, 2019, from https://www.ncdc.noaa.gov/cdo-web/datatools/lcd.

NWS (National Weather Service) (2020). *Normal Depth Demonstration Tool*. Normal Depth Calculator. Retrieved February 21, 2020, from https://www.weather.gov/aprfc/NormalDepthCalc.

Pandey, B. R. (2015). Open Channel Surges. *Journal of Advanced College of Engineering and Management, 1*, 35-43.

Petersen-Overleir, A., & Reitan, T. (2009). Bayesian analysis of stage–fall–discharge models for gauging stations affected by variable backwater. *Hydrological Processes: An International Journal*, *23*(21), 3057-3074.

Plant, W. J., Keller, W. C., & Hayes, K. (2005). Measurement of river surface currents with coherent microwave systems. *IEEE Transactions on Geoscience and Remote Sensing*, *43*(6), 1242-1257.

Polatel, C. (2006). *Large-scale roughness effect on free-surface and bulk flow characteristics in open-channel flows* (Doctoral dissertation, University of Iowa).

PRISM (2004). *PRISM Climate Group*, Oregon State University, http://prism.oregonstate.edu, created 4 Feb 2004

Rantz, S. E. (1982). Measurement and computation of streamflow: Volume 1, Measurement of stage and discharge. *U.S. Geological Survey Water Supply Paper 2175.*

Schmidt, A. R. (2002). *Analysis of Stage-Discharge Relations for Open-Channel Flows and Their Associated Uncertainties* (Doctoral dissertation, University of Illinois at Urbana-Champaign).

Servat, E., & Dezetter, A. (1991). Selection of calibration objective fonctions in the context of rainfall-ronoff modelling in a Sudanese savannah area. *Hydrological Sciences Journal*, *36*(4), 307-330.

Shemdin, O. H. (1972). Wind-generated current and phase speed of wind waves. *Journal of Physical oceanography*, *2*(4), 411-419.

Smart, G. M. (1999). Turbulent velocity profiles and boundary shear in gravel bed rivers. *Journal of Hydraulic Engineering*, *125*(2), 106-116.

Smith, C. F., Cordova, J. T., & Wiele, S. M. (2010). The continuous slope-area method for computing event hydrographs. *U.S. Geological Survey Scientific Investigations Report-5241*, 37.

Sommer GmbH (2014). *Discharge Measurement System for RQ-30, RQ-30a Firmware version 1.8x: User Manual (V02)*, Koblach, Austria: Author

Sun, X., Shiono, K., Chandler, J. H., Rameshwaran, P., Sellin, R. H. J., & Fujita, I. (2010). Discharge estimation in small irregular river using LSPIV. In *Proceedings of the Institution of Civil Engineers-Water Management,163*(5), 247-254.

Swarno, H. A., Zaki, S. A., Hagishima, A., & Yusup, Y. (2020). Characteristics of wind speed during rainfall event in the tropical urban city. *Urban Climate*, *32*, 100620.

Tauro, F., Piscopia, R., & Grimaldi, S. (2017). Streamflow observations from cameras: Large-scale particle image velocimetry or particle tracking velocimetry? *Water Resources Research*, *53*(12), 10374-10394.

TSU (Texas State University) (2020). *Endangered Species,* The Meadows Center for Water and the Environment. Retrieved June 1, 2020,from www.meadowscenter.txstate.edu/ExploreSpringLake/EndangeredSpecies.html,

USDA (United States Department of Agriculture) (2019). *Runoff Event for Digital Flumes*. Online Data Access: Southwest Watershed Research Center. Retrieved May 08, 2019, from https://www.tucson.ars.ag.gov/dap/digital/runoff_event.asp.

USGS (United States Geological Survey (2019). *How do I interpret gage height and streamflow values?* How do I interpret gage height and streamflow values? - USGS Water Data for the Nation Help System. Retrieved October 25, 2019, from https://help.waterdata.usgs.gov/tutorials/surface-water-data/how-do-i-interpret-gage-height-and-streamflow-values.

USGS (United States Geological Survey) (2018). *Daily Streamflow Conditions*, USGS Current Water Data for the Nation. Retrieved September 10, 2018, from https://waterdata.usgs.gov/nwis/rt.

USGS (United States Geological Survey) (2020a). *Streamgaging Basics,* Water Science School. Retrieved March 10, 2020, from https://www.usgs.gov/mission-areas/water-resources/science/streamgaging-basics?qt-science_center_objects=0#qt-science_center_objects.

USGS (United States Geological Survey) (2020b). *How Streamflow is Measured*, Water Science School. Retrieved March 10, 2020, from https://www.usgs.gov/special-topic/water-science-school/science/how-streamflow-measured?qt-science_center_objects=0.

USGS (United States Geological Survey) (2020c). *TNM Download (V1.0)*, The National Map. Retrieved February 02, 2020, from https://viewer.nationalmap.gov/basic/.

Welber, M., Le Coz, J., Laronne, J. B., Zolezzi, G., Zamler, D., Dramais, G., ... & Salvaro, M. (2016). Field assessment of noncontact stream gauging using portable surface velocity radars (SVR). *Water Resources Research*, *52*(2), 1108-1126.

WMO (World Meteorological Organization) (2010). *Manual on Stream Gauging. Computation of discharge*, *1044*(2), 195.

APPENDIX – A

Python Code for k-value Optimization

Figure AA.1 shows the code developed in Python to run the trials for a single-k optimization, while Figure AA.2 represents the code for double-k.

```
@author: MRKhan
"""
import numpy as np
from pandas import DataFrame, read_excel

f0 = read_excel('All_data.xlsx')
h = f0['h']
v = f0['v']
A = f0['A']
O = f0['O']
Q = 0
Q_all=[]
index = []
H_index = []
k_index = []
Q_SR = []
sum1=[]
sum2=[]
Chi = []

sum_E1_US = sum (O[0:22])
P1_US = O[7]
sum_E2_US = sum (O[73:288])
P2_US = O[166]
P3_US = O[193]
sum_E3_US = sum (O[288:387])
P4_US = O[317]
sum_E4_US =sum(O[628:654])
P5_US = O[630]
P6_US = O[642]
O_bar = np.average(O)

alpha = np.arange (0.7,1.0,0.001)
```

```
for k in range (0, len(alpha)):
    k = alpha[k]
    for m in range (0, len (h)):
        stage = h[m]
        surf_vel = v[m]
        wt_area = A[m]
        Q = k*surf_vel*wt_area
        del_Q = (O[m] - Q)**2
        Q_SR.append(Q)
        del_O_bar = (O[m]-O_bar)**2
        sum1.append(del_Q)
        sum2.append(del_O_bar)
    denomero = sum (sum1)
    numero = sum (sum2)
    NSE = 1 - (denomero/numero)
    sum_E1_SR = sum (Q_SR [0:22])
    P1_SR = Q_SR[7:8]
    sum_E2_SR = sum (Q_SR [73:288])
    P2_SR = Q_SR[166:167]
    P3_SR = Q_SR[193:194]
    sum_E3_SR =sum (Q_SR [288:387])
    P4_SR = Q_SR[318:319]
    sum_E4_SR =sum (Q_SR [628:654])
    P5_SR = Q_SR[630:631]
    P6_SR = Q_SR[643:644]
    ve1= abs (sum_E1_SR - sum_E1_US)/sum_E1_US*100
    ve2= abs (sum_E2_SR - sum_E2_US)/sum_E2_US*100
    ve3= abs (sum_E3_SR - sum_E3_US)/sum_E3_US*100
    ve4= abs (sum_E4_SR - sum_E4_US)/sum_E4_US*100
    VE = np.average((ve1,ve2,ve3,ve4))
    pe1= abs (P1_SR -P1_US)/P1_US*100
    pe2= abs (P2_SR -P2_US)/P2_US*100
    pe3= abs (P3_SR -P3_US)/P3_US*100
    pe4= abs (P4_SR -P4_US)/P4_US*100
    pe5= abs (P5_SR -P5_US)/P5_US*100
    pe6= abs (P6_SR -P6_US)/P6_US*100
    PE = np.average((pe1,pe2,pe3,pe4,pe5,pe6))
    chii = NSE/3 + (1-VE/100)/3 + (1-PE/100)/3
    k_ind = k
    k_index.append (k_ind)
    Chi.append(chii)
    Q_all.append(Q_SR)
    Q_SR = []

Chi_max = max (Chi)
max_index = Chi.index (Chi_max)
k_opt = k_index[max_index]

print k_opt,  Chi_max
```

Figure AA. 1: Python code for single-k optimization

```
@author: MRKhan
"""

import numpy as np
from pandas import DataFrame, read_excel

f0 = read_excel('All_data.xlsx')
h = f0['h']
v = f0['v']
A = f0['A']
O = f0['O']
Q = 0
Q_all=[]
index = []
H_index = []
k1_index = []
k2_index = []
Q_SR = []
sum1=[]
sum2=[]
Chi = []

sum_E1_US = sum (O[0:22])
P1_US = O[7]
sum_E2_US = sum (O[73:288])
P2_US = O[166]
P3_US = O[193]
sum_E3_US = sum (O[288:387])
P4_US = O[317]
sum_E4_US =sum(O[628:654])
P5_US = O[630]
P6_US = O[642]
O_bar = np.average(O)

alpha1 = np.arange (0.75,0.85,0.001)
alpha2 = np.arange (0.9,1.0,0.001)

W = np.arange (6.0,7.0,0.1)
```

```
for i in range (0,len (W)):
    H = W[i]
    for j in range (0, len(alpha1)):
        k1 = alpha1[j]
        for k in range (0, len(alpha2)):
            k2 = alpha2[k]
            for m in range (0, len (h)):
                stage = h[m]
                surf_vel = v[m]
                wt_area = A[m]
                if stage > H:
                    Q = k2*surf_vel*wt_area
                else:
                    Q = k1*surf_vel*wt_area
                Q_SR.append(Q)
                del_Q = (O[m] - Q_SR[m])**2
                del_O_bar = (O[m]-O_bar)**2
                sum1.append(del_Q)
                sum2.append(del_O_bar)
            denomero = sum (sum1)
            numero = sum (sum2)
            NSE = 1 - (denomero/numero)
            sum_E1_SR = sum (Q_SR [0:22])
            P1_SR = Q_SR[7:8]
            sum_E2_SR = sum (Q_SR [73:288])
            P2_SR = Q_SR[166:167]
            P3_SR = Q_SR[193:194]
            sum_E3_SR =sum (Q_SR [288:387])
            P4_SR = Q_SR[318:319]
            sum_E4_SR =sum (Q_SR [628:654])
            P5_SR = Q_SR[630:631]
            P6_SR = Q_SR[643:644]
            ve1= abs (sum_E1_SR - sum_E1_US)/sum_E1_US*100
            ve2= abs (sum_E2_SR - sum_E2_US)/sum_E2_US*100
            ve3= abs (sum_E3_SR - sum_E3_US)/sum_E3_US*100
            ve4= abs (sum_E4_SR - sum_E4_US)/sum_E4_US*100
            VE = np.average((ve1,ve2,ve3,ve4))
            pe1= abs (P1_SR -P1_US)/P1_US*100
            pe2= abs (P2_SR -P2_US)/P2_US*100
            pe3= abs (P3_SR -P3_US)/P3_US*100
            pe4= abs (P4_SR -P4_US)/P4_US*100
            pe5= abs (P5_SR -P5_US)/P5_US*100
            pe6= abs (P6_SR -P6_US)/P6_US*100
            PE = np.average((pe1,pe2,pe3,pe4,pe5,pe6))
            chii = NSE/3 + (1-VE/100)/3 + (1-PE/100)/3
            k2_ind = k2
            k1_ind = k1
            H_ind = H
            H_index.append (H_ind)
            k1_index.append (k1_ind)
            k2_index.append (k2_ind)
            Chi.append(chii)
            Q_all.append(Q_SR)
            Q_SR = []
```

```
Chi_max = max (Chi)
max_index = Chi.index (Chi_max)
H_opt = H_index[max_index]
k1_opt = k1_index[max_index]
k2_opt = k2_index[max_index]
print H_opt, k1_opt, k2_opt,  Chi_max
```

Figure AA. 2: Python code for double-k optimization

APPENDIX – B

Event Hydrographs with Optimized k-value for the Collocated Stations

B.1 Mill Creek

Figure AB.1 shows the event-hydrograph comparisons of Mill Creek for double-k optimization.

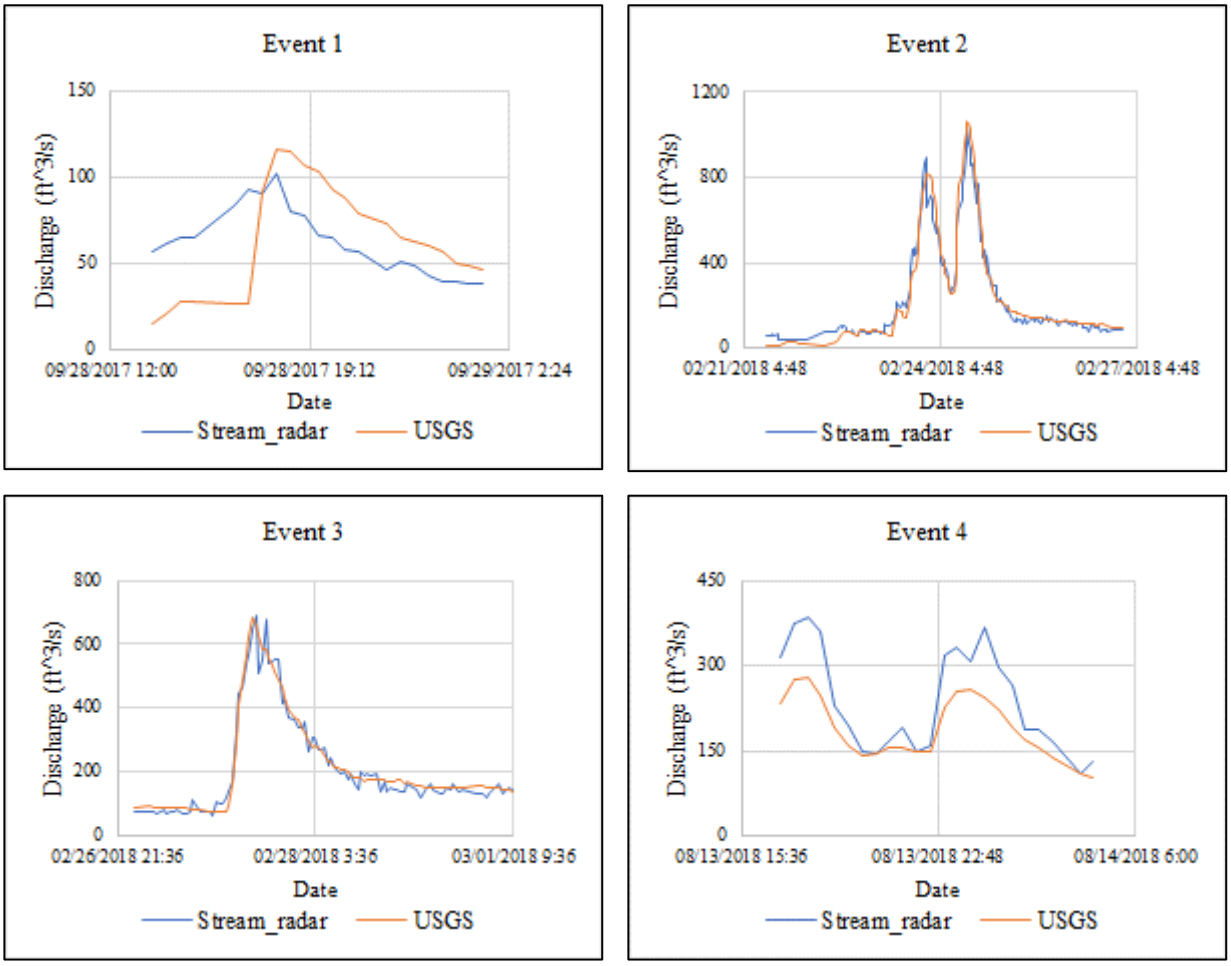

Figure AB. 1: Event-hydrograph comparisons for Mill Creek with double-k

B.2 Cherry Creek

Figure AB.2 shows the event-hydrograph comparisons of Cherry Creek for double-k optimization.

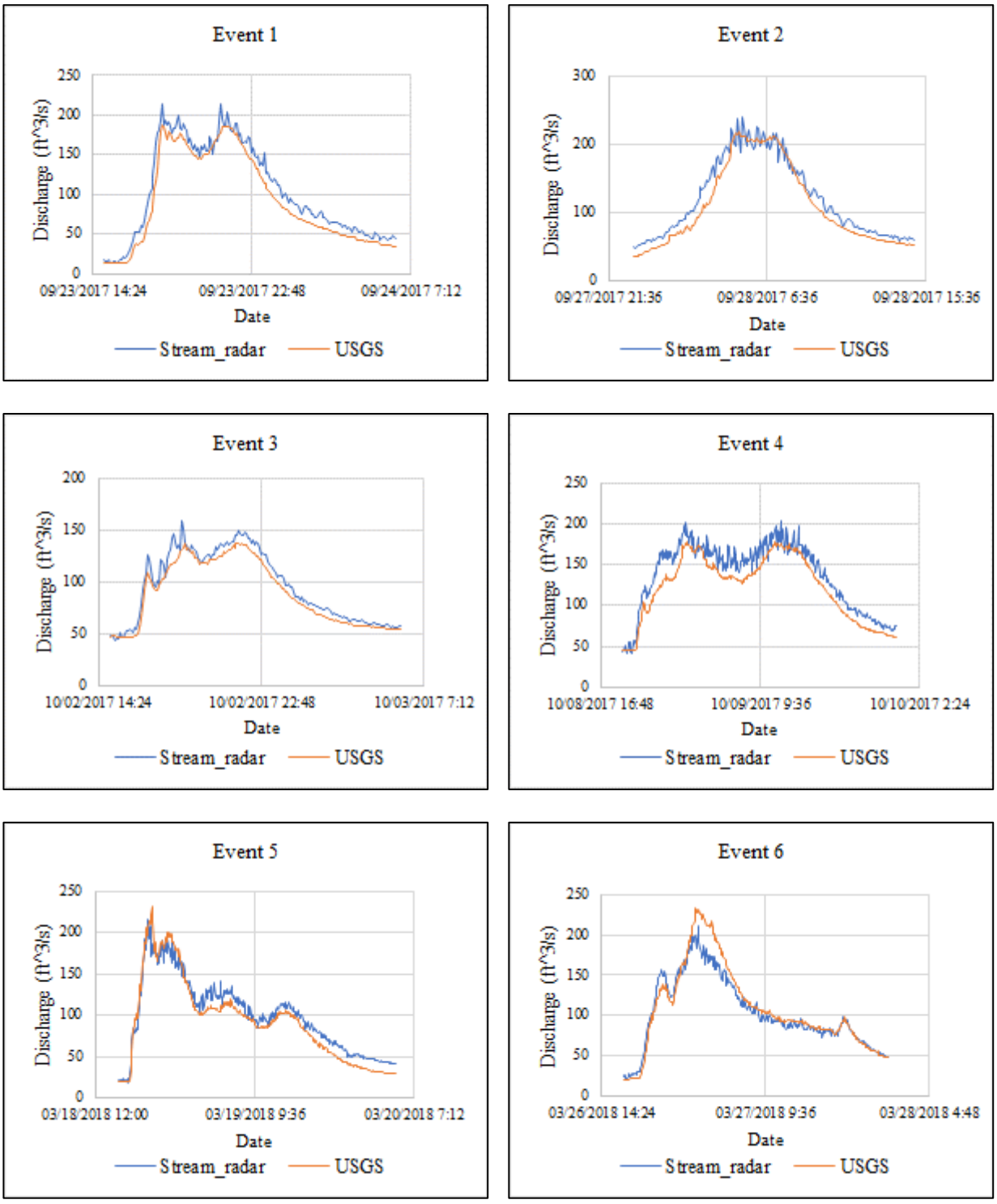

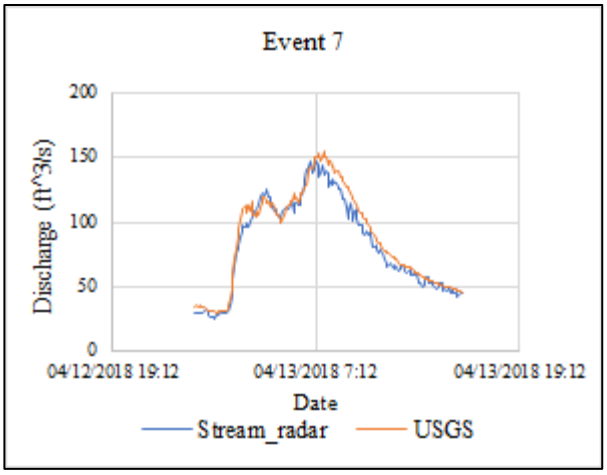
Event 7
Discharge (ft^3/s)
200
150
100
50
0
04/12/2018 19:12
04/13/2018 7:12
04/13/2018 19:12
Date
Stream_radar
USGS

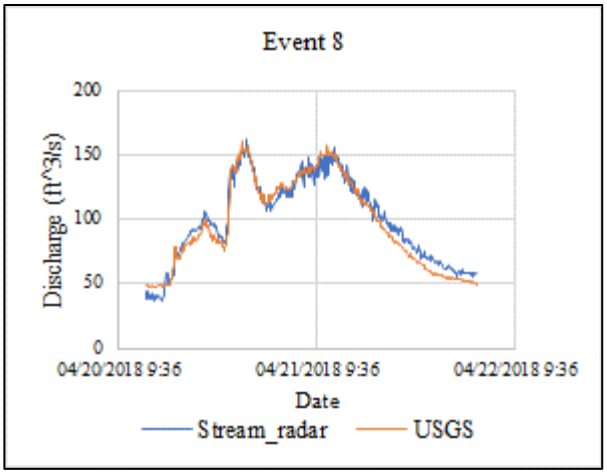
Event 8
Discharge (ft^3/s)
200
150
100
50
0
04/20/2018 9:36
04/21/2018 9:36
04/22/2018 9:36
Date
Stream_radar
USGS

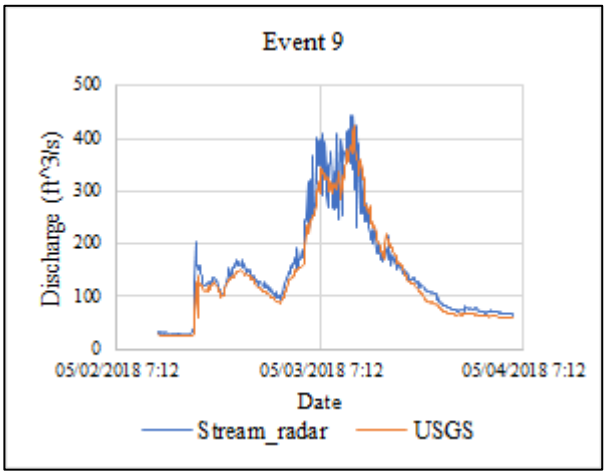
Event 9
Discharge (ft^3/s)
500
400
300
200
100
0
05/02/2018 7:12
05/03/2018 7:12
05/04/2018 7:12
Date
Stream_radar
USGS

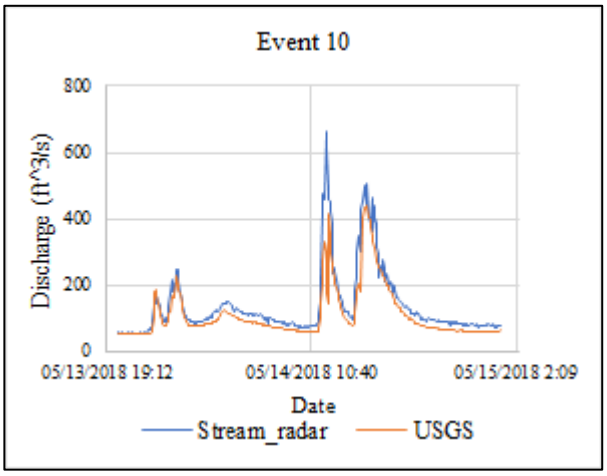
Event 10
Discharge (ft^3/s)
800
600
400
200
0
05/13/2018 19:12
05/14/2018 10:40
05/15/2018 2:09
Date
Stream_radar
USGS

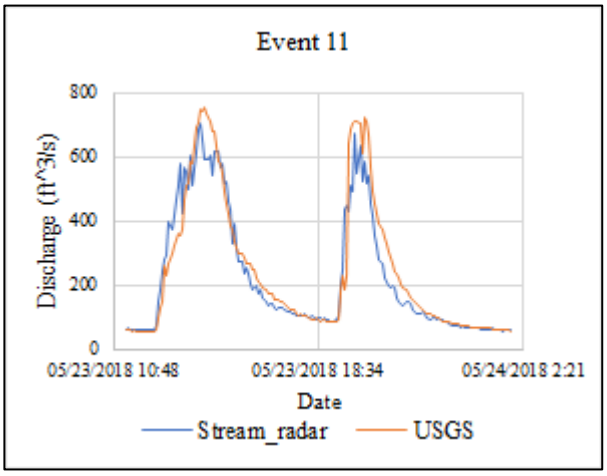
Event 11
Discharge (ft^3/s)
800
600
400
200
0
05/23/2018 10:48
05/23/2018 18:34
05/24/2018 2:21
Date
Stream_radar
USGS

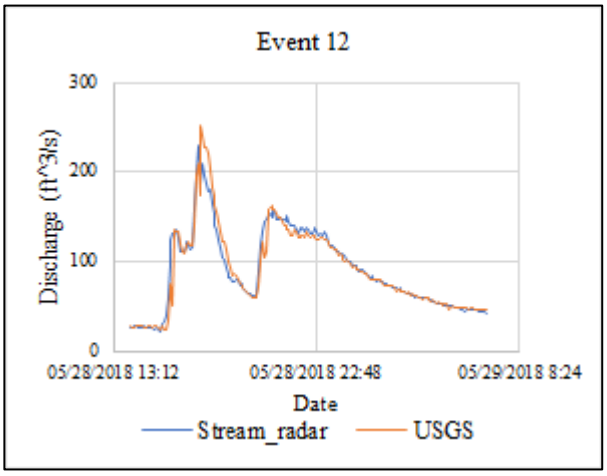
Event 12
Discharge (ft^3/s)
300
200
100
0
05/28/2018 13:12
05/28/2018 22:48
05/29/2018 8:24
Date
Stream_radar
USGS

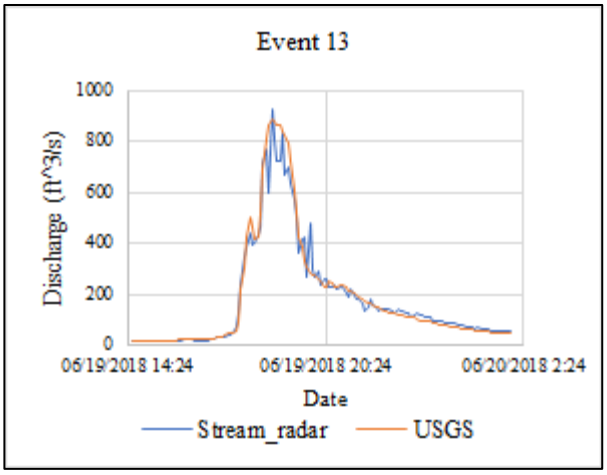
Event 13
Discharge (ft^3/s)
1000
800
600
400
200
0
06/19/2018 14:24
06/19/2018 20:24
06/20/2018 2:24
Date
Stream_radar
USGS

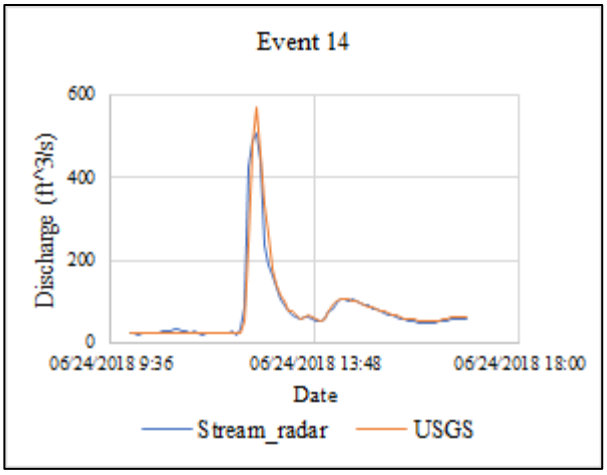
Event 14
Discharge (ft^3/s)
600
400
200
0
06/24/2018 9:36
06/24/2018 13:48
06/24/2018 18:00
Date
Stream_radar
USGS

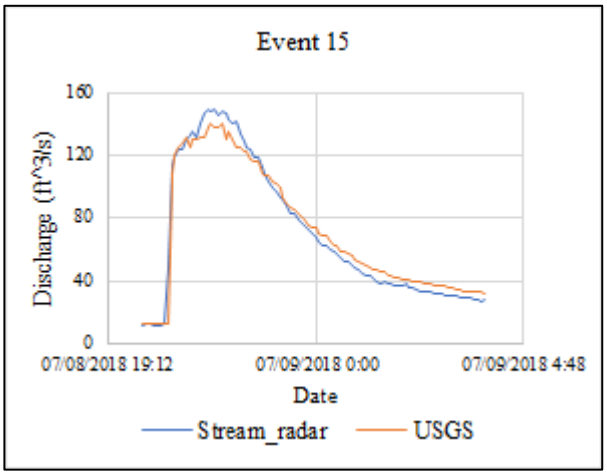
Event 15
Discharge (ft^3/s)
160
120
80
40
0
07/08/2018 19:12
07/09/2018 0:00
07/09/2018 4:48
Date
Stream_radar
USGS

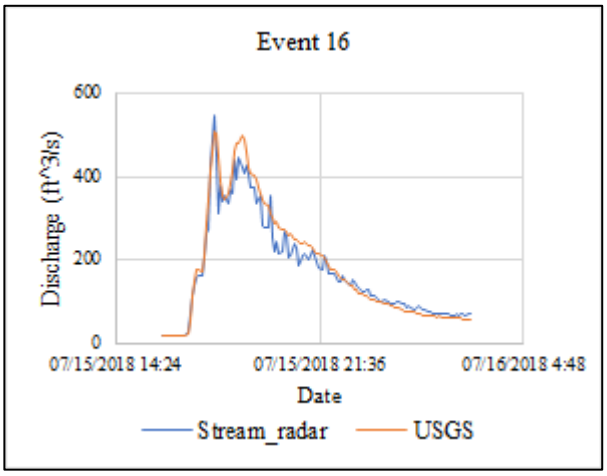
Event 16
Discharge (ft^3/s)
600
400
200
0
07/15/2018 14:24
07/15/2018 21:36
07/16/2018 4:48
Date
Stream_radar
USGS

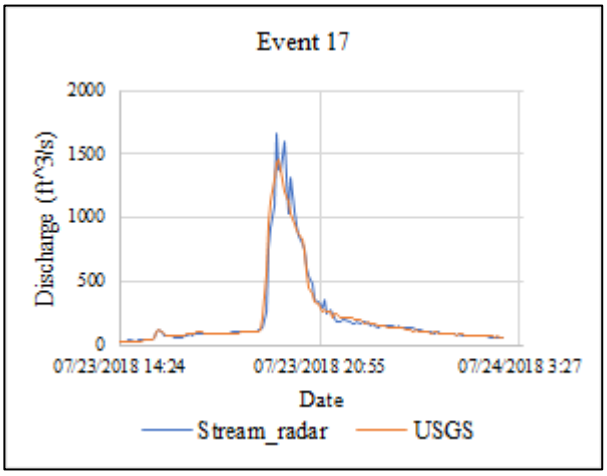
Event 17
Discharge (ft^3/s)
2000
1500
1000
500
0
07/23/2018 14:24
07/23/2018 20:55
07/24/2018 3:27
Date
Stream_radar
USGS

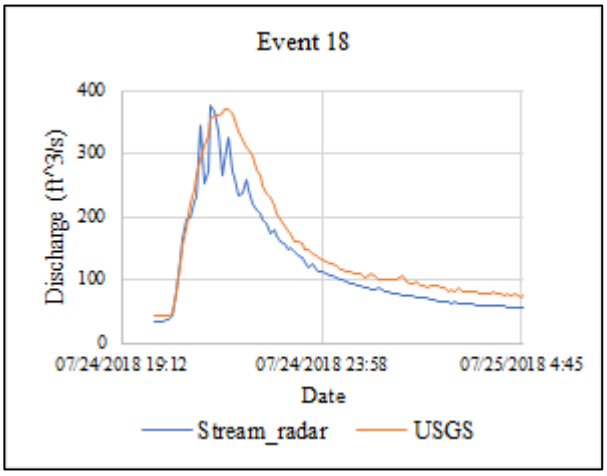
Event 18
Discharge (ft^3/s)
400
300
200
100
0
07/24/2018 19:12
07/24/2018 23:58
07/25/2018 4:45
Date
Stream_radar
USGS

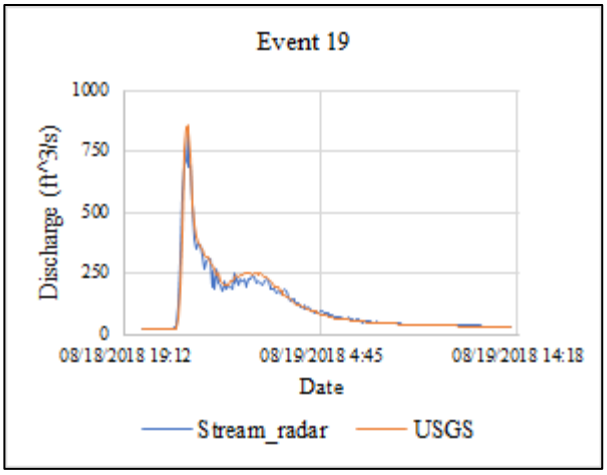
Event 19
Discharge (ft^3/s)
1000
750
500
250
0
08/18/2018 19:12
08/19/2018 4:45
08/19/2018 14:18
Date
Stream_radar
USGS

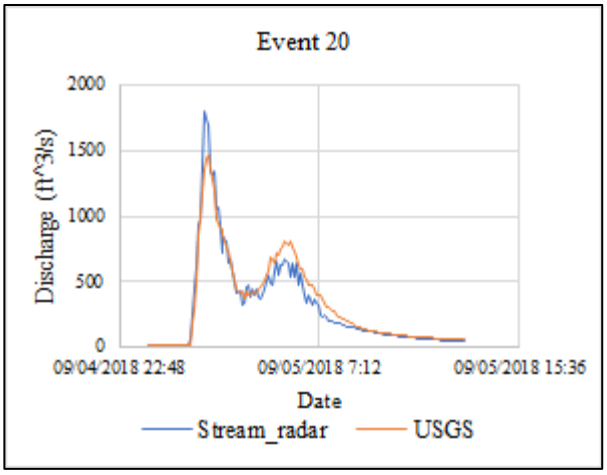
Event 20
Discharge (ft^3/s)
2000
1500
1000
500
0
09/04/2018 22:48
09/05/2018 7:12
09/05/2018 15:36
Date
Stream_radar
USGS

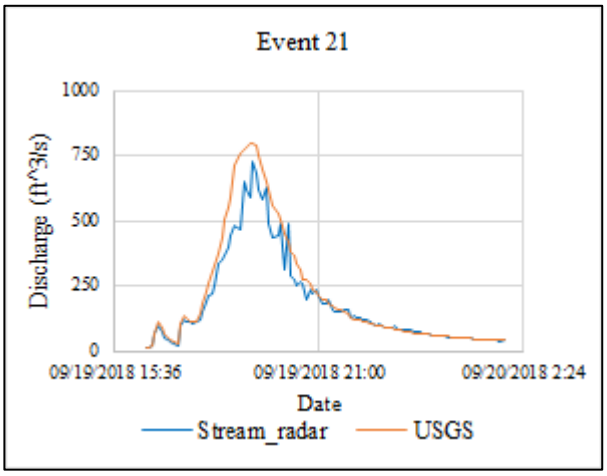
Event 21
Discharge (ft^3/s)
1000
750
500
250
0
09/19/2018 15:36
09/19/2018 21:00
09/20/2018 2:24
Date
Stream_radar
USGS

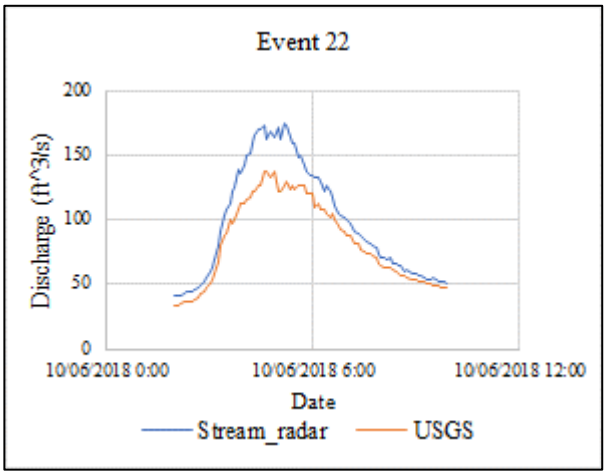
Event 22
Discharge (ft^3/s)
200
150
100
50
0
10/06/2018 0:00
10/06/2018 6:00
10/06/2018 12:00
Date
Stream_radar
USGS

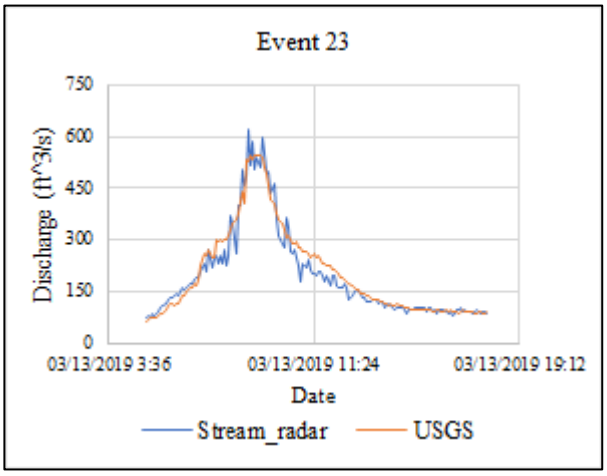
Event 23
Discharge (ft^3/s)
750
600
450
300
150
0
03/13/2019 3:36
03/13/2019 11:24
03/13/2019 19:12
Date
Stream_radar
USGS

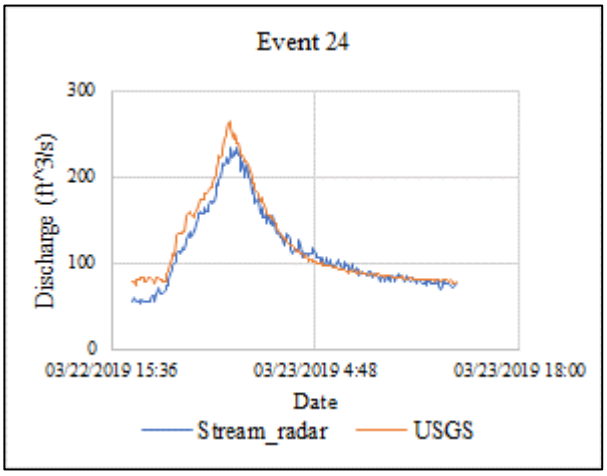
Event 24
Discharge (ft^3/s)
300
200
100
0
03/22/2019 15:36
03/23/2019 4:48
03/23/2019 18:00
Date
Stream_radar
USGS

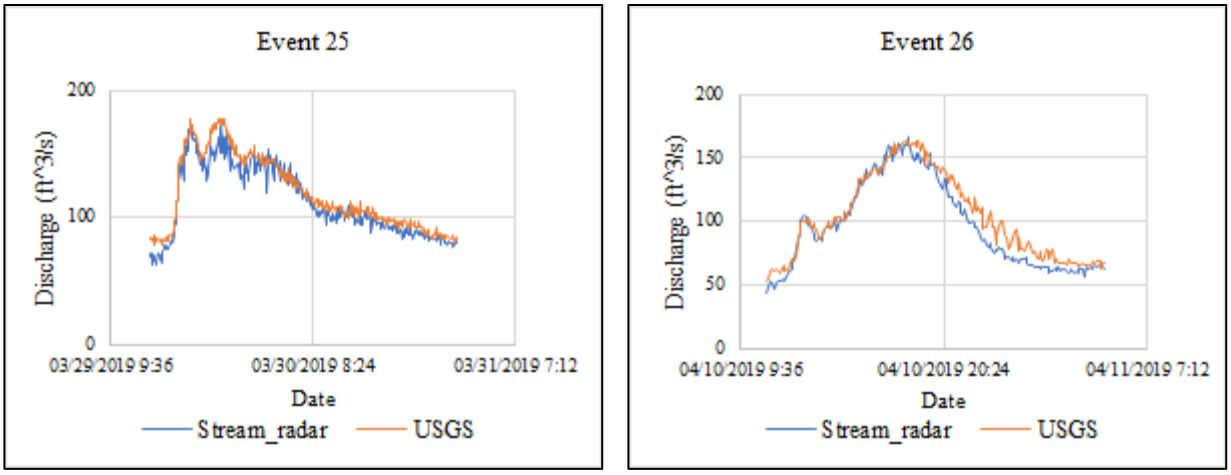

Figure AB. 2: Event-hydrograph comparisons for Cherry Creek with double-k

B.3 Walnut Gulch

Figure AB.3 shows the event-hydrograph comparisons of Walnut Gulch for double-k optimization.

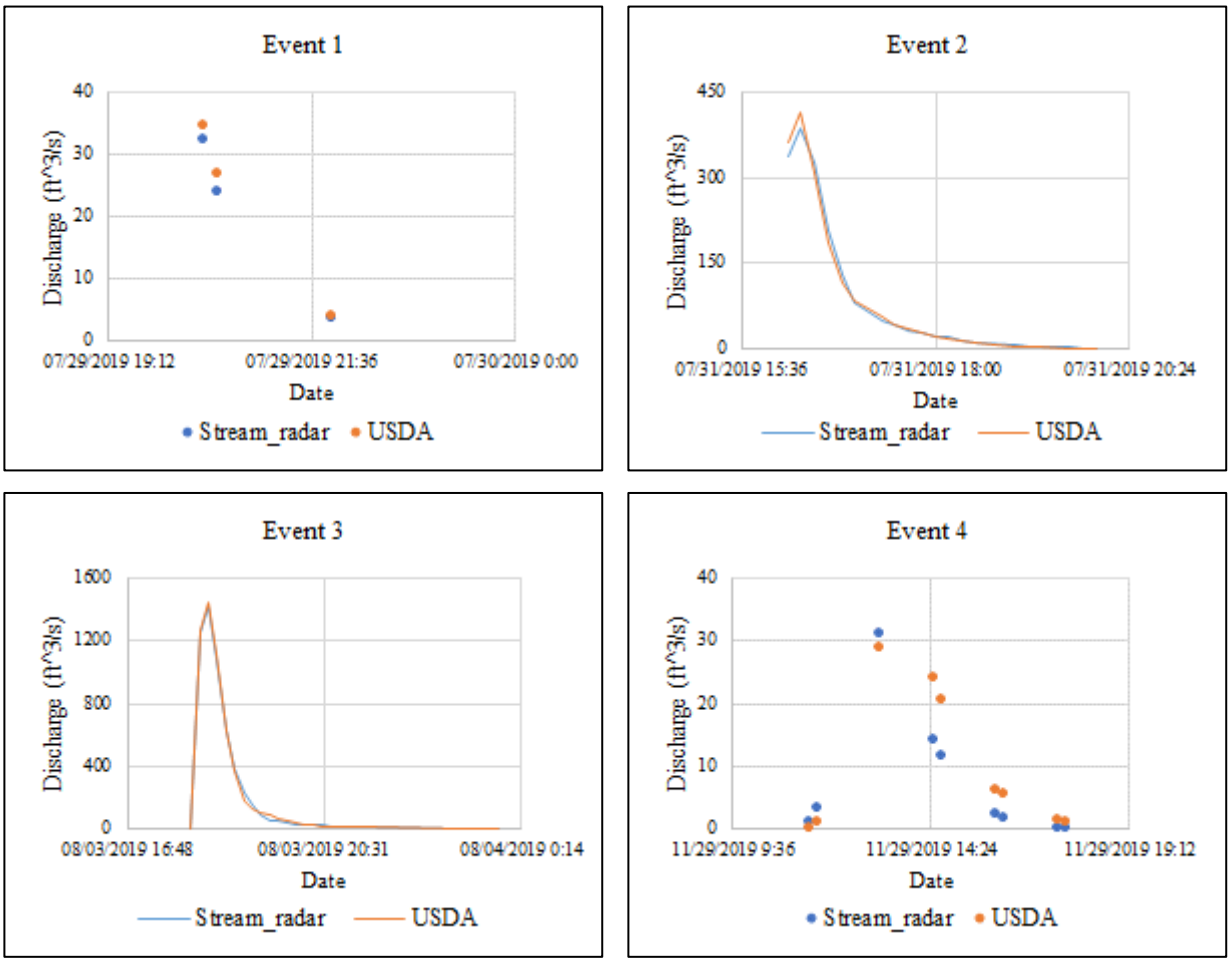

Figure AB. 3: Event-hydrograph comparisons for Walnut Gulch with double-k

B.4 Paria River

Figure AB.4 shows the event-hydrograph comparisons of Paria River for k-value of 1.0.

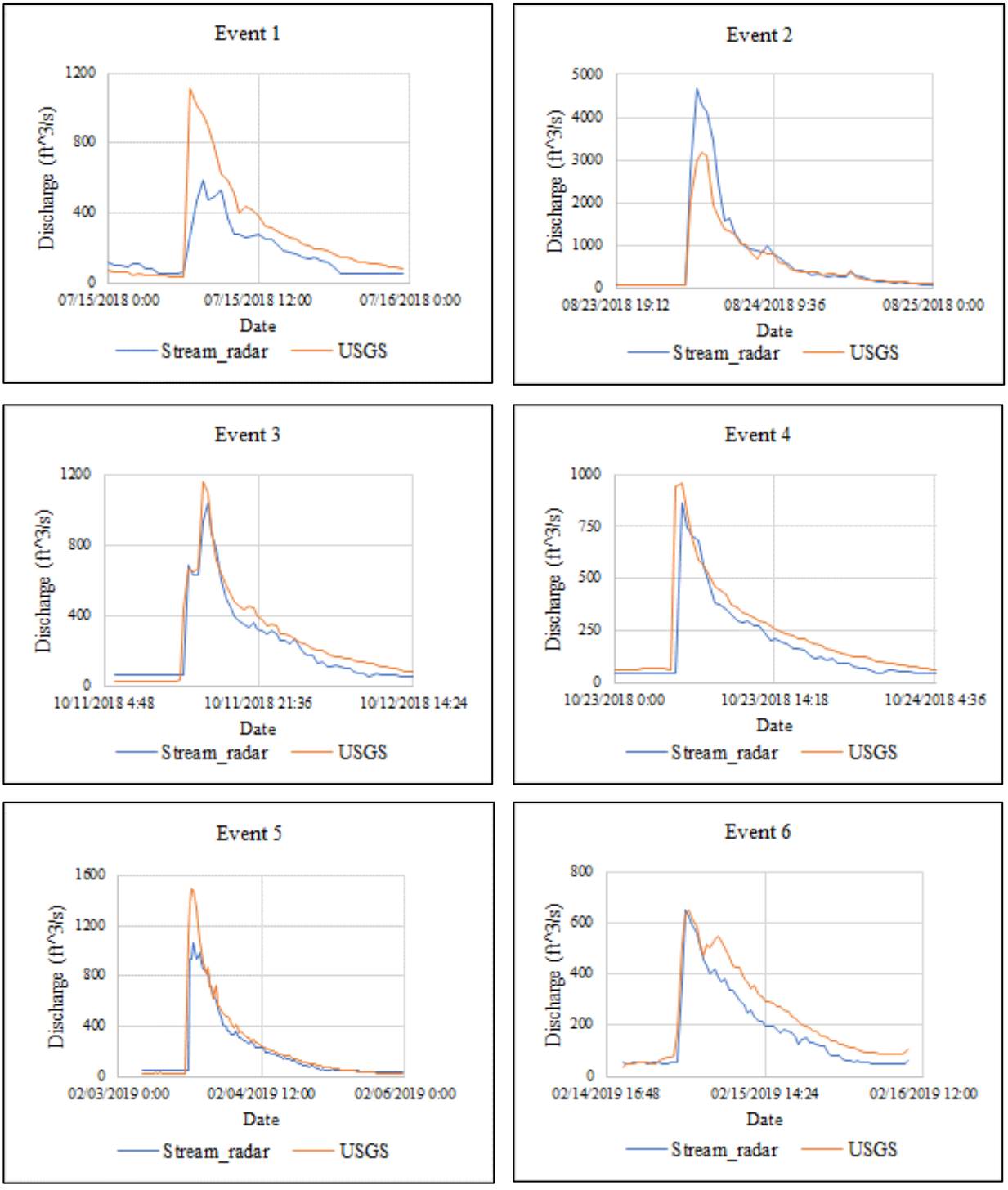

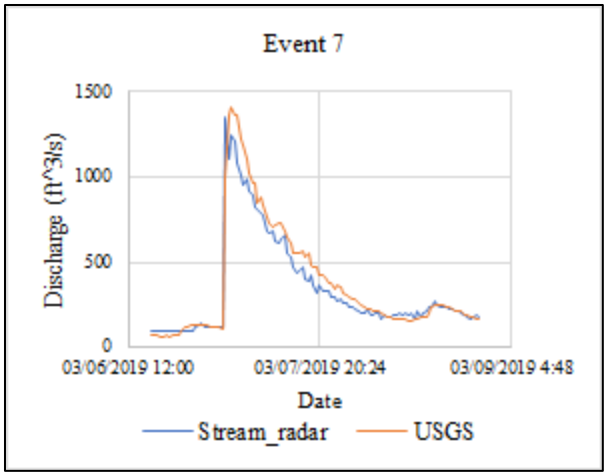

Figure AB. 4: Event-hydrograph comparisons for Paria River with k-value of 1.0

APPENDIX – C

Events Having Stage Led by Surface Velocity

C.1 Mill Creek

Figure AC.1 shows the rest of the event-hydrographs of Mill Creek where surface velocity leads the stage.

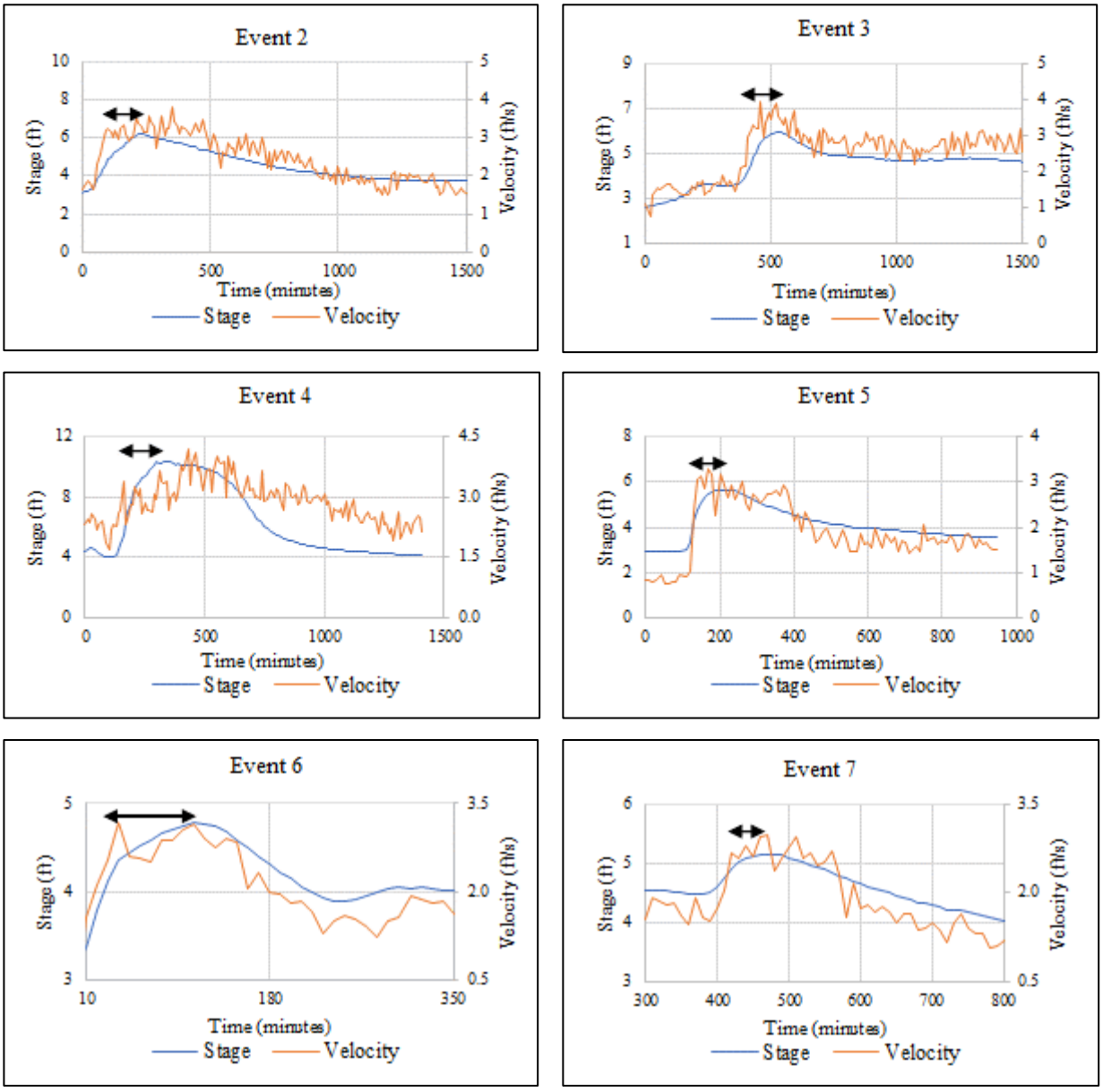

Figure AC. 1: Events of Mill Creek having stage led by surface velocity

C.2 Paria River

Figure AC.2 shows the rest of the event-hydrographs of Paria River where surface velocity leads the stage.

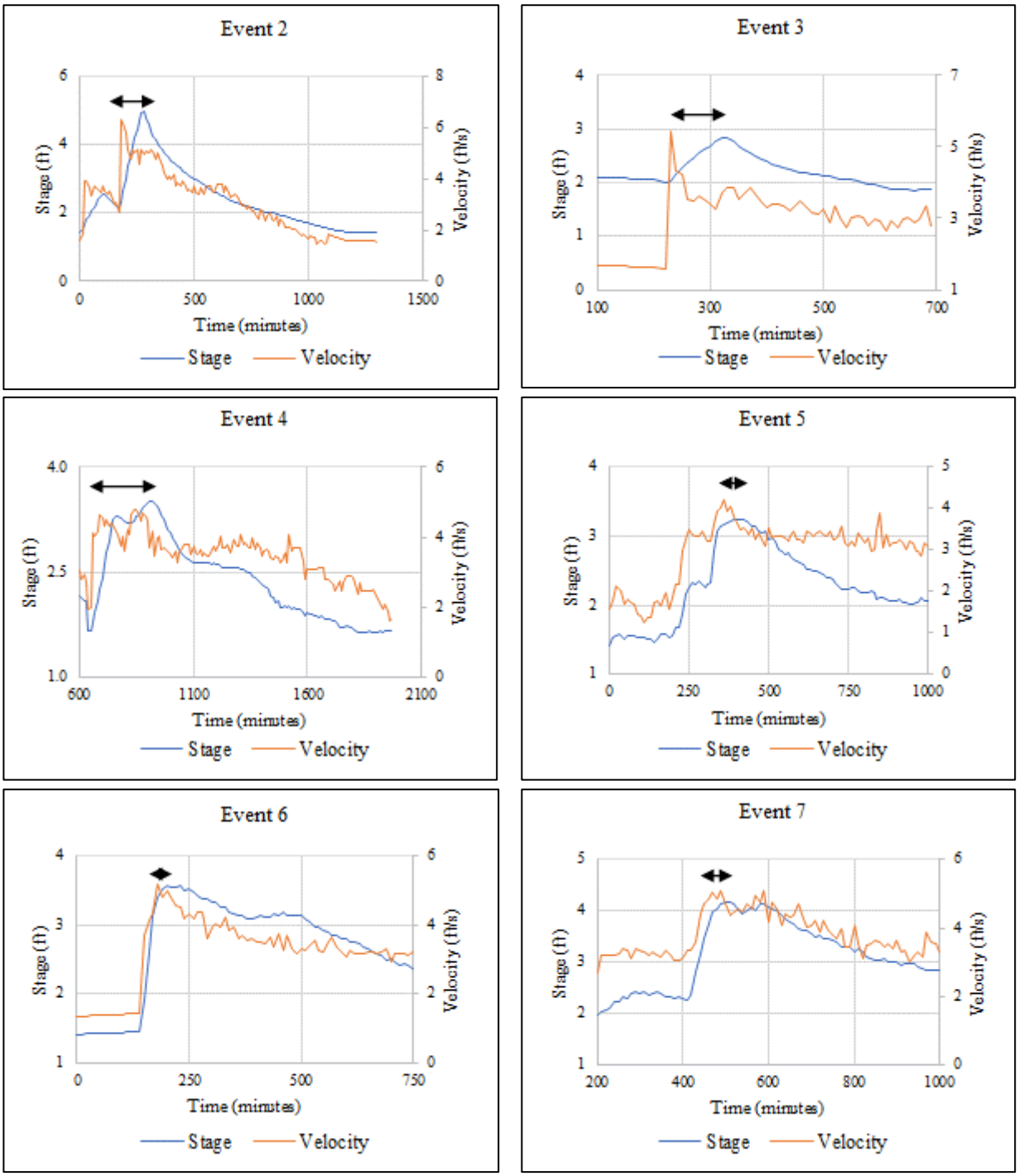

Figure AC. 2: Events of Paria River having stage led by surface velocity

C.3 Falls Creek

Figure AC.3 shows the rest of the event-hydrographs of Falls Creek where surface velocity leads the stage.

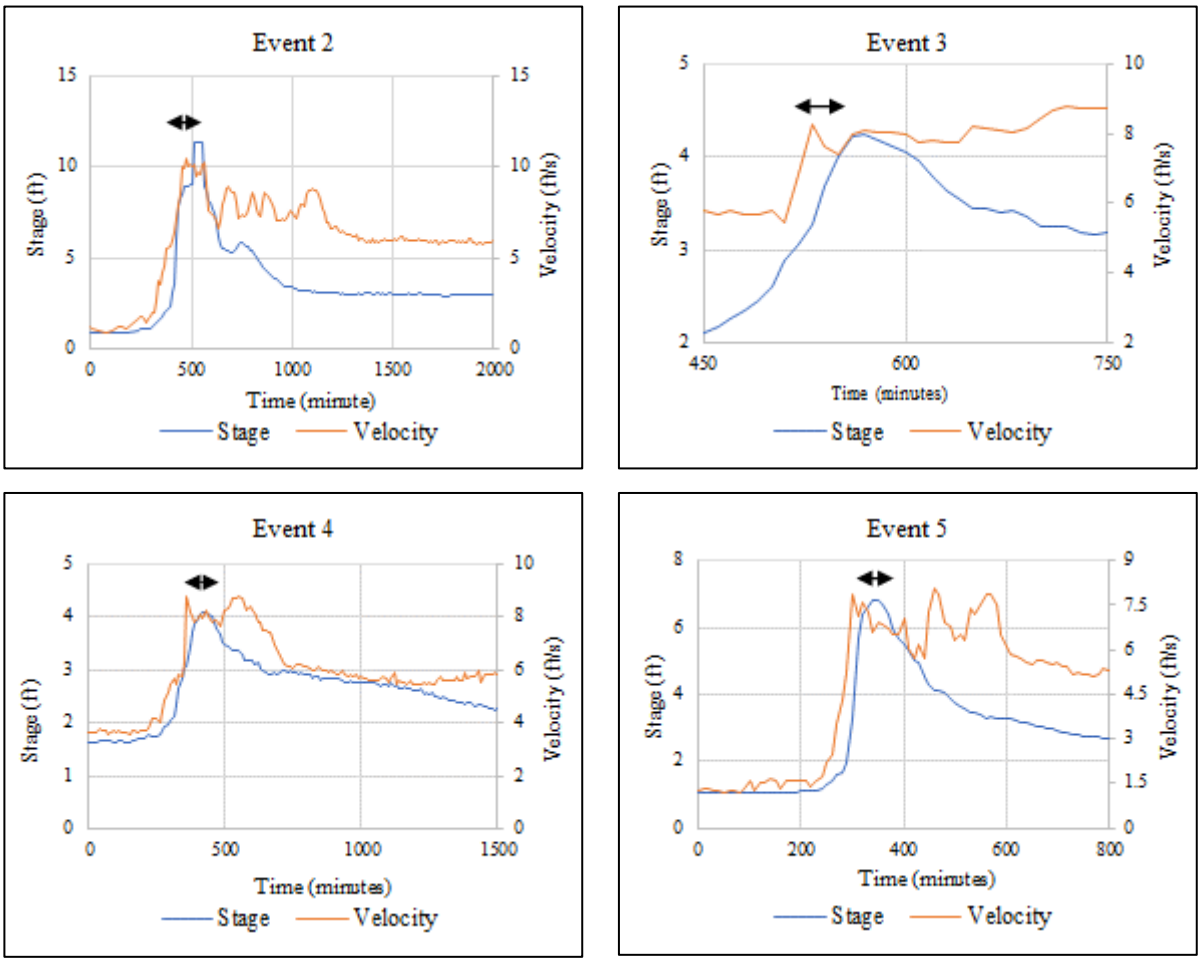

Figure AC. 3: Events of Falls Creek having stage led by surface velocity

C.4 Sessom Creek

Figure AB.4 shows the rest of the event-hydrographs of Sessom Creek where surface velocity leads the stage.

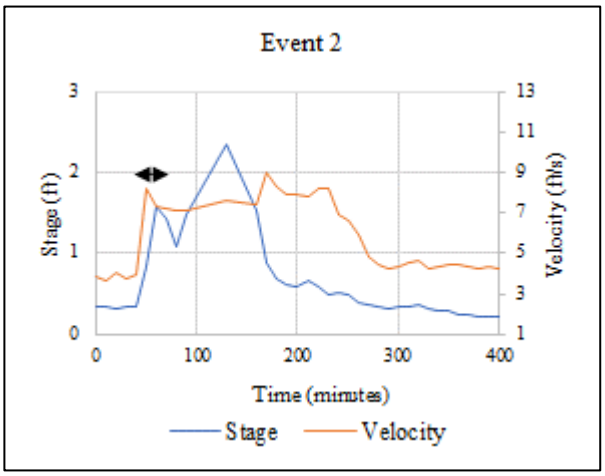

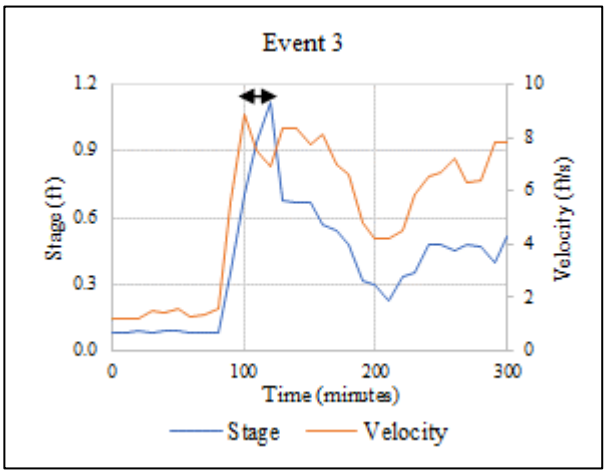

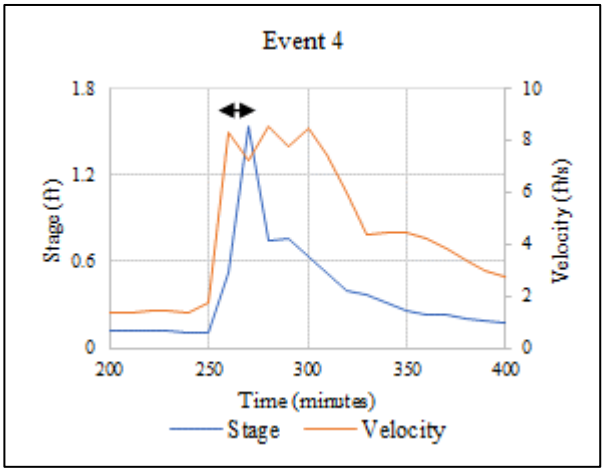

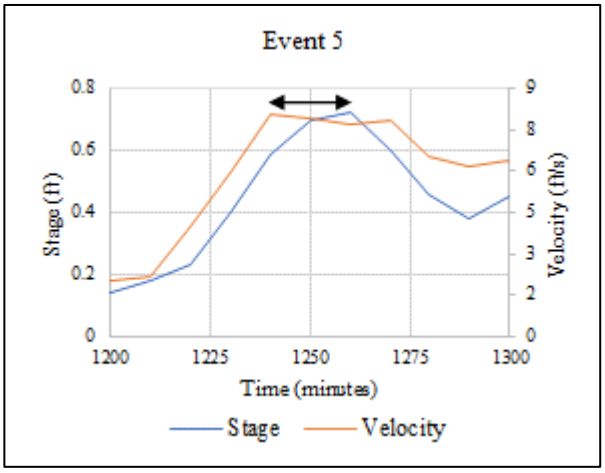

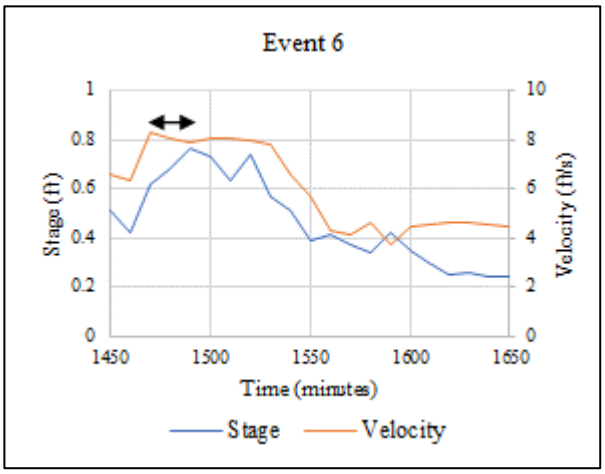

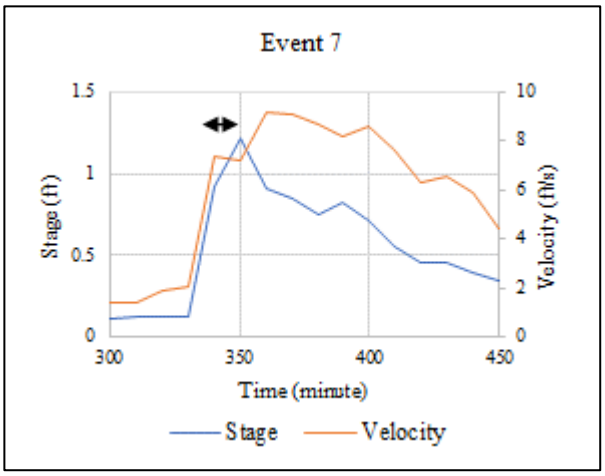

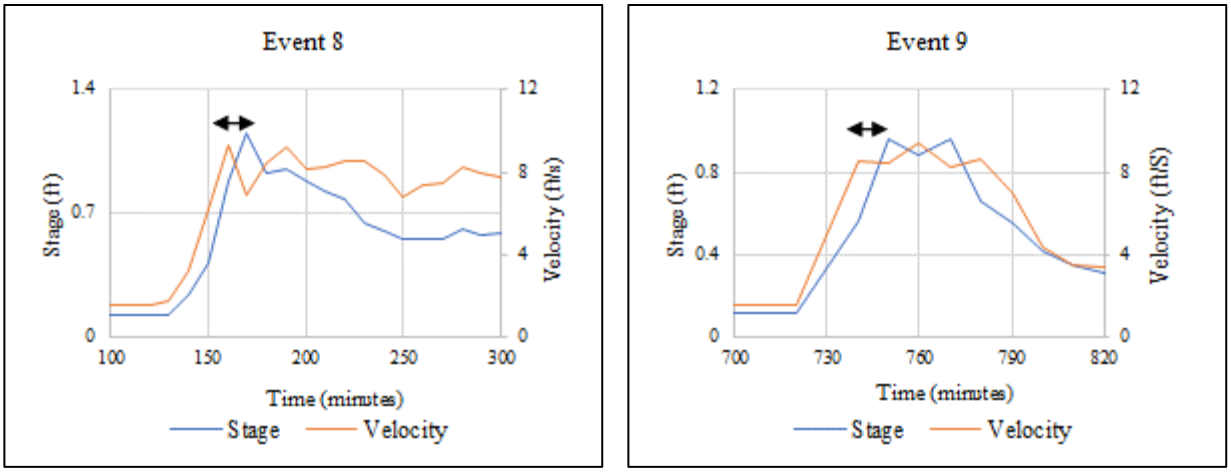

Figure AC. 4: Events of Sessom Creek having stage led by surface velocity